RUB

RUHR-UNIVERSITÄT BOCHUM

Advanced Materials Processing and Microfabrication

VORLESUNG Wintersemester 2025/2026

Prof. Dr.-Ing. Alfred Ludwig

Advanced Materials Processing and Microfabrication

Übersicht Themen Prof. Ludwig

1. Grenzflächendominierte Werkstoffe
2. Oberflächenprozessierung
3. Mikrosystemtechnik
4. Nanotechnologie

„Megatrends“:
→ Miniaturisierung und Integration
→ Dünnschichttechnologie

Grundlagen:
- Werkstoffe und Fertigungsverfahren der Mikrosystemtechnik (Bachelor)

Vertiefung im Master:
- MEMS und Nanotechnologie (SoSe)
- Dünne Schichten und Hochdurchsatzmethoden in der Materialforschung (WiSe)

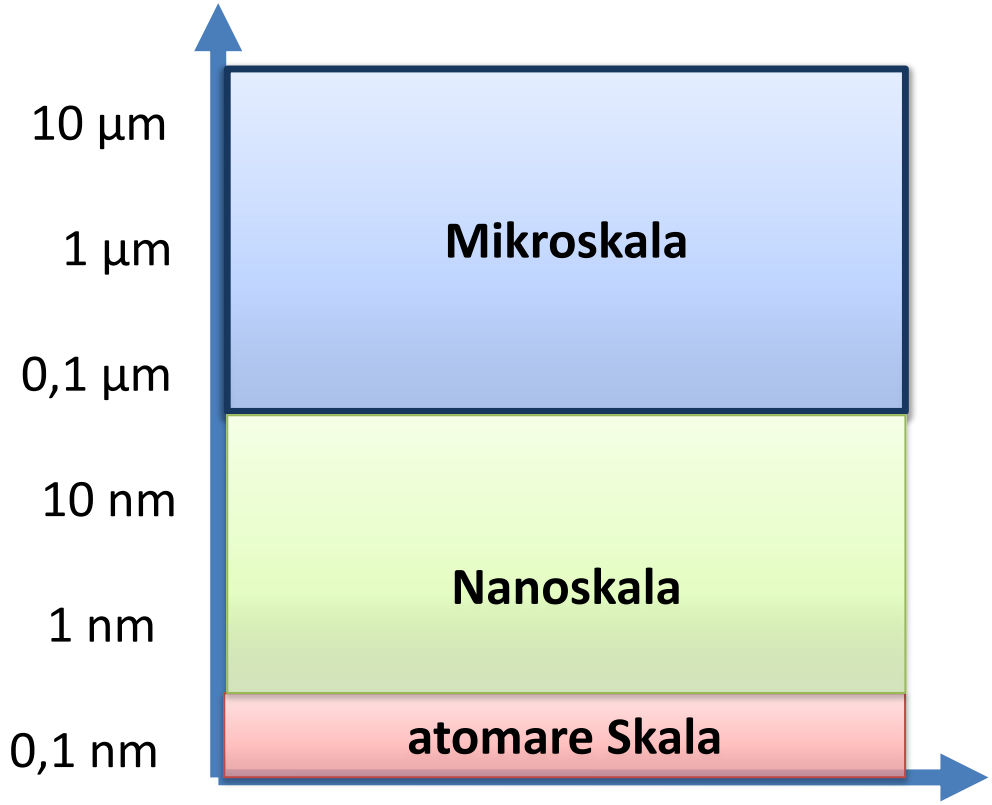

Advanced Materials Processing and Microfabrication

Advanced Materials Processing

- **Synthese anorganische Festkörper**
  - Herstellung in unterschiedlicher Form (Einkristall, Polykristall, Volumenwerkstoff, mikro- oder nanostrukturierte Materialien)
  - in situ Kontrolle der Herstellung
- **Grenzflächendominierte Höchstleistungswerkstoffe**
  - Grenzflächenbauteile
  - Viellagenschichtsysteme
  - Nanomaterialien
  - funktionelle Oberflächen
- **extreme Prozesse**
  - (fast) perfekte Kristalle
  - metallische Gläser
  - Hochdruckphasen
- **spezielle Prozessierungsmethoden**
- **stabile/metastabile Materialien (Legierungen und Verbindungen)**

Advanced Materials Processing for Micro- and Nanofabrication

- **Mikrosysteme**
  - bestehen zum Großteil aus mikrostrukturierten Schichtwerkstoffen
  - großer Oberflächenanteil
- **Nanosysteme**
  - extrem hoher Oberflächenanteil
  - z.B. Nanopartikel

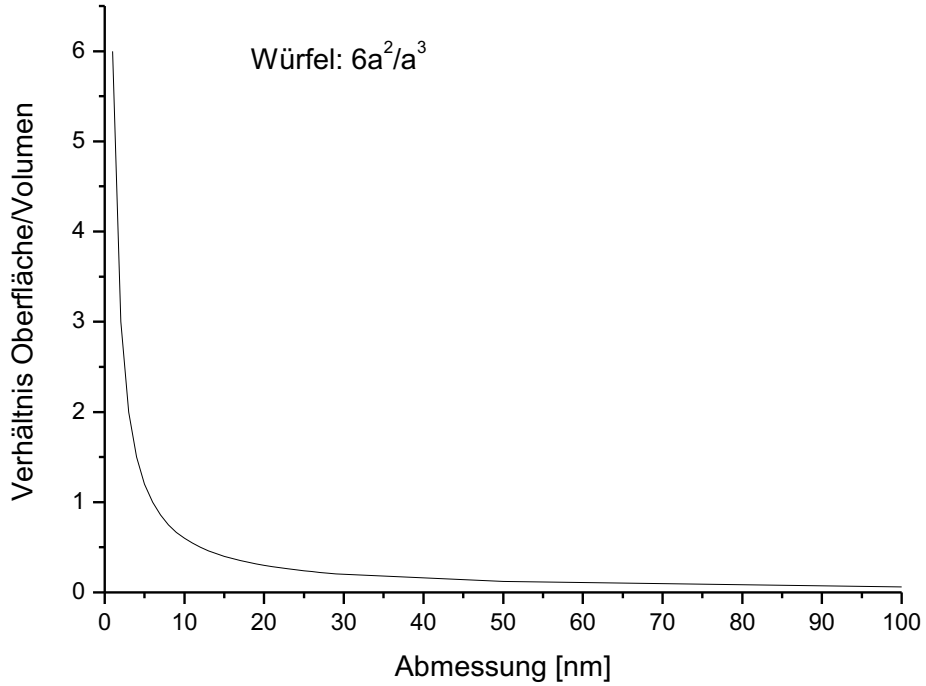

Skalierung:
immer mehr Grenzflächen bei Miniaturisierung

Advanced Materials Processing and Microfabrication

Mikrosystemtechnik

MEMS:

Micro-**E**lectro-**M**echanical **S**ystems

Mit welchen Werkstoffen und Methoden kann man Maschinen mit charakteristischen Abmessungen im Mikrometerbereich herstellen?

Mask Aligner and UV-Exposure Unit

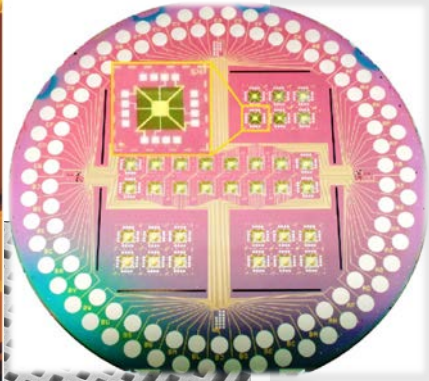

Beispiel: Gyroskop für PKW

Nanotechnologie

- Herstellung und Charakterisierung von Objekten mit charakteristischen Abmessungen im Nanometerbereich
- Nanomaterialien ermöglichen neue Anwendungen

Integration in Systeme

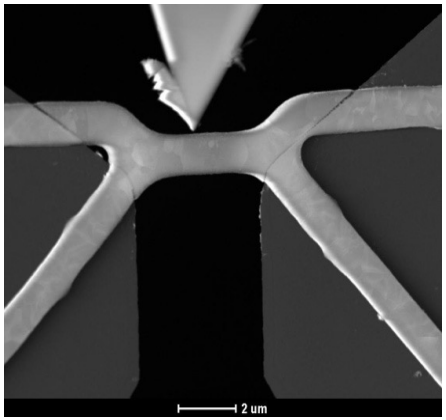

Mikro/Nanosysteme (MEMS/NEMS)

Nanopartikel

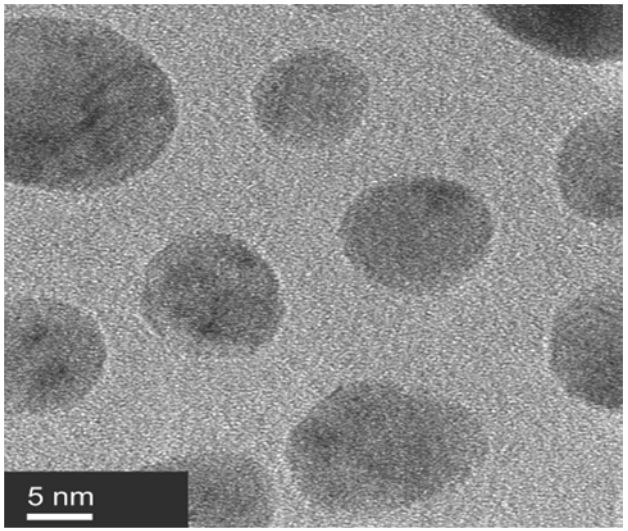

Nanosäulen

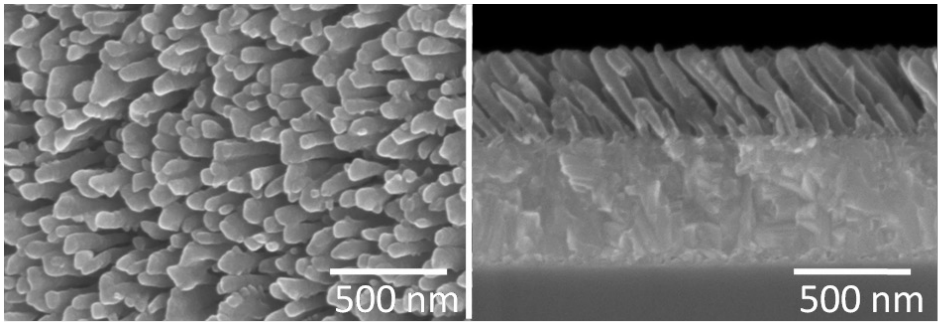

Advanced Materials Processing and Microfabrication

Grenzflächen in der Materialwissenschaft

- **innere Grenzflächen**
  - Korngrenzen (innerhalb einer Phase)
  - Phasengrenzflächen
    (zwischen mehreren Phasen, z.B. Matrix-Ausscheidung)
  - Zwillingsgrenzen

- **Oberflächen**
  - Grenzflächen zum Vakuum oder Umgebungsmedium

Grenzflächendominierte Höchstleistungswerkstoffe

Oberflächen und Schichten

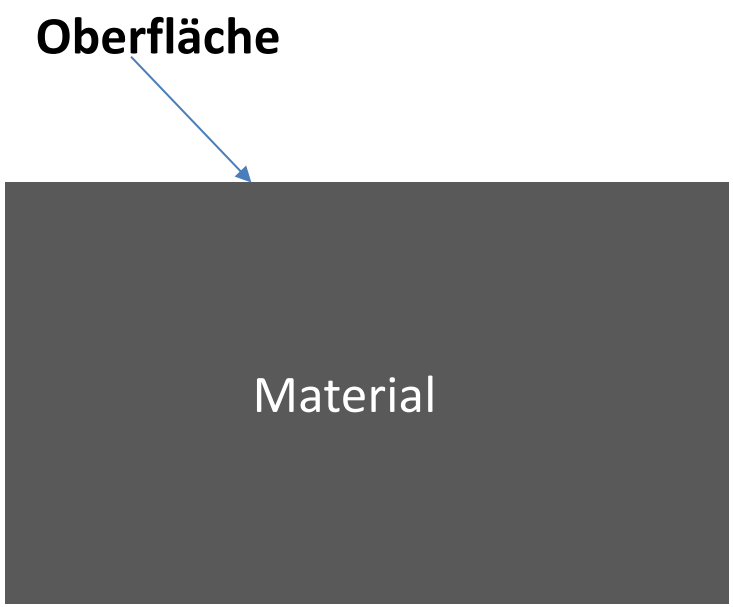

Flächen:
d.h. zweidimensional,
aber reale Oberflächen und Grenzflächen haben eine Dicke (mindestens eine Atomlage)

Oberflächentechnik
Behandeln
(mechanisch, thermisch, thermomechanisch)
Abscheiden
(phys., chem., galvanisch)
Auftragen
(mechanisch, thermisch, mechanothermisch)

Beanspruchung von Oberflächen

- mechanisch
- thermisch
- chemisch
- elektrochemisch
- elektrisch
- durch Strahlung

Grenzflächendominierte Höchstleistungswerkstoffe

Grenzflächen

Grenzflächen:

- zwischen Körnern in kristallinen Gefügen
- zwischen Phasen (fest/fest, fest/flüssig, fest/gas, …)
- zwischen Schichten in Mikro- und Nanosystemen

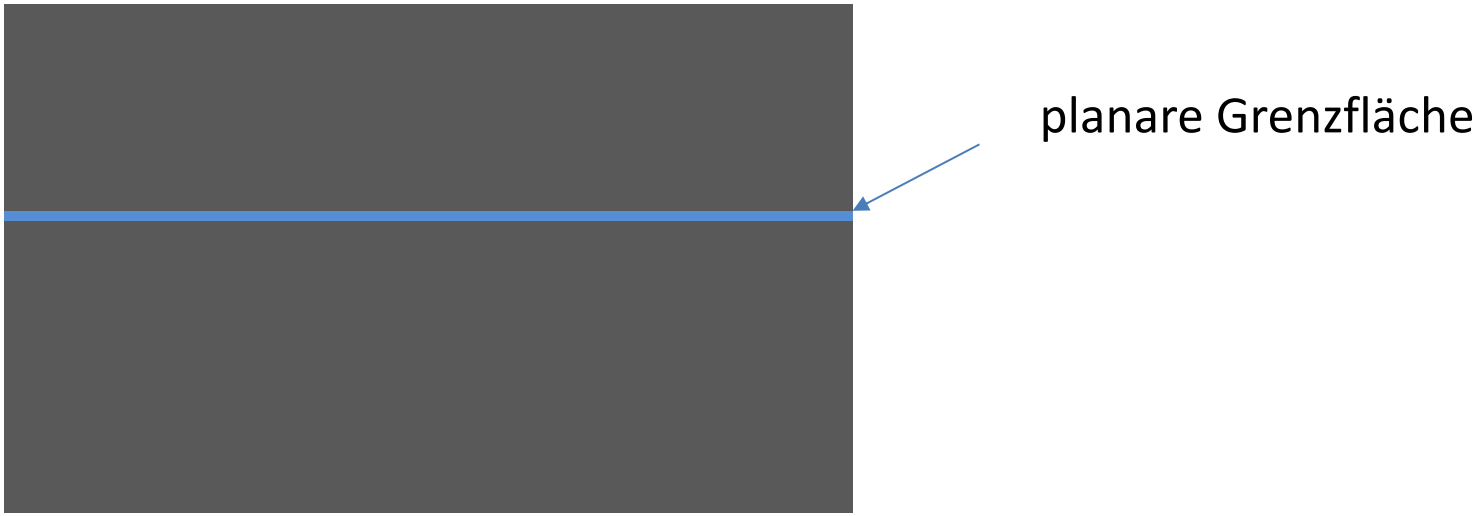

Grenzflächendominierte Höchstleistungswerkstoffe

Vielleicht die wichtigste Grenzfläche: pn Übergang

p-n-Übergang

- atomar glatte Grenzfläche zwischen p- und n-Halbleiter
- **Transistoren**, **Solarzellen** und hocheffizienten Lichtemitter (**LEDs**) basieren auf pn-Übergäng(en).

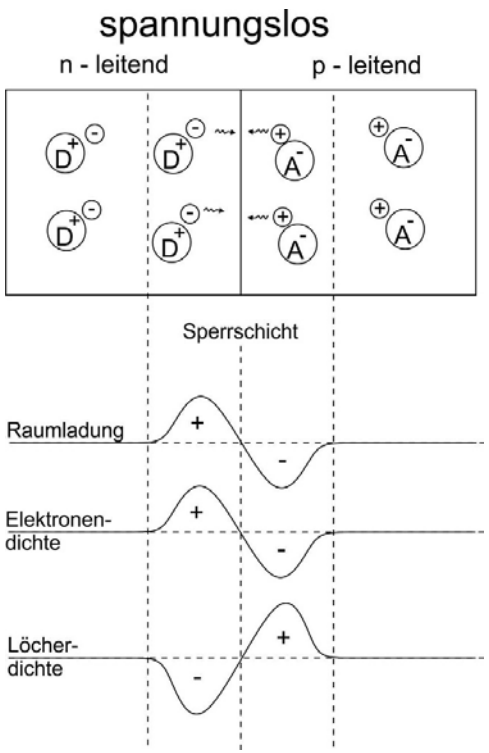

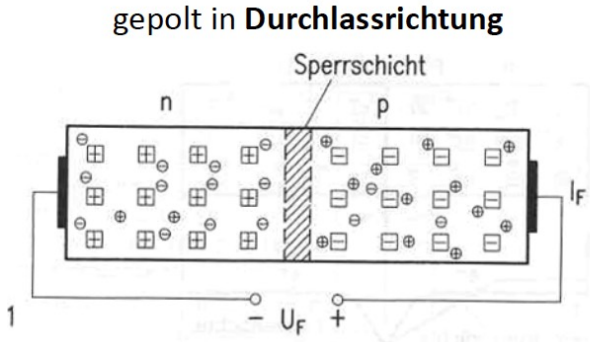

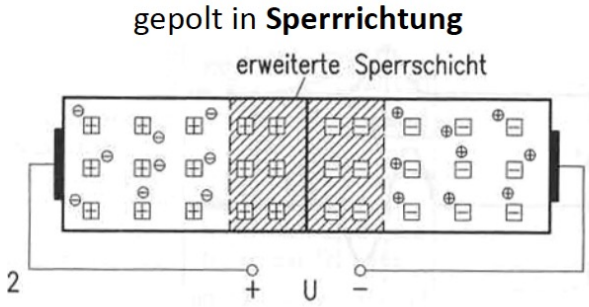

Beim Anlegen einer elektrischen Spannung an einen p-n Übergang kommt es, je nach Polung, zum Fließen oder zur Sperrung des Stromes. Die freien Ladungsträger folgen der angelegten Spannung und verkleinern (Durchlassrichtung) oder vergrößern (Sperrrichtung) die Sperrschicht.

1= p–n–Übergang in Durchlaßrichtung
2= p–n–Übergang in Sperrrichtung
Symbolerklärung: ⊞ = ionisiertes Donatoratom
⊟ = ionisiertes Akzeptoratom
⊕ = Defektelektron
⊖ = Leitungselektron

Grenzflächendominierte Höchstleistungswerkstoffe

Transistor

The Nobel Prize in Physics 1956

Summary

Laureates

William B. Shockley
John Bardeen
Walter H. Brattain

Presentation Speech

Share this

The Nobel Prize in Physics 1956

Photo from the Nobel Foundation archive.
William Bradford Shockley
Prize share: 1/3

John Bardeen
Prize share: 1/3

Photo from the Nobel Foundation archive.
Walter Houser Brattain
Prize share: 1/3

The Nobel Prize in Physics 1956 was awarded jointly to William Bradford Shockley, John Bardeen and Walter Houser Brattain "for their researches on semiconductors and their discovery of the transistor effect"

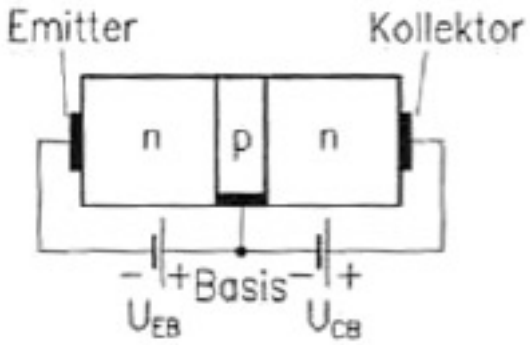

Bipolartransistor

Transistor: „Ein-Aus-Schalter“

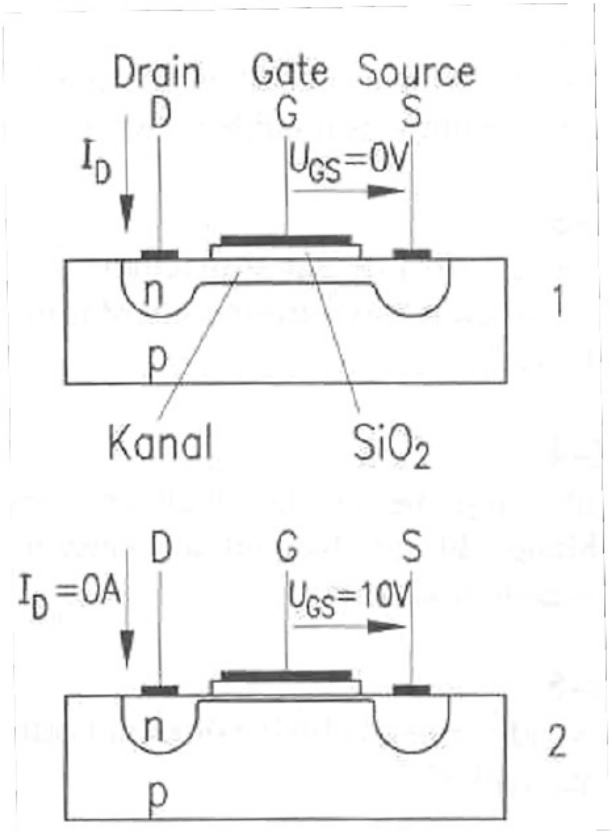

1 - ohne Steuerspannung U_{GS}
2 - mit Steuerspannung U_{GS}

Feldeffekttransistor

Grenzflächendominierte Höchstleistungswerkstoffe

Solarzellen und LEDs

Solarzellen

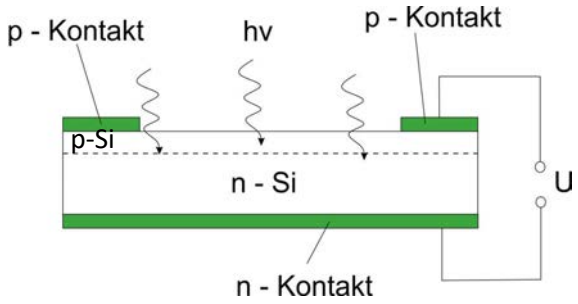

LEDs

LEDs: light emitting devices (diodes)

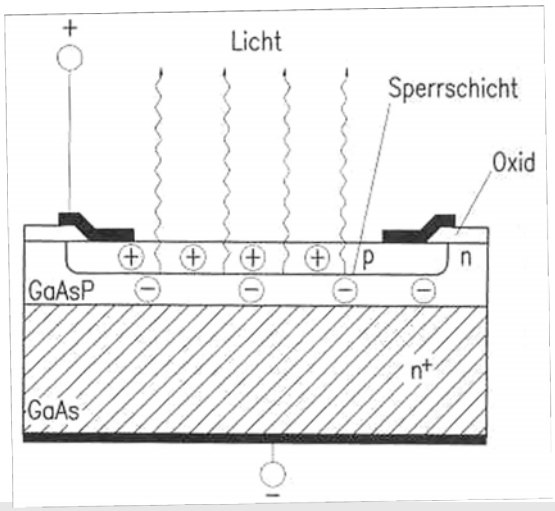

Grenzflächendominierte Höchstleistungswerkstoffe

Blaue LED

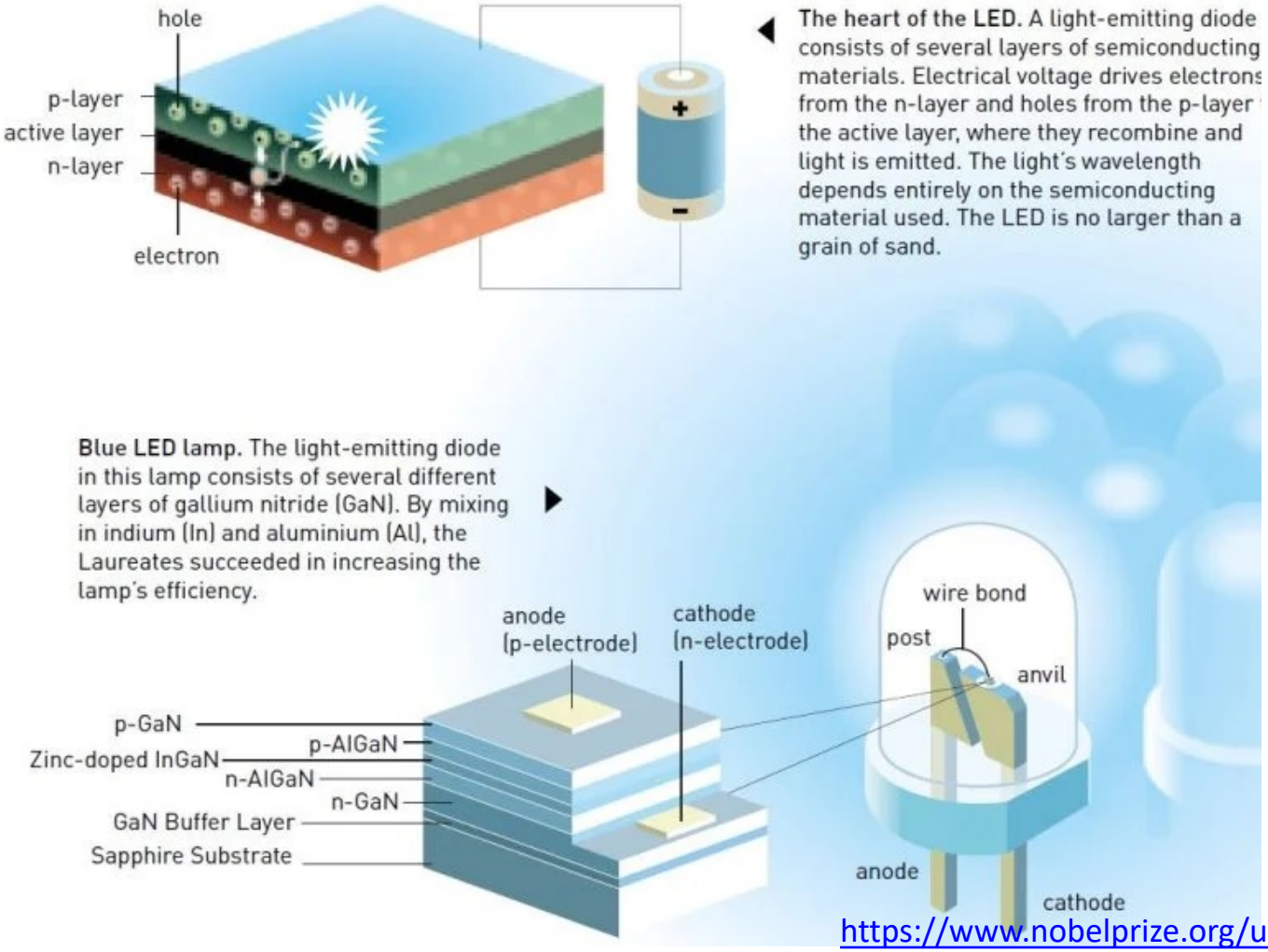

GaN,
direkte Bandlücke 3,39 eV
Metalorganic vapor phase epitaxy (MOVPE)
MOCVD
Epitaktische Schichten auf Saphir-EinkristallSubstrat

https://www.nobelprize.org/uploads/2018/06/advanced-physicsprize2014-1.p

The principle for a light-emitting diode – LED (upper left) and an example of a blue LED lamp.
Illustration: © Johan Jarnestad/The Royal Swedish Academy of Sciences https://www.nobelprize.org/prizes/physics/2014/popular-information/

Grenzflächendominierte Höchstleistungswerkstoffe

Blaue LED: Probleme

1. Epitaktische Schichten auf Saphir-Einkristall-Substrat

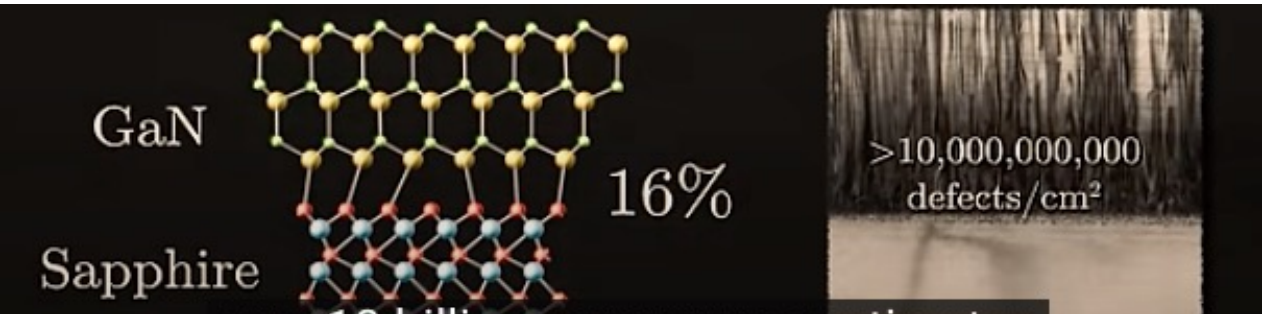

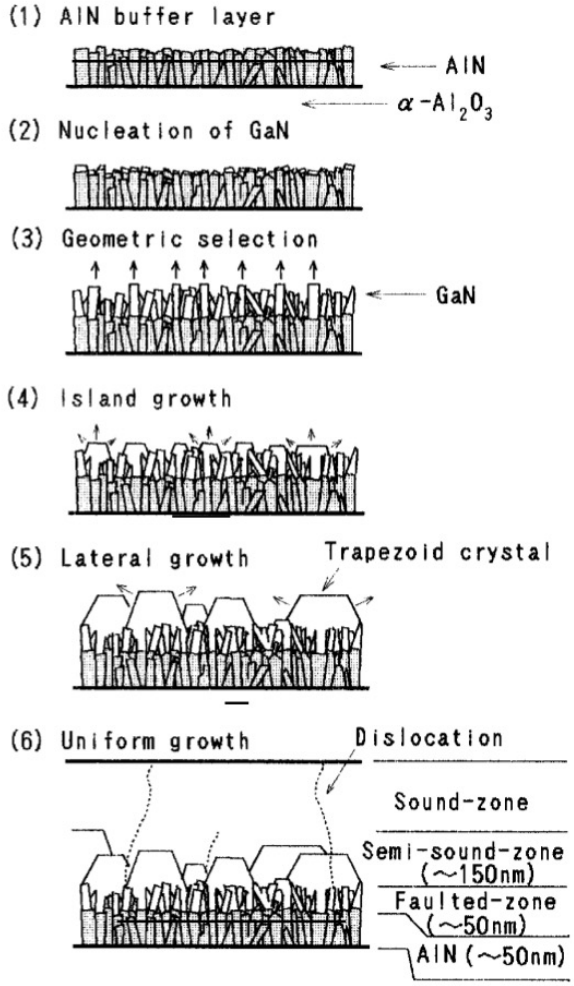

Fig. 6. Schematic diagrams showing the growth process of GaN on the AlN buffer layer as the cross sectional views.

https://youtu.be/AF8d72mA41M?feature=shared
https://www.nobelprize.org/uploads/2018/06/advanced-physicsprize2014-1.pdf
https://www.nobelprize.org/prizes/physics/2014/popular-information/

Grenzflächendominierte Höchstleistungswerkstoffe

Blaue LED: Probleme

2. p und n Materialien werden benötigt:
n einfach, p problematisch, Dotierung ?

Mg funktioniert,
nach Elektronenbestrahlung

Besser skalierbarer Prozess:
Glühen

Funktionsprinzip:
Beseitigung von Wasserstoff

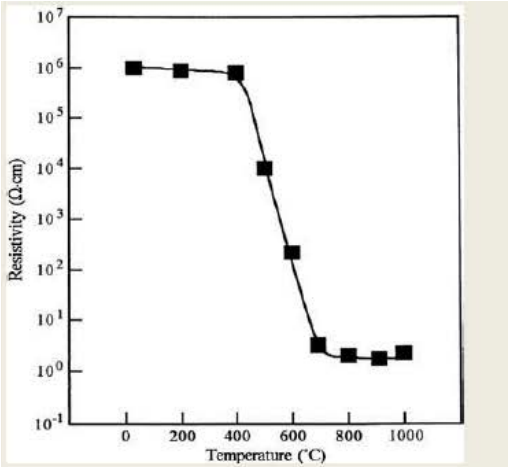

b) Resistivity of Mg doped GaN as a function of annealing temperature [32]

3. Hohe Effizienz notwendig

https://youtu.be/AF8d72mA41M?feature=shared
https://www.nobelprize.org/uploads/2018/06/advanced-physicsprize2014-1.pdf
https://www.nobelprize.org/prizes/physics/2014/popular-information/

Grenzflächendominierte Höchstleistungswerkstoffe

“The interface is the device“

H. Kroemer:
Im Jahr 2000 zusammen mit Schores Alfjorow Nobelpreis für Physik für die Entwicklung von Halbleiter-Heterostrukturen für Hochgeschwindigkeits- und Optoelektronik. Der dritte Preisträger war Jack Kilby für die Entwicklung Integrierter Schaltkreise.

The interface is still the device

Oxide materials show an amazing variety of electronic and ionic phenomena. However, despite considerable advances in understanding and utilizing these effects, experimental and theoretical challenges still need to be addressed before the promised applications can be realized.

When Nobel laureate Herbert Kroemer coined the famous phrase that “the interface is the device”, he referred to the astonishing success of devices based on thin semiconductor films for photonic and electronic applications that started more than 40 years ago. Now we are once more in the midst of a similar revolution, this time for oxide materials. Exhibiting a wide range of phenomena such as magnetism, superconductivity, ionic conduction and ferroelectricity, oxide materials are finding applications that include batteries, fuel cells, information storage and more. In particular, oxide interfaces, like their coventional semiconductor counterparts, offer the unique opportunity to control and enhance the effects by controlling the interaction between layers.

But where does this broad range of phenomena come from? For a start, the bonds between the ions in an oxide crystal tend to have a more polar character than in a conventional semiconductor such as silicon, which means that the electrons have stronger interactions with each other; they are said to be correlated. Moreover, the crystal structure of oxides is highly adaptable to changes in composition — many different chemical elements can be incorporated into the prototypical perovskite structure. This can not only be used for a very broad tuning of the carrier density in the crystal through doping, but it also increases the design flexibility in crystal composition. The latter is crucial to the development of improved materials such as ionic conductors for electrochemical applications, and moreover facilitates a wide range of different oxide compounds that can be deposited on top of each other in thin-film devices.

Progress — particularly in oxide thin-film growth technology — during the past decade has led to a large number of breakthroughs. For example, $LaAlO_3$ and $SrTiO_3$ are electrical insulators, but, grown on top of each other under the right conditions, they form a highly conducting layer at their interface (see image). This is just one of many cases where new functionality arises at oxide interfaces. A more detailed summary of these and other emergent phenomena is provided in the Review by Yoshinori Tokura and colleagues on page 103 of this issue[1].

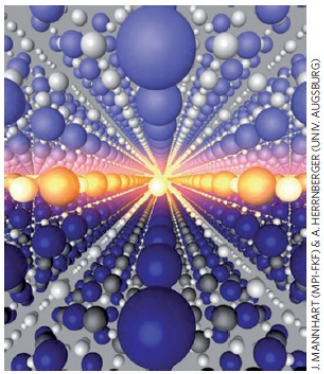

J. MANNHART (MPI-FKF) & A. HERRNBERGER (UNIV. AUGSBURG)

A highly conducting layer forms at the interface between thin films of the insulators $LaAlO_3$ and $SrTiO_3$.

For a quantitative measure of just how much progress in this field comes from developments in crystal-growth technologies, ZnO thin-films provide a good case study. The achievable speed at which electrons move through the thin film, crucially dependent on sample quality, has increased by more than a factor of 1,000 within only three years — enabling even observation of the fractional quantum Hall effect.

Yet, despite all these promises, significant obstacles to a systematic understanding of oxide interfaces remain. As Jak Chakhalian and colleagues argue[2] in their Commentary on page 92, one of the reasons is that a theoretical description of these complex materials and their electronic interactions continues to pose challenges, which at this stage prevents the possibility of designing oxide interfaces with the same ease as for semiconductor interfaces. Furthermore, sample growth continues to face its own obstacles. For example, even though samples grown with different crystallographic orientations can lead to new properties, such growth can prove difficult owing to unfavourable energetics.

Researchers in the field therefore can't be complacent. Many of the applications touted in the past haven't materialized yet. Often the properties that make the oxides so interesting are difficult to realize, particularly at room temperature, or are too weak to be of practical use. Moreoever, some of these compounds contain expensive, rare elements that prohibit broader commercialization. At the fundamental level, some promising phenomena, such as topological insulating behaviour, have not yet been realized in oxides despite considerable efforts.

Nevertheless, progress has been made even under difficult circumstances. Oxide thin-films such as $LaAlO_3$ and $SrTiO_3$ have already been grown on silicon substrates, where avoiding the growth of undesired SiO_2 is a considerable challenge. Although the full potential of emergent phenomena has not yet been realized for oxides grown on silicon, the marriage between conventional semiconductors and oxides clearly promises to combine semiconductor electronics with correlated electron systems.

It is clear that the advances made so far certainly warrant further research and strong funding for the field. Oxide thin-films have come a remarkably long way, and we are now beginning to understand how to design and control emergent phenomena in these materials systems. To appreciate just how far research in oxides has come and how exciting the prospects are for future research, *Nature Materials*, along with the Jülich-Aachen Research Alliance, is organizing a conference in June 2012 on ‘Frontiers in Electronic Materials: Correlation Effects and Memristive Phenomena’, where many of these advances will be discussed[3]. The programme will feature some of the most prolific researchers in the field, and will provide plenty of opportunity for discussion. We hope to see you there! ❐

References
1. Hwang, H. Y. *et al. Nature Mater.* **11,** 103–113 (2012).
2. Chakhalian, J., Millis, A. & Rondinelli, J. *Nature Mater.* **11,** 92–94 (2012).
3. http://www.nature.com/natureconferences/fem2012

Grenzflächendominierte Höchstleistungswerkstoffe

Phasen an Korngrenzen

Science Paper Prof. Dr. Christian Liebscher (RC FEMS, ZGH)

Editor's summary

The structure of grain boundaries in alloys can strengthen or embrittle, which makes understanding grain boundary structure important for materials design. Devulapalli *et al*. used high-resolution microscopy to investigate the grain boundary structure of a titanium-iron alloy (see the Perspective by Luo). The authors found that the iron in the grain boundary is accommodated by the formation of cages with fivefold symmetry. This prevents the formation of ordered phases and is reminiscent of quasi-crystals or glass. Simulations were able to reproduce this unexpected structure, which creates a method for engineering grain boundary structure for other alloy compositions. — Brent Grocholski

RESEARCH

METALLURGY

Topological grain boundary segregation transitions

Vivek Devulapalli[1]*, Enze Chen[2], Tobias Brink[1], Timofey Frolov[3]*, Christian H. Liebscher[1,4,5]*

Engineering the structure of grain boundaries (GBs) by solute segregation is a promising strategy to tailor the properties of polycrystalline materials. Solute segregation triggering phase transitions at GBs has been suggested theoretically to offer different pathways to design interfaces, but an understanding of their intrinsic atomistic nature is missing. We combined atomic resolution electron microscopy and atomistic simulations to discover that iron segregation to GBs in titanium stabilizes icosahedral units ("cages") that form robust building blocks of distinct GB phases. Owing to their five-fold symmetry, the iron cages cluster and assemble into hierarchical GB phases characterized by a different number and arrangement of the constituent icosahedral units. Our advanced GB structure prediction algorithms and atomistic simulations validate the stability of these observed phases and the high excess of iron at the GB that is accommodated by the phase transitions.

Grenzflächendominierte Höchstleistungswerkstoffe

Phasen an Korngrenzen

RUB

of *Vps34* worsens the disease phenotype (*4*). This may relate to the multiple roles of Vps34, particularly its involvement in the initiation of autophagy, given that zebrafish and mouse models of XLMTM are sensitive to dysregulation of autophagy (*10*, *11*). Because menadione sodium bisulfite does not inhibit autophagy, it could be effective without deleterious effects. However, additional preclinical work is needed to assess the benefit of Vps34 inhibition, either alone or in combination with other small-molecule therapies that have shown efficacy in the XLMTM mouse model (*12*). There is also the emerging challenge of the underlying liver disease in XLMTM. It is intriguing to consider whether menadione sodium bisulfite may improve—or, instead, potentially worsen—XLMTM liver disease.

Vps34 is the primary generator of PI(3)P, a low-abundance membrane-bound phospholipid that serves as a signaling molecule to regulate membrane trafficking. Vps34 attracts proteins with PI(3)P-binding motifs, which in turn are involved with dynamic membrane remodeling and initiation of vesicle transport. The identification of menadione sodium bisulfite as an inhibitor of Vps34 by Swamynathan *et al.* is notable in that it selectively acts on the endosomal fraction of Vps34 but leaves autophagy undisturbed. Also, they uncover that a redox checkpoint is crucial for Vps34-dependent maturation of the endosome. The authors coin the term "triaptosis" to describe this new form of cell death promoted by redox-dependent depletion of endosomal PI(3)P (see the figure). Uncovering the function of triaptosis in cellular homeostasis and tissue biology will require further exploration. ■

REFERENCES AND NOTES

1. E. A. Klein *et al.*, *JAMA* **306**, 1549 (2011).
2. M. M. Swamynathan *et al.*, *Science* **386**, eadk9167 (2024).
3. M. W. Lawlor, J. J. Dowling, *Neuromuscul. Disord.* **31**, 1004 (2021).
4. N. Sabha *et al.*, *J. Clin. Invest.* **126**, 3613 (2016).
5. C. Kutchukian *et al.*, *Proc. Natl. Acad. Sci. U.S.A.* **113**, 14432 (2016).
6. H. J. Forman, H. Zhang, *Nat. Rev. Drug Discov.* **20**, 689 (2021).
7. H. Sies, R. J. Mailloux, U. Jakob, *Nat. Rev. Mol. Cell Biol.* **25**, 701 (2024).
8. M. J. Iqbal *et al.*, *Cell Commun. Signal.* **22**, 7 (2024).
9. F. Pouremamali, A. Pouremamali, M. Dadashpour, N. Soozangar, F. Jeddi, *Cell Commun. Signal.* **20**, 100 (2022).
10. J. J. Dowling, S. E. Low, A. S. Busta, E. L. Feldman, *Hum. Mol. Genet.* **19**, 2668 (2010).
11. H. Tasfaout, B. S. Cowling, J. Laporte, *J. Neuromuscul. Dis.* **5**, 387 (2018).
12. P. B. Shieh *et al.*, *Lancet Neurol.* **22**, 1125 (2023).

ACKNOWLEDGMENTS

E.P. and J.J.D. acknowledge support through grants from the Canadian Institutes of Health Research and the US National Institutes of Health. J.J.D. has received funding related to XLMTM gene therapy from Astellas Pharma, Inc.

10.1126/science.adt2538

IMAGES (FROM TOP): YU ET AL., T. HU, ET AL., *NAT. COMMUN.* 9, 2754 (2018). DOI: 10.1038/S41467-018-05117-7; DEVULAPALLI ET AL.

MATERIALS SCIENCE

Distinct interfacial structures between grains

Adsorption transitions at grain boundaries in a polycrystal result in structures that are forbidden in bulk crystals

By Jian Luo[1,2]

Most solid materials are composed of small crystals (called grains) that comprise the same constituents but with different orientations within the polycrystal. Grain boundaries (GBs) form between two grains and control various properties. Adsorption of impurities or alloying elements at these interfaces can substantially alter a material's properties, such as strength and toughness. GB adsorption, also called segregation, can transform the structures and properties of an interface. Despite the importance of GB transitions in engineering materials, they are not well understood because of the challenges in characterizing structural transformations at the atomic level. On page 420 of this issue, Devulapalli *et al.* (*1*) report a detailed description of a GB transition in titanium that is induced by iron adsorption. It allows the formation of icosahedral structures that are forbidden in bulk crystals. The observation suggests new types of distinct interfacial structures and properties.

In 1968, first-order GB adsorption transitions were proposed (*2*) that were based on an extension of the Fowler-Guggenheim model for surface adsorption (*3*). This model can be derived by treating a GB as a regular solution (a solution model considering pair-wise interactions) (*4*). A first-order adsorption transition occurs when the effective regular solution parameter, Ω_{GB} (a measure of mixing enthalpy that is related to adsorbate-adsorbate interaction at the GB), exceeds $2RT$ (R is the gas constant and T is the absolute temperature) (*4*). This corresponds to a discontinuity in the slope of the GB energy versus bulk composition curve and a finite jump in the adsorption amount at the boundary, which was shown in a lattice model for nickel-bismuth (*5*). In addition, a GB transition can result in disinct interfacial structures such as an ordered bilayer in a nickel-bismuth alloy (*6*, *7*) or two types of disordered interfaces in a nickel-sulfur alloy (*8*).

In a broader context, GBs can be treated as two-dimensional (2D) interfacial phases, which are also called complexions to differentiate them from thin layers of bulk phases sandwiched between two grains (*4*). Such an interfacial phase is thermodynamically 2D because the structural and compositional profiles along the direction perpendicular to the GB are fixed (there is no degree of freedom in the third dimension) at the equilibrium. Such a 2D interfacial phase can have distinct structures that are neither observed nor stable in bulk phases. Consequently, they may possess properties unattainable by bulk materials.

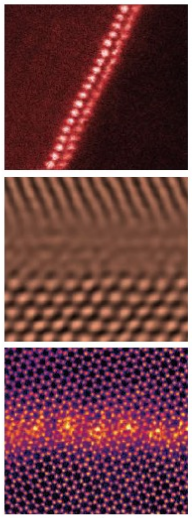

Scanning transmission electron microscopy images show three types of two-dimensional interfacial phases: nickel-bismuth (top), nickel-sulfur (middle), and titanium-iron (bottom).

Devulapalli *et al.* report adsorption-induced transitions at a (nearly) symmetric tilt GB in a titanium-iron alloy by combining scanning transmission electron microscopy and atomistic simulations. They observed a GB structure with three subunits (A, B, and C) in an undoped titanium thin film. The authors systematically varied the amount of iron in titanium to study its role in the atomic arrangement at these GBs. Upon iron adsorption (segregation from the bulk material), Devulapalli *et al.* observed a transition from the ABC structure in polycrystalline titanium-iron alloy to one bearing icosahedral cages with fivefold symmetry. Such structural units are forbidden in a bulk crystal because they violate translational symmetry but can exist in glasses or quasicrystals. As the amount of iron doped into the titanium increased, the GB transited into a series of structures. These observations confirm a new type of 2D interfacial phases that have quasicrystal-like structures but are different from thin layers of quasicrystals. Devulapalli *et al.* described these transformations as topological GB segregation transitions, which are unrelated to the topological phases in condensed matter physics. Instead, these transformations indicate interfacial transitions that change the topological structure of the local bonding environment.

The results of Devulapalli *et al.* make an important contribution to the previously known cases of 2D interfacial phases at GBs. Atomic-level observations have shown periodically ordered bilayer adsorption of bismuth at GBs in a nickel-bismuth alloy (*6*). An adsorbed bismuth layer on each GB facet underwent reconstruction, which changed the 2D translational symmetry of each grain surface (*7*). For example, bismuth atoms adsorbed on (100) GB facets went through a $c(2\times2)$ reconstruction, in which the adsorbed atoms form a centered 2×2 supercell that was double the size of the underlying nickel grain surface (*7*). Another type of interfacial structures are amorphous-like intergranular films, which differ from their crystalline or amorphous bulk counterpart. These structures are much more disordered but still exhibit partial structural order, as shown in the 2D interfacial phase that is formed anisotopically on the (100) GB facets in a nickel-sulfur alloy (*8*). Similar liquid-like complexions can be formed by segregation-driven GB premelting (structural disordering at an interface below the bulk melting temperature) in binary alloys such as tungsten-nickel (*9*).

Based on the observations made to date, three classes of adsorption-based 2D interfacial phases have now been identified (see the figure). A 2D crystal-like GB contains highly ordered adsorbates, which change 2D translational symmetries of both grain surfaces. An amorphous-like boundary has a disordered interfacial structure with partial order within. A quasicrystal-like GB, revealed by Devulapalli *et al.*, can form from a new type of adsorption-driven 2D structural transition at an interface. Moreover, GB structural transitions can also take place without adsorption. A transition between domino and pearl motifs has been observed at a boundary in elemental copper (*10*). Thus, it would be interesting to also investigate GB transitions that occur with changes of other conditions such as temperature and pressure.

Further studies should investigate whether 2D interfacial phases based on icosahedral cages form broadly at other types of GBs and in different materials and the resulting properties. In general, studies of GB phase-like transitions have helped resolve decades-old mysteries in materials science, such as the atomic-level origins of liquid-metal embrittlement (*6*, *7*), activated sintering (*9*), and abnormal grain growth (*4*, *11*). For example, ordered (*6*, *7*) and disordered (*8*) 2D interfacial phases have been shown to cause embrittlement in nickel-bismuth and nickel-sulfur, respectively, which are two classical GB embrittlement systems in physical metallurgy. Analogous to using 2D surface phases to improve the functional properties of battery materials (*12*), the 2D interfacial phases at GBs can potentially be engineered to achieve exotic properties, such as superior ionic conductivity.

Given that bulk phase diagrams are arguably the most useful tool in materials science, computing GB phase diagrams can be equally important (*13*). In addition to the common thermodynamic potentials such as temperature, chemical potentials, and pressure, GB transitions can also be driven electrochemically by applying electric fields to alter the microstructural evolution of an oxide (*14*). Because adsorption at the boundary results in more diverse 2D interfacial phases in alloys with multiple elements than in unary (one-component) systems, it would be fascinating to further investigate the GB transitions in multicomponent and high-entropy alloys, including the emerging concept of high-entropy GBs (*15*). ■

[1]Aiiso Yufeng Li Family Department of Chemical and Nano Engineering, University of California San Diego, La Jolla, CA, USA. [2]Program in Materials Science and Engineering, University of California San Diego, La Jolla, CA, USA. Email: jluo@alum.mit.edu

REFERENCES AND NOTES

1. V. Devulapalli, E. Chen, T. Brink, T. Frolov, C. H. Liebscher, *Science* **386**, 420 (2024).
2. E. W. Hart, *Scr. Metall.* **2**, 179 (1968).
3. R. H. Fowler, E. A. Guggenheim, *Statistical Thermodynamics* (Cambridge Univ. Press, 1939).
4. P. R. Cantwell *et al.*, *Acta Mater.* **62**, 1 (2014).
5. N. Zhou, Z. Yu, Y. Zhang, M. P. Harmer, J. Luo, *Scr. Mater.* **130**, 165 (2017).
6. J. Luo, H. Cheng, K. M. Asl, C. J. Kiely, M. P. Harmer, *Science* **333**, 1730 (2011).
7. Z. Yu *et al.*, *Science* **358**, 97 (2017).
8. T. Hu, S. Yang, N. Zhou, Y. Zhang, J. Luo, *Nat. Commun.* **9**, 2764 (2018).
9. J. Luo, V. Gupta, D. Yoon, H. Meyer III, *Appl. Phys. Lett.* **87**, 231902 (2005).
10. T. Meiners, T. Frolov, R. E. Rudd, G. Dehm, C. H. Liebscher, *Nature* **579**, 375 (2020).
11. S. J. Dillon, M. Tang, W. C. Carter, M. P. Harmer, *Acta Mater.* **55**, 6208 (2007).
12. J. Luo, *Energy Storage Mater.* **21**, 50 (2019).
13. J. Luo, *Interdiscip. Mater.* **2**, 137 (2023).
14. Q. Yan, C. Hu, J. Luo, *Mater. Today* **73**, 66 (2024).
15. J. Luo, N. Zhou, *Commun. Mater.* **4**, 7 (2023).

ACKNOWLEDGMENTS

The author acknowledges support from the National Science Foundation (DMR-2011967), US Army Research Office (W911NF2210071), and US Air Force Office of Scientific Research (FA9550-22-1-0413).

10.1126/science.ads5954

Downloaded from https://www.science.org at University College London on January 01, 2025

Adsorption-induced interfacial transitions

Adsorption of impurities or alloying elements can result in various types of structural transitions at grain boundaries. Quasicrystal-like boundaries in titanium-iron alloy form fivefold symmetry units, contributing to the previously known cases of two-dimensional (2D) interfacial phases.

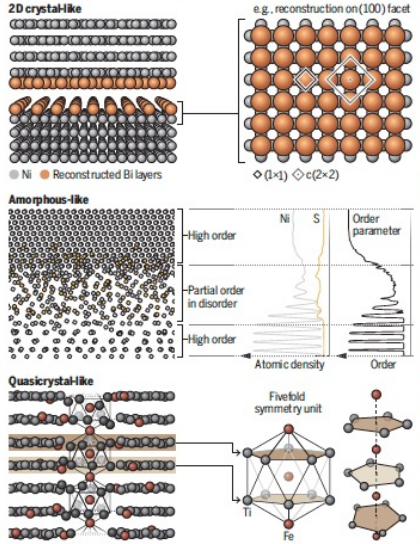

Grenzflächendominierte Höchstleistungswerkstoffe

Phasen an Korngrenzen

Science Paper Chr. Liebscher

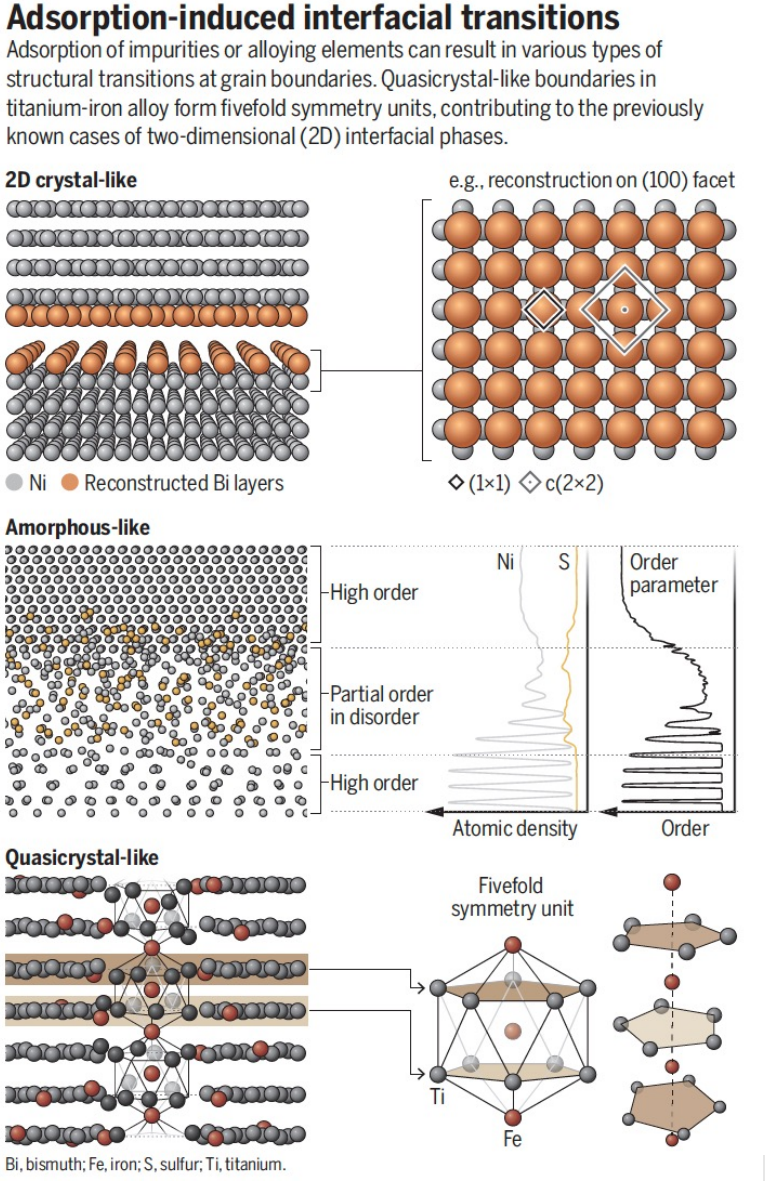

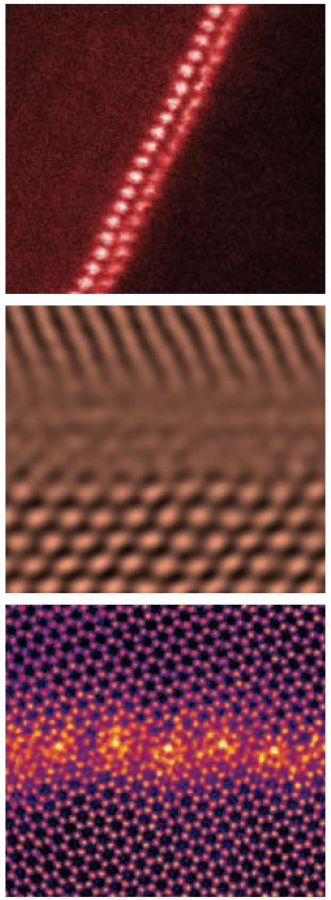

Scanning transmission electron microscopy images show three types of two-dimensional interfacial phases: nickel-bismuth (top), nickel-sulfur (middle), and titanium-iron (bottom).

Grenzflächen zwischen Schicht und Substrat

mechanisch

Monoschicht/Monoschicht

Verbindung

Diffusion

Pseudodiffusion

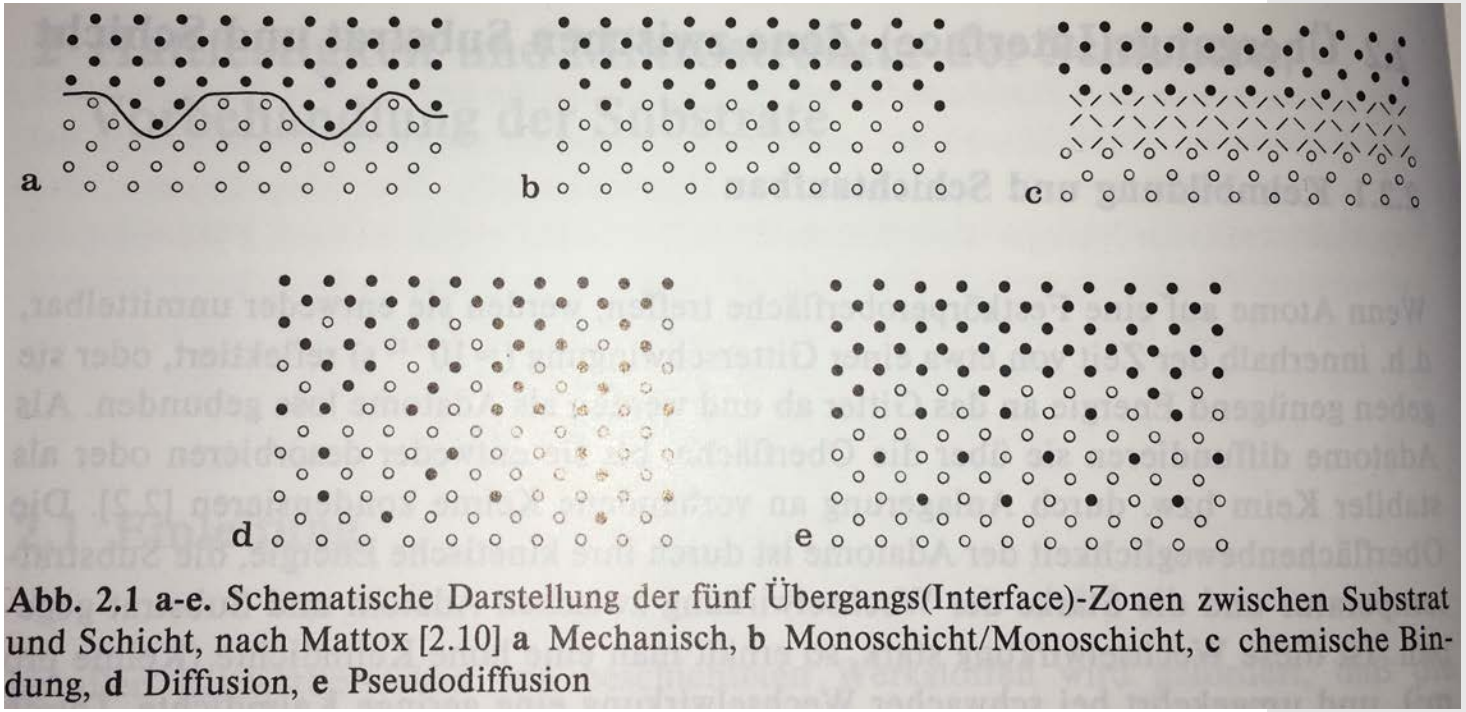

Abb. 2.1 a-e. Schematische Darstellung der fünf Übergangs(Interface)-Zonen zwischen Substrat und Schicht, nach Mattox [2.10] **a** Mechanisch, **b** Monoschicht/Monoschicht, **c** chemische Bindung, **d** Diffusion, **e** Pseudodiffusion

material systems. Results on bulk materials[1] suggest a picture as shown in Fig. 5 for three different possibilities. Coherent or partially coherent interfaces with a "boundary phase" and interaction free interfaces. Metallic hard materials are able to form coherent or semicoherent interfaces with metals or other metallic hard materials. As a result low-energy interfaces with optimum adherence can be obtained (e.g., TiC/TiB_2).[2] Interfaces between metallic and ionic hard materials often show intermediate regions of variable composition (e.g., TiC/Al_2O_3).[3] The behavior is strongly dependent on the constitution and structure of this boundary phase. Interfaces between covalent hard material seems to be quasi-interaction-free with the consequence of bad adherence of the phases (e.g., B_4C/B_4C or B_4C/Al_2O_3).

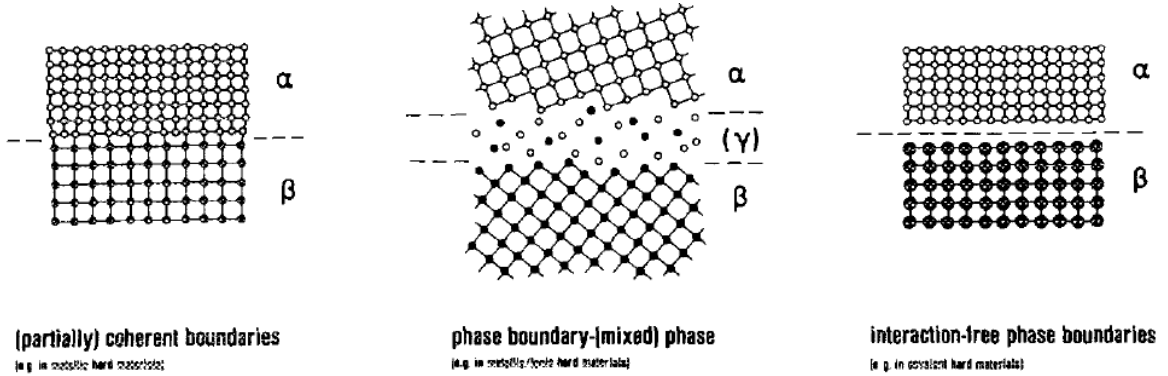

FIG. 5. Different natures of interfaces in multiphase coatings or at the substrate/layer interface.

J. Vac. Sci. Technol. A, Vol. 4, No. 6, Nov/Dec 1986

Advanced Materials Processing and Microfabrication

Grenzflächendominierte Werkstoffe: Nanoskalige Viellagenschichten

H. Holleck, V. Schier/Surface and Coatings Technology 76–77 (1995) 328–336

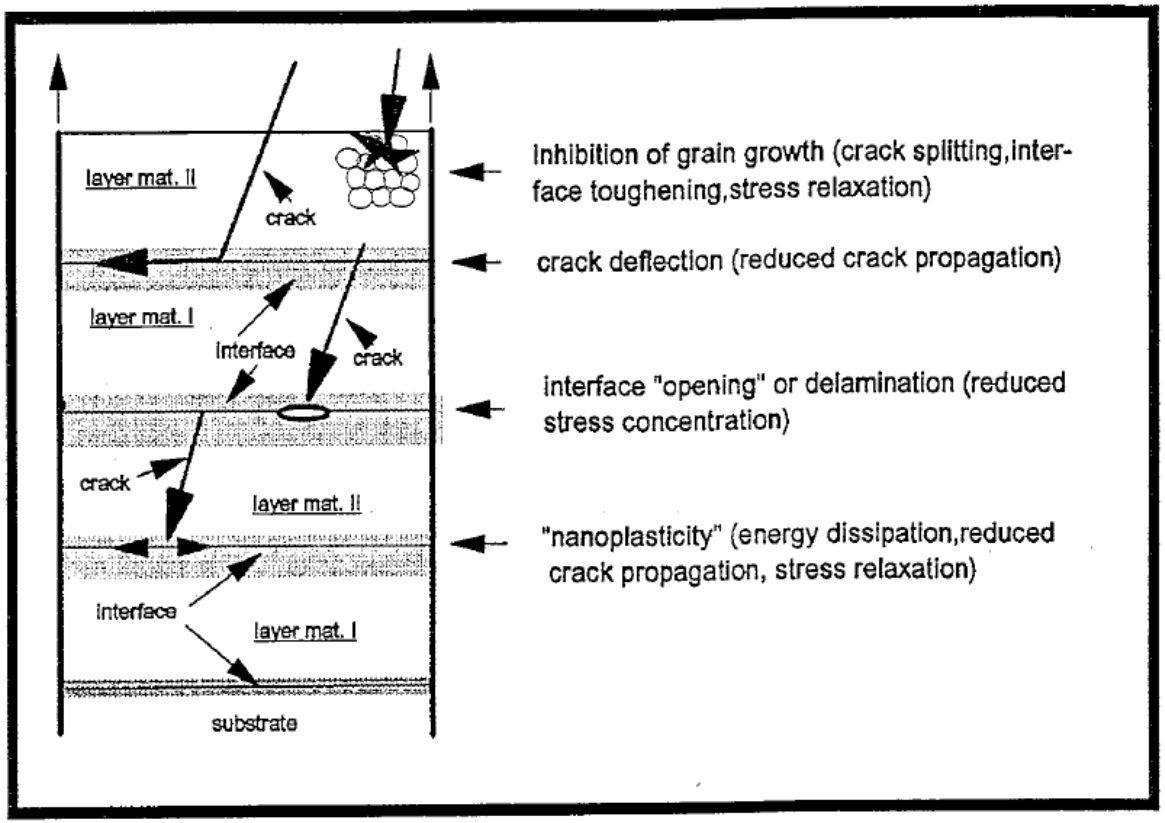

Fig. 4. Toughening mechanism in ceramic multilayer materials (schematic representation).

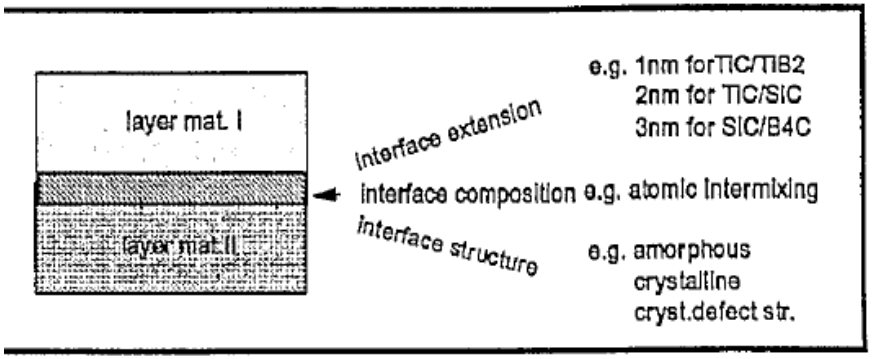

ig. 3. Constitution characteristics of interfaces in multilayer coatings.

Grenzflächendominierte Werkstoffe: Nanoskalige Viellagenschichten: CrN/AlN

New J. Phys. 17 (2015)093004 doi:10.1088/1367-2630/17/9/093004

New Journal of Physics
The open access journal at the forefront of physics

Published in partnership with: Deutsche Physikalische Gesellschaft and the Institute of Physics

PAPER

Synergy of atom-probe structural data and quantum-mechanical calculations in a theory-guided design of extreme-stiffness superlattices containing metastable phases

M Friák[1,2], D Tytko[1], D Holec[3], P-P Choi[1], P Eisenlohr[1,4], D Raabe[1] and J Neugebauer[1]

[1] Max-Planck-Institut für Eisenforschung GmbH, D-40237 Düsseldorf, Germany
[2] Institute of Physics of Materials, Academy of Sciences of the Czech Republic, v. v. i., 61662 Brno, Czech Republic
[3] Montanuniversität Leoben, A-8700 Leoben, Austria
[4] Michigan State University, East Lansing, MI 48824, USA

E-mail: friak@ipm.cz

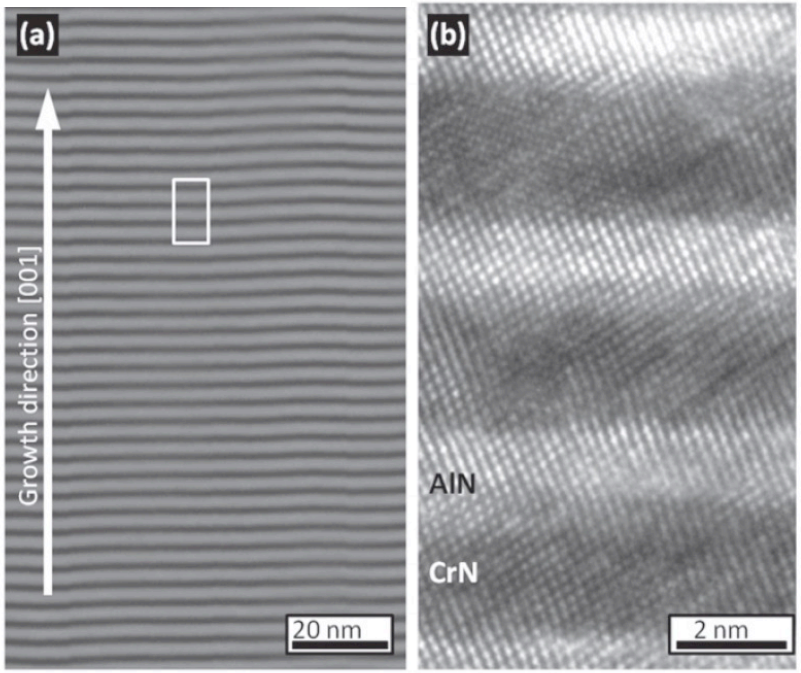

Figure 2. (a) Scanning transmission electron microscopy high angle annular dark field (STEM HAADF) image of the as-deposited AlN/CrN superlattice showing chemically sharp layers (bright and dark contrast corresponds to CrN and AlN, respectively); (b) high-resolution transmission electron microscopy (HR-TEM) image of the region marked by the rectangle in (a) showing coherent multilayers. The multilayers are stacked along the [001] direction.

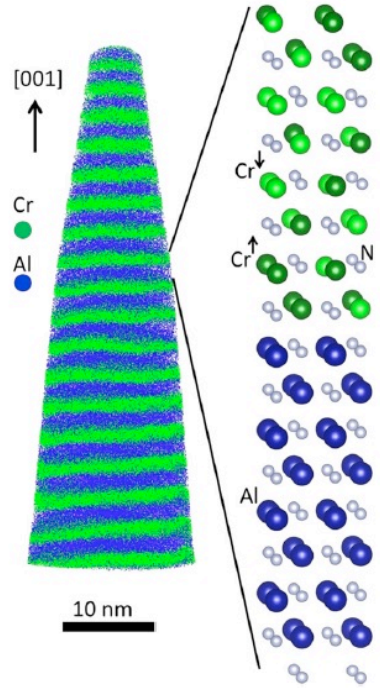

Figure 3. Spatial distribution of Cr and Al in an AlN/CrN superlattice measured by atom probe tomography (left, see also [25]) and the computational model derived from these data (right).

Grenzflächendominierte Werkstoffe:
Nanoskalige Viellagenschichten: TiNi/W

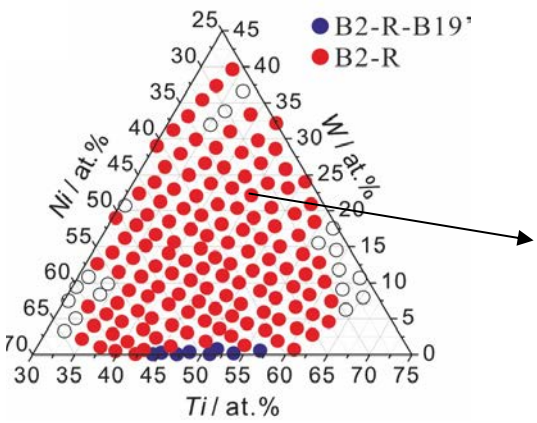

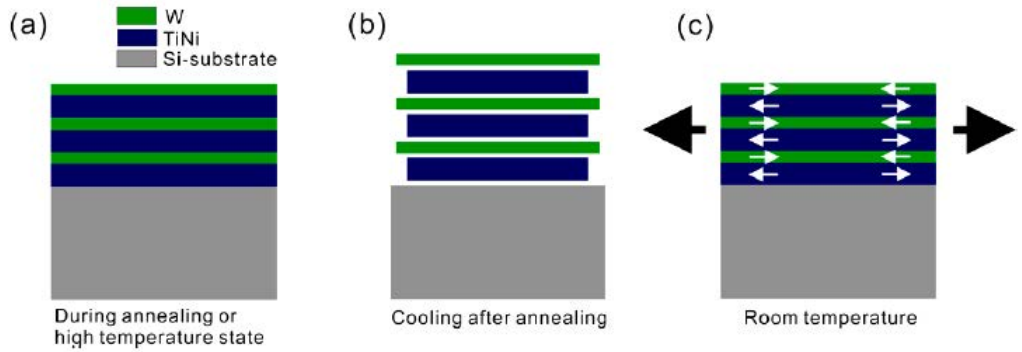

HAADF-STEM image

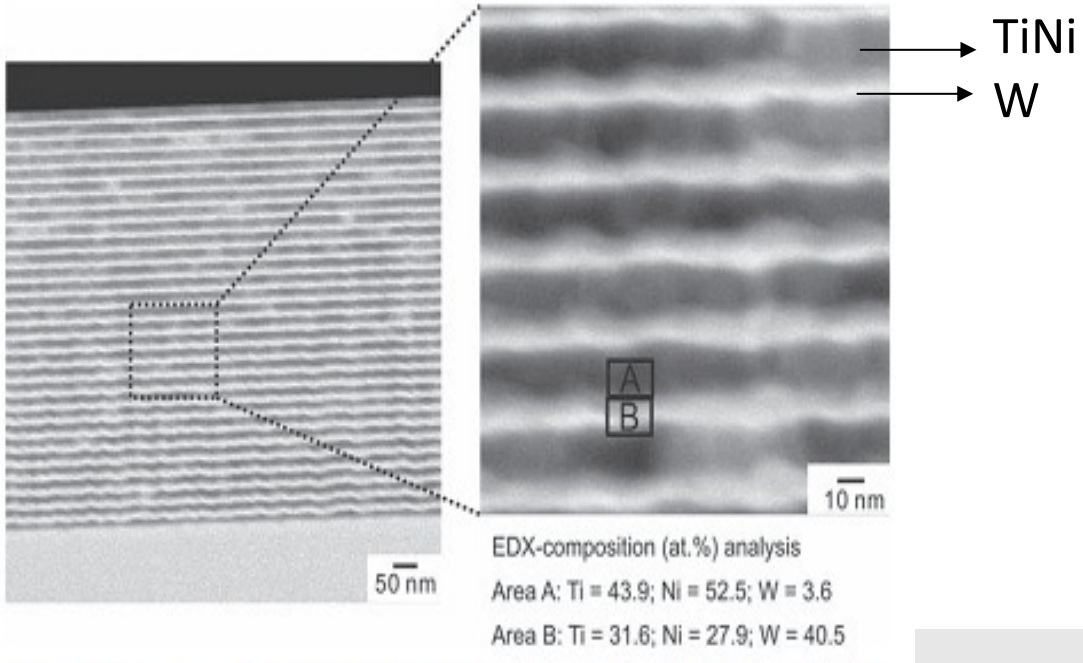

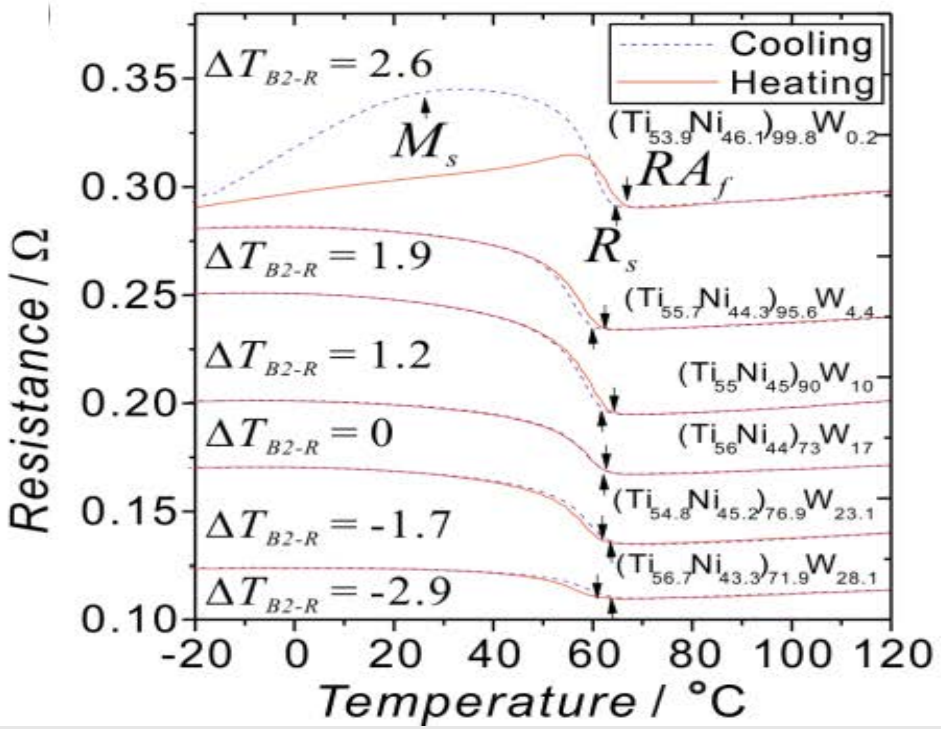

P. Buenconsejo, A. Ludwig, et al., Adv. Funct. Mat. **2011**, 21, 113-118

Nanoscale shape memory materials: Downscaling Ni-Ti-X (film thickness)

- shape change of ρ(T) curves for thicknesses < 150 nm

$Ti_{51}Ni_{38}Cu_{11}$
continuous thin films

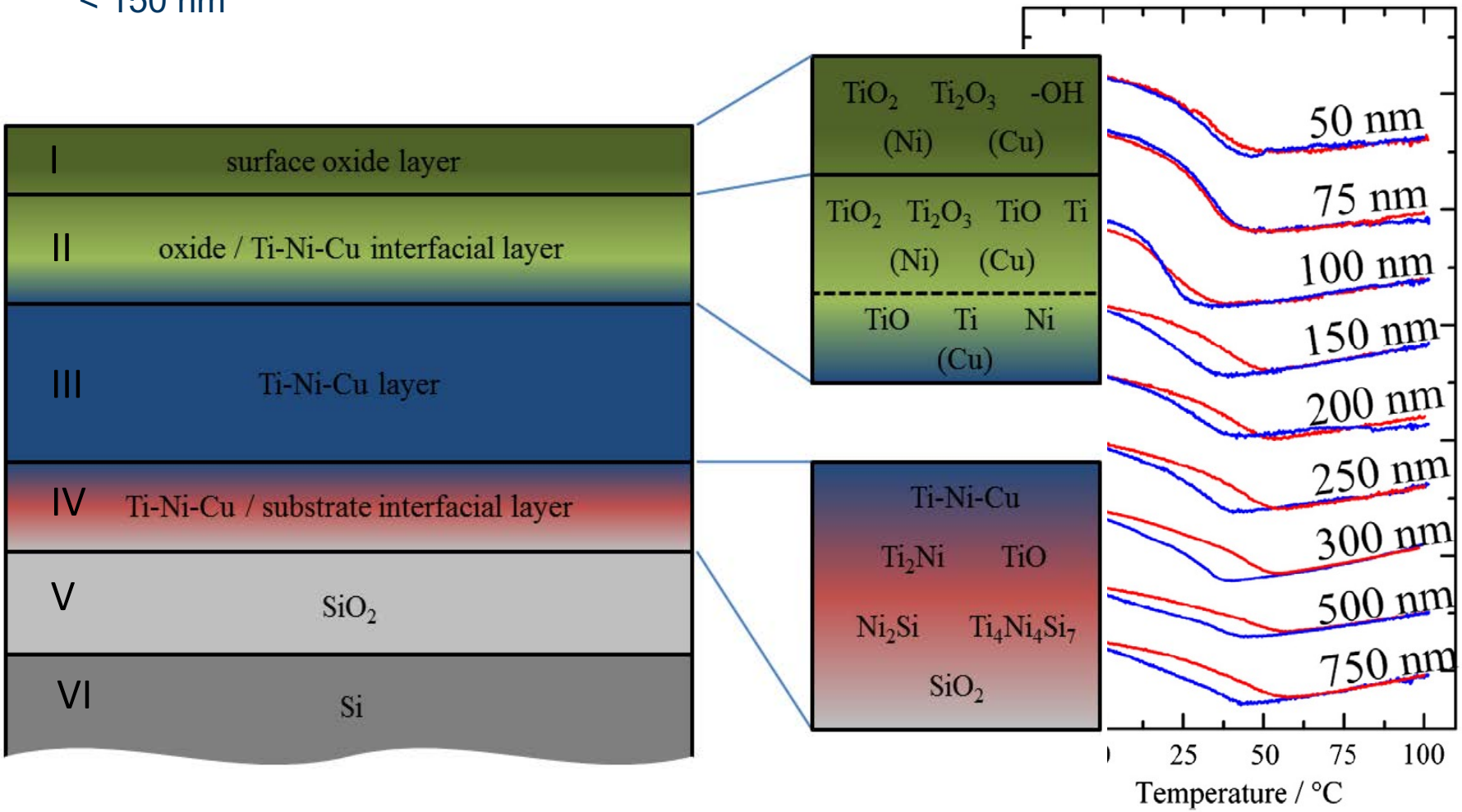

D.König, P.J.S. Buenconsejo, D. Grochla, S. Hamann, J. Pfetzing-Micklich, A. Ludwig, *Acta Mater.*, **60**, 306-313, (2012).

Advanced Materials Processing and Microfabrication

Grenzflächendominierte Werkstoffe: Durch Grenzfläche erzeugte verzerrte Phase

FeCo: kubisch

tetragonal verzerrtes FeCo zeigt
nach theoretischen Berechnungen
stark veränderte magnetische Eigenschaften

VOLUME 93, NUMBER 2 PHYSICAL REVIEW LETTERS week ending 9 JULY 2004

Giant Magnetic Anisotropy in Tetragonal FeCo Alloys

Till Burkert,[1,*] Lars Nordström,[1] Olle Eriksson,[1] and Olle Heinonen[2]
[1]*Department of Physics, Uppsala Universitet, Box 530, 751 21 Uppsala, Sweden*
[2]*Seagate Technology, 7801 Computer Avenue S., Bloomington, Minnesota 55435, USA*
(Received 15 January 2004; published 9 July 2004)

In order to further increase the recording density in hard disk drives, new media materials are required. Two essential parameters of future recording media are a large uniaxial magnetic anisotropy energy (MAE) K_u and a large saturation magnetization M_s. Based on first-principles theory, we predict that very specific structural distortions of FeCo alloys possess these desired properties. The discovered alloy has a saturation magnetization that is about 50% larger than that of FePt—a compound that has received considerable attention lately—with a uniaxial MAE that can easily be tailored reaching a maximum value that is 50% larger than that of FePt.

DOI: 10.1103/PhysRevLett.93.027203 PACS numbers: 75.30.Gw, 75.50.Bb, 75.50.Ss

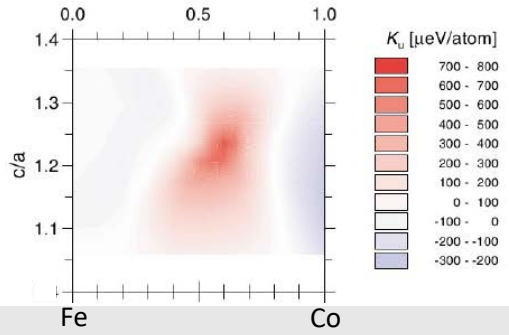

Fe-Co
$c/a > 1$

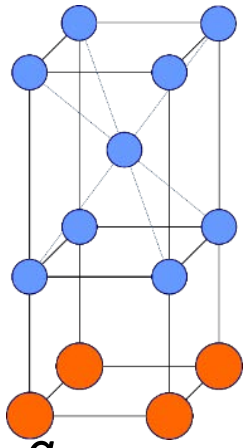

$a_{Substrat}$

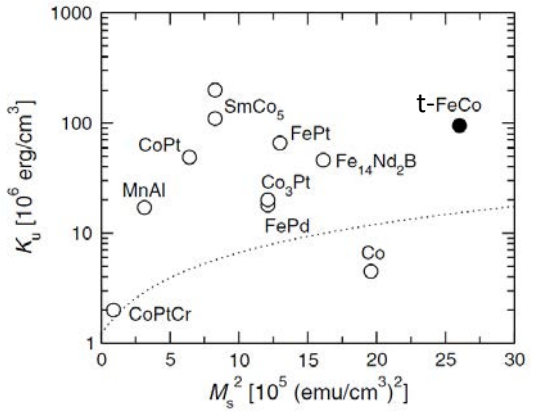

FIG. 2. Stability contour plot of high K_u materials, drawn after Fig. 1 of Ref. [3] (open circles). The present result for the tetragonal FeCo alloy with the maximum uniaxial MAE is included for comparison (closed circle). The dotted line is the 40 Gbits/in^2 stability boundary according to Charap *et al.* [23], assuming a write field of 5100 Oe and 12 nm grains.

Lattice constant library, i.e. a materials library of epitaxial buffer layers with tailored lattice parameters needed for the deposition of distorted Fe-Co-X-Y

Development of the appropriate buffer layer system for epitaxial growth of FeCo: Au_xCu_{1-x} on Si and MgO tuning of in-plane lattice of Au_xCu_{1-x}

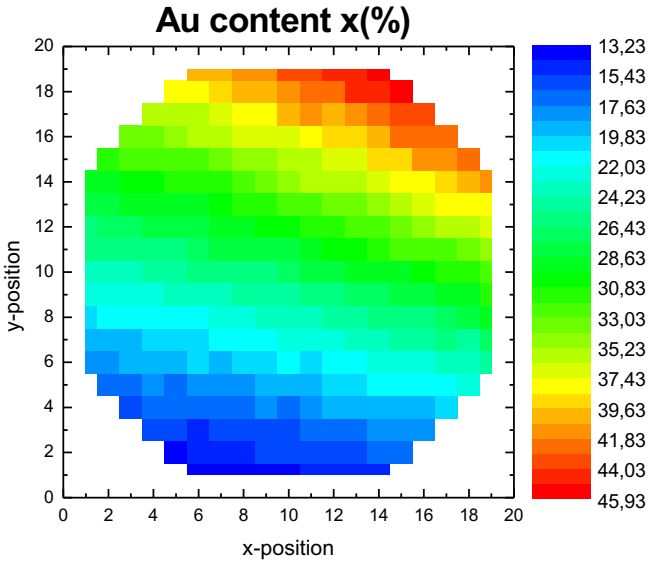

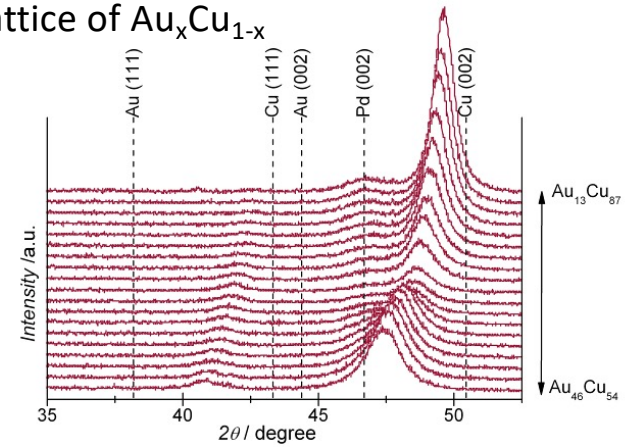

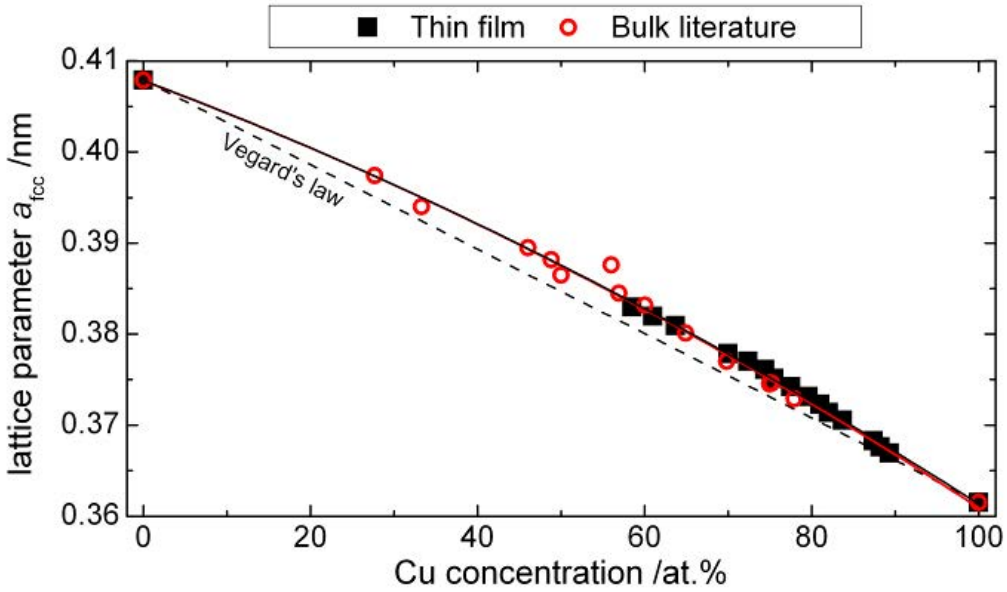

S. Kauffmann-Weiss, S. Hamann, L. Reichel, A. Siegel, V. Alexandrakis, R. Heller, L. Schultz, A. Ludwig, S. Fähler (2014), *The Bain library: A Cu-Au buffer template for a continuous variation of lattice parameters in epitaxial films*, APL Materials 2, 046107

Advanced Materials Processing and Microfabrication

Werkstoffe und Werkstoffsysteme

eine einzelne Schicht im Vergleich zu:
mehrere Schichten im Verbund

Bei der Miniaturisierung treten viele Werkstoffe in engen Kontakt, dadurch Bildung von Grenzflächen

Beispiel:
Dünnschichtbatterie

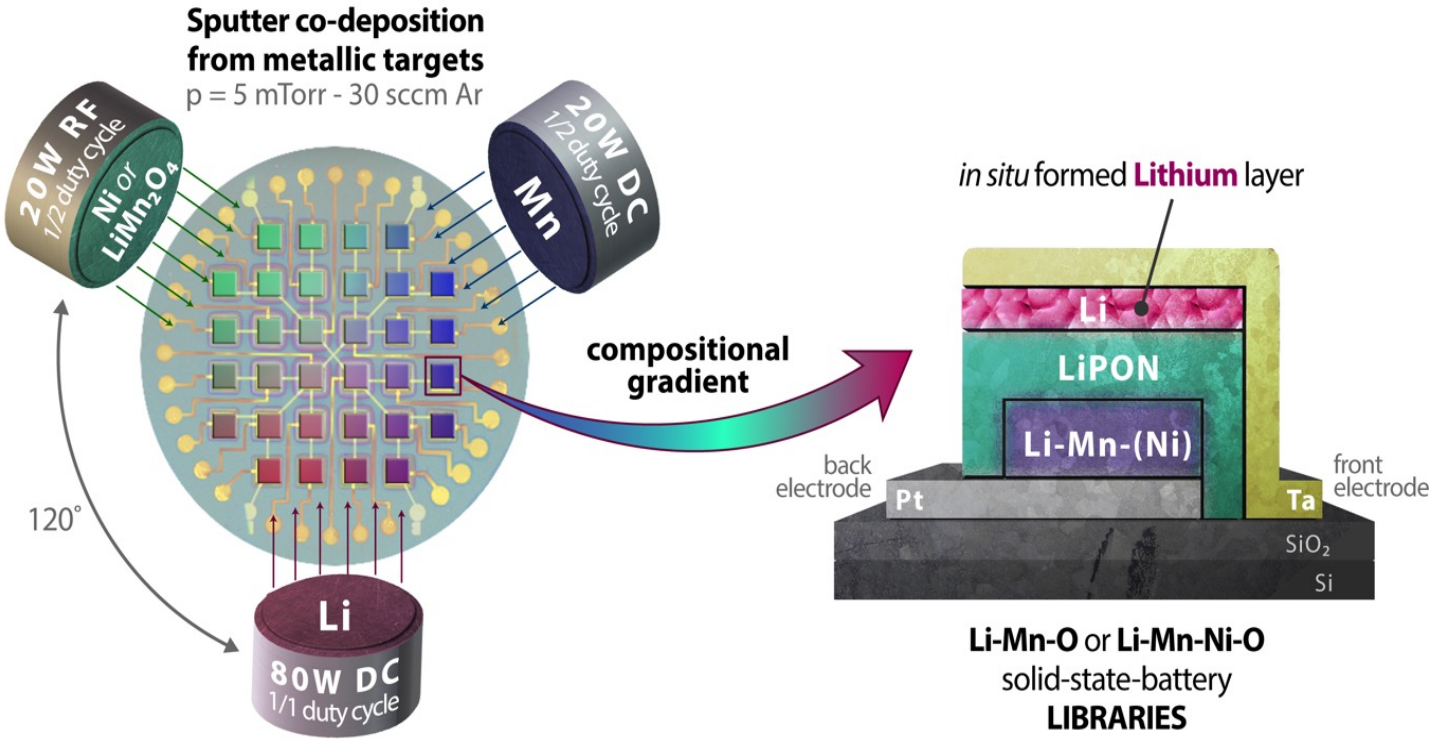

Grenzflächendominierte Werkstoffe

ZGH
Zentrum für Grenzflächendominierte Höchstleistungswerkstoffe

ZGH: Ziele

Ministerium für Innovation, Wissenschaft und Forschung des Landes Nordrhein-Westfalen

RUHR-UNIVERSITÄT BOCHUM

Zentrum für Grenzflächendominierte Höchstleistungswerkstoffe (ZGH)

Antrag Forschungsbau (Neubau) | Förderphase 2013

Materials Research Department

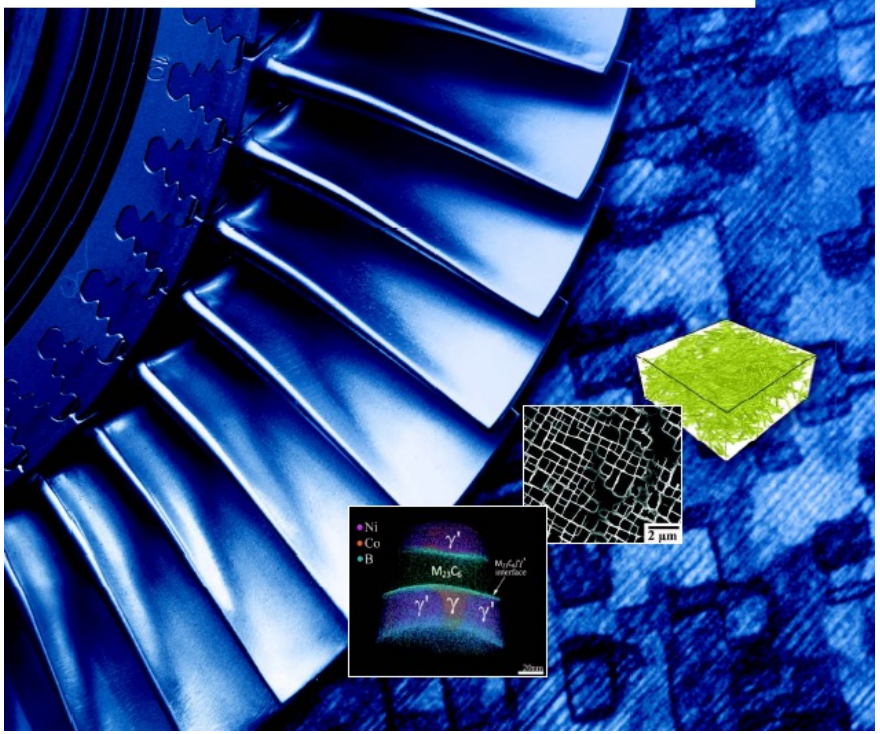

Für einen ressourceneffizienten und nachhaltigen Fortschritt in den Bereichen Mobilität, Energie und Umwelt ist die **Entwicklung neuer Höchstleistungswerkstoffe** für die Industrie und unsere Gesellschaft zwingend erforderlich

Ziele:

- leistungsfähiges und einzigartiges Kompetenzzentrum, das Deutschland im Bereich der grenzflächendominierten Höchstleistungswerkstoffe eine Spitzenstellung verschaffen soll
- gleichzeitiges Aufgreifen grundlegender und angewandter Fragestellungen in einem interdisziplinären Team aus Ingenieur/innen und Naturwissenschaftler/innen mit gemeinsamen Fokus auf Grenzflächen in Höchstleistungs-werkstoffen
- ZGH wird interdisziplinäre Grenzflächenforschung zur Entwicklung von Höchstleistungswerkstoffen als Arbeitsgebiet etablieren
- es ermöglichen, auf gesellschaftliche/technologische Anforderungen schneller und besser mit innovativen Werkstoffen reagieren zu können

Die Einrichtung des ZGH hat größte Bedeutung für die Werkstoffforschung und für angrenzende ingenieur- und naturwissenschaftliche Forschungsbereiche.

ZGH: Neuartige Höchstleistungswerkstoffe

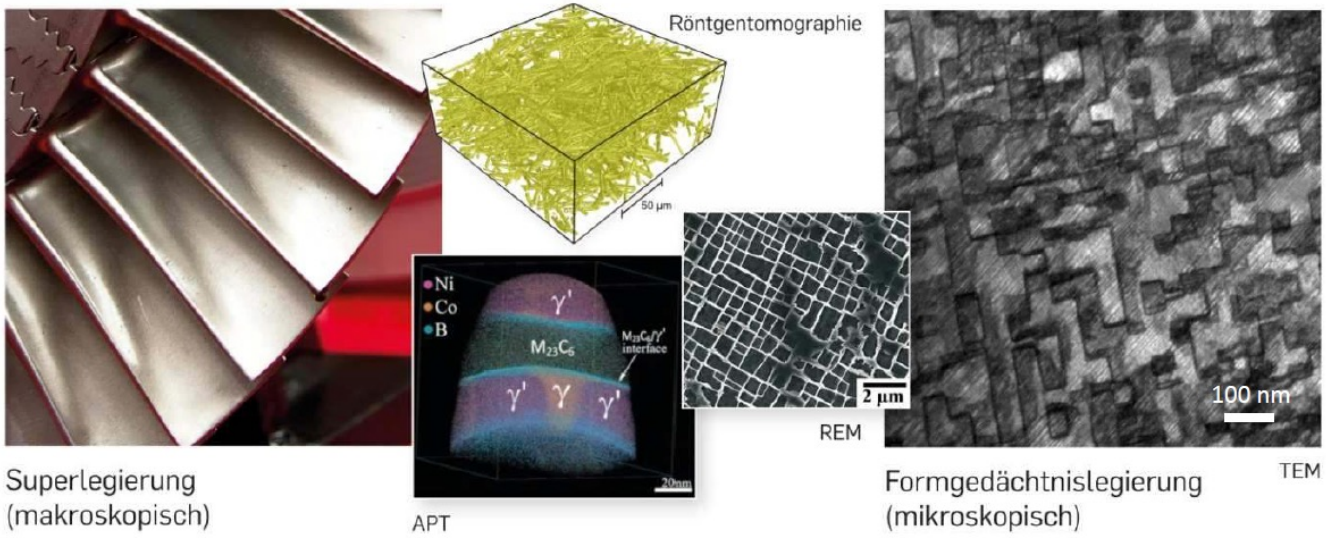

Strukturwerkstoffe Funktionswerkstoffe

Neuartige Werkstoffe
mit bisher ungenutzten
strukturell-funktionell verknüpften
Eigenschaftsprofilen

Höchstleistungswerkstoffe
müssen ihre strukturelle Integrität und Multifunktionalität unter extremen Bedingungen, z.B. in einer Turbine, in automobilen Hybrid- oder Elektroantrieben oder in elektrochemischen Zellen nachhaltig, unter voller Erhaltung der Eigenschaften gewährleisten

ZGH: Werkstoff-Design durch Grenzflächen-Engineering und generische Konzepte

Grenzflächen-Engineering:
basiert auf dem grundlegenden Verständnis der Grenzflächen auf atomarer Ebene und reicht bis zu komplexen Werkstoffen im technischen Einsatz

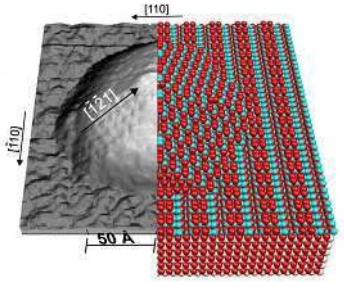

skalenübergreifende dreidimensionale Analyse von Werkstoffgrenzflächen
bis hin zu atomarer Auflösung, führt zum Design neuer Werkstoffe

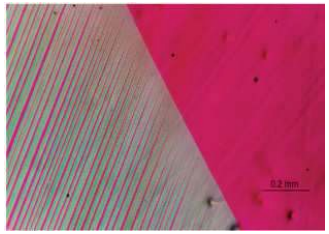

- (Im)Mobilisierung von Grenzflächen
- geometrisch kompatible Phasengrenzflächen
- Funktionalisierung von Oberflächen
- Verschmelzung von Struktur und Funktion
- strukturelle und funktionelle Integrität unter extremen Bedingungen
- *in situ* Sensorik und Selbstheilung
- Kombinationen von Simulation/Experiment
- atomare Analyse/tomographische dreidimensionale Messungen als übergreifende Methoden

ZGH: Core Facilities

Um die atomare Struktur, die Geometrie und die Eigenschaften von Grenzflächen verstehen zu können, müssen diese mit höchstauflösenden Verfahren möglichst dreidimensional analysiert werden

CF I: Höchstauflösende tomographische Werkstoffcharakterisierungsverfahren	a-TEM, Atomsondentomographie, Röntgentomographie
CF II: Oberflächencharakterisierung	Elektronenmikroskopie
CF III: Reinraum zur Herstellung mikrostrukturierter Oberflächen und mikrotechnischer Werkzeuge für die skalenübergreifende Analyse von grenzflächendominierten Werkstoffen	Schichtherstellung, Strukturierung, Photolithographie
CF IV: Computer-Cluster für die Grenzflächensimulation	

ZGH: Drei kohärente Forschungsschwerpunkte

Zur effizienten Umsetzung der generischen Konzepte ist die Forschungsprogrammatik in drei kohärente Forschungsschwerpunkte gegliedert

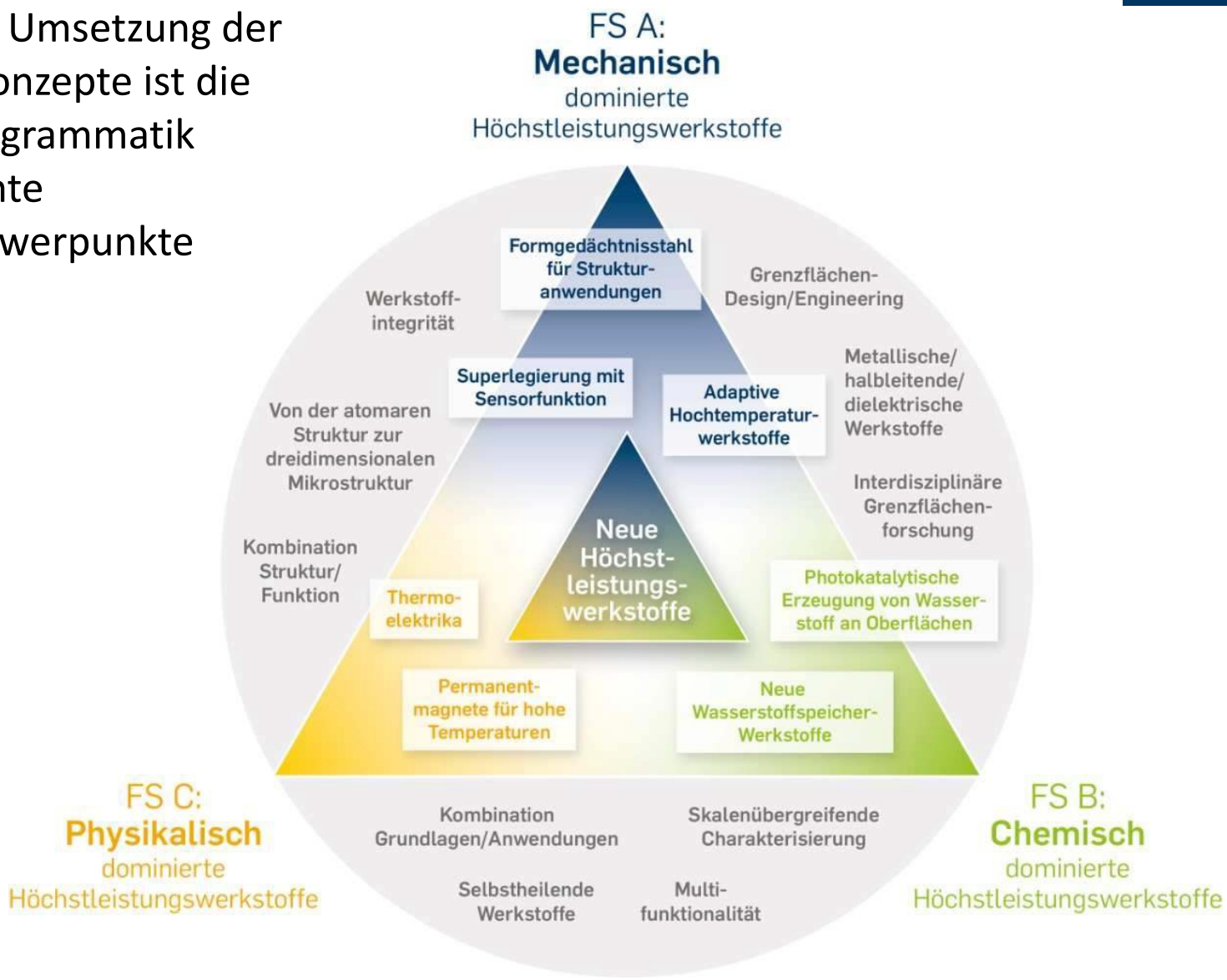

ZGH: Forschungsschwerpunkt A

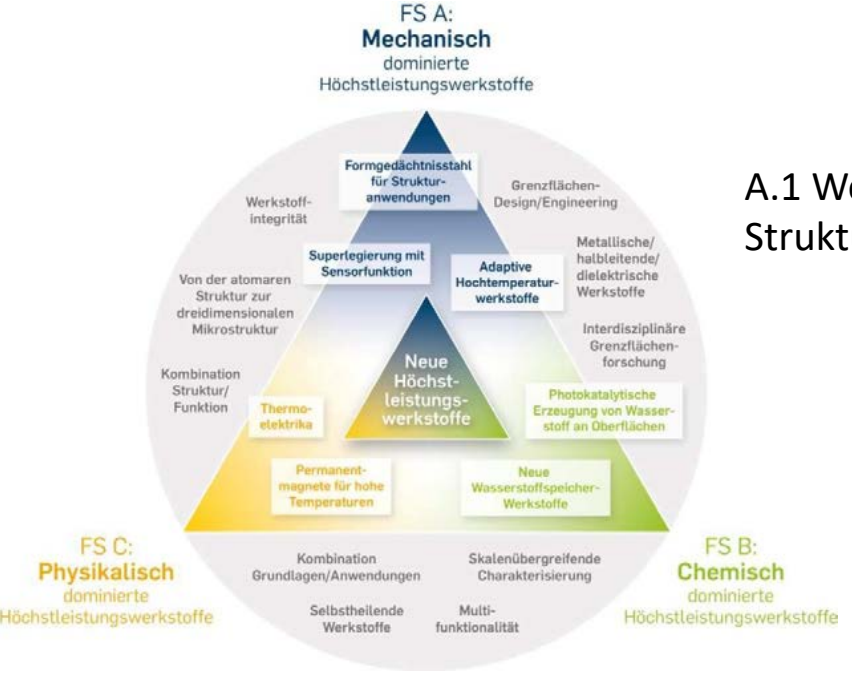

A.1 Weiterentwicklung von Strukturwerkstoffen zu Struktur/Funktionswerkstoffen durch Oberflächenfunktionalisierung

Beispiel: Funktionalisierung von Strukturwerkstoffen durch Integration energiewandelnder Werkstoffe

Strukturwerkstoffe wie Stahl- und Glasflächen in Gebäuden bekommen neben ihren tragenden und schützenden Aufgaben zusätzlich Funktionen für die Energieversorgung des Gebäudes.

Die Verbindung von Struktur und Funktion kann z.B. durch hybride Integration erfolgen, indem ein Strukturwerkstoff mit einer Funktionswerkstoffschicht versehen wird (photoaktive Schicht, z.B. für Selbstreinigung, Solarstrom, Wasserstoffproduktion).

A.2 Stahl mit Formgedächtniseigenschaften/Formgedächtnislegierungen als Strukturwerkstoffe

A.3 Formgedächtnislegierungen (FGL) für hohe und höchste Anwendungstemperaturen

A.4 Höchstleistungswerkstoffe mit Selbstheilungsfunktionalität

ZGH: Forschungsschwerpunkt B, Chemisch dominierte Höchstleistungswerkstoffe

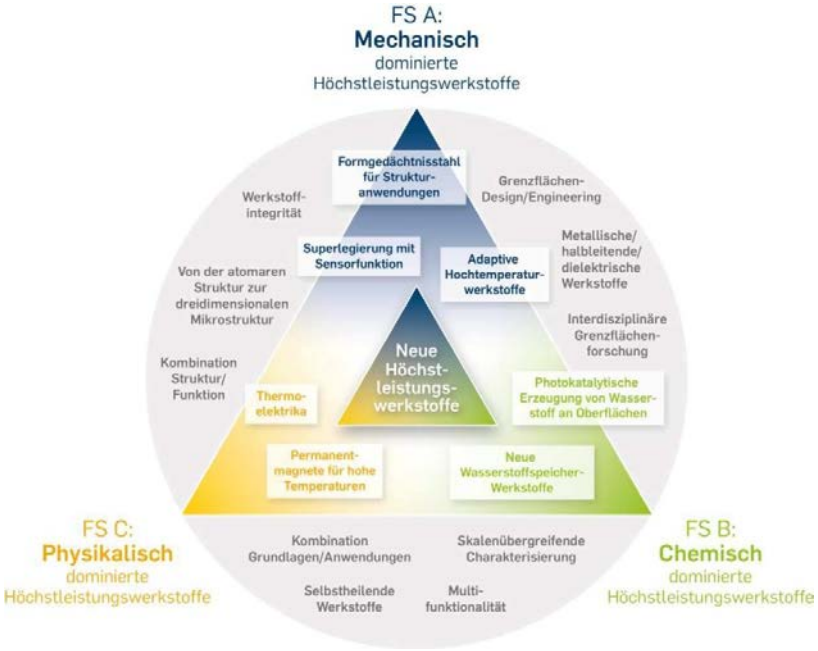

Elektrokatalytische Oberflächen

(Photo)Elektrokatalyse

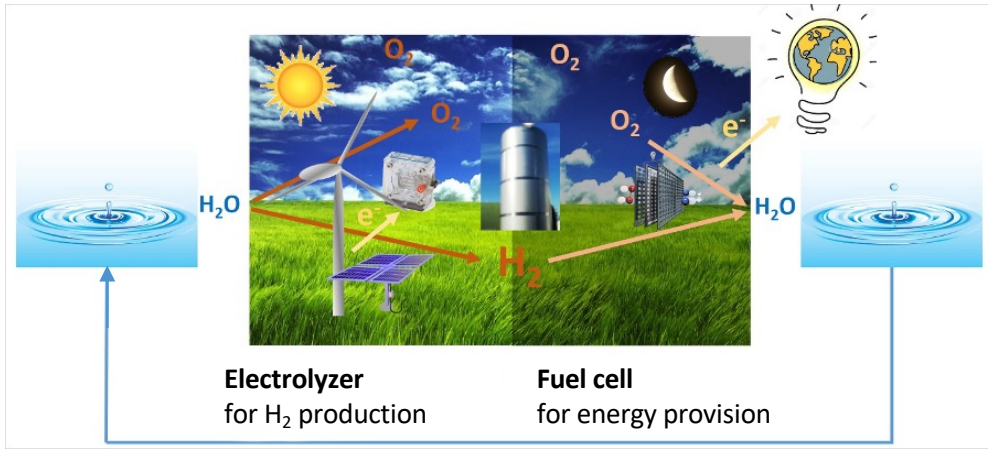

ER: evolution reaction
RR: reduction reaction
H, O: Wasserstoff, Sauerstoff

Wichtige Reaktionen für die Energiesysteme der Zukunft:
HER, OER, ORR, (water splitting)
CO2RR
…

Advanced Materials Processing and Microfabrication

Elektrokatalytische Oberflächen

Motivation for compositionally complex solid solutions (CCSS) and surface atom arrangements (SAA)

Goal of
Collaborative Research Centre 1625
fundamental scientific understanding
of CCSS surfaces,
i.e. mastering poly-elemental SAA
by fusion of simulation,
synthesis,
characterisation,
and data science

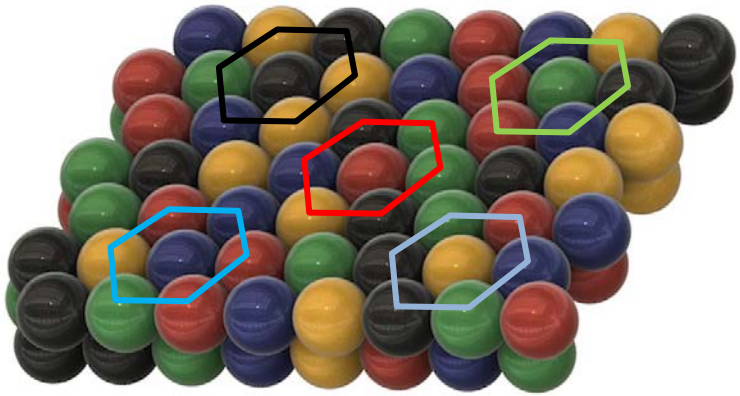

Advanced Materials Processing and Microfabrication

Elektrokatalytische Oberflächen

SAA make CCSS exceptional electrocatalysts

Example:
Hydrogen evolution reaction

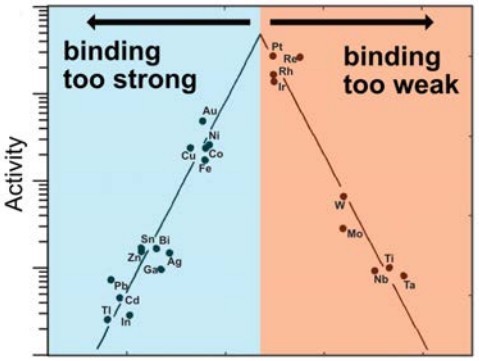

Binding energy as descriptor for catalytic activity

Single element (ideal surface)	Binary intermetallic phase	Doped phase	**Quinary CCSS phase**

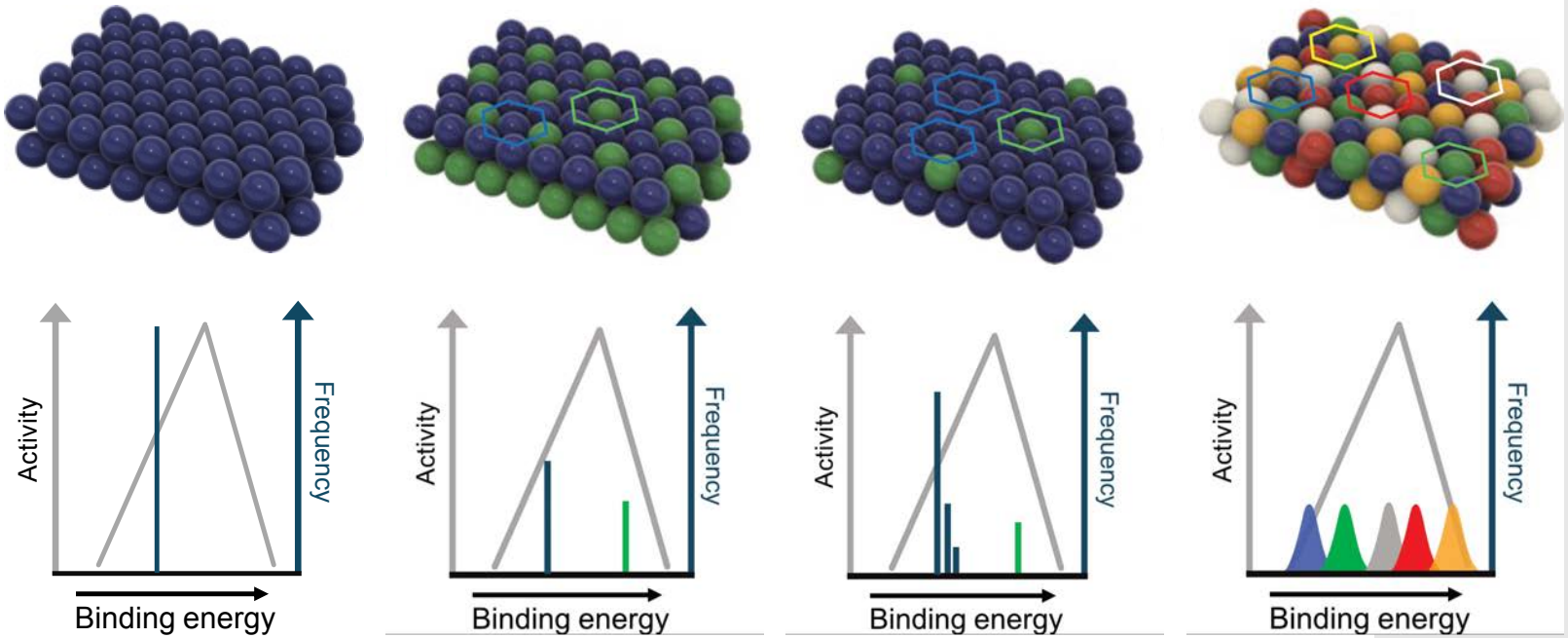

T. Löffler, **A. Ludwig, J. Rossmeisl, W. Schuhmann** (2021) *What makes high-entropy alloys exceptional electrocatalysts?* Angew. Chem. Int. Ed. 2021, 60, 26894

Elektrokatalytische Oberflächen

Universal applicability and multifunctionality of CCSS

Hypothesis
Electrochemical properties of CCSS can be tailored for any reaction,
if we can master their poly-elemental surface atom arrangements

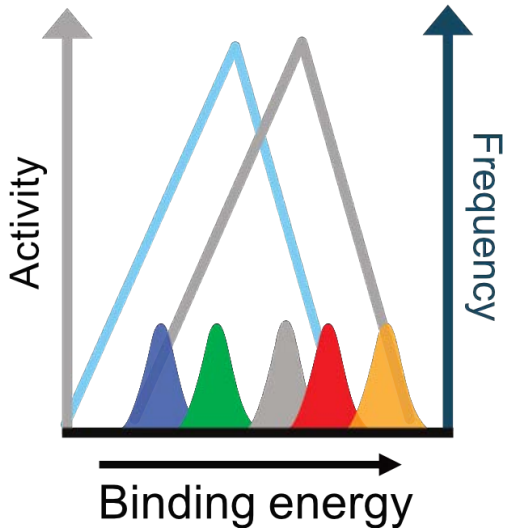

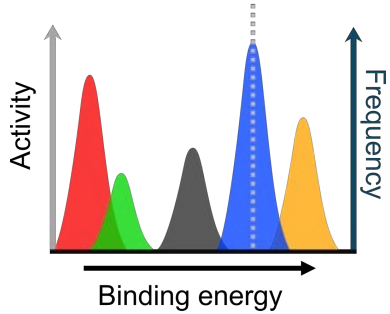

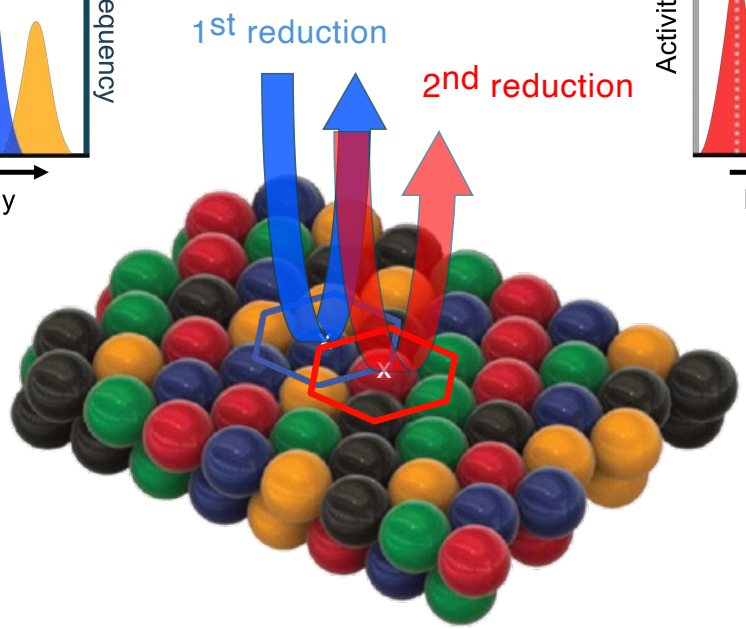

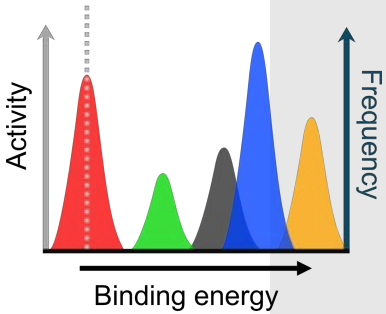

Multifunctional CCSS surface

Activity and stability **Cascade reactions**

Advanced Materials Processing and Microfabrication

Elektrokatalytische Oberflächen

Exploration and exploitation of CCSS by data-driven science

Phase I:

- 9 noble metals
- 126 quinary systems
- 10^4 compositions in 1 system
- 10^5 of SAA for 1 composition

Combinatorial explosion
➞ data-driven science

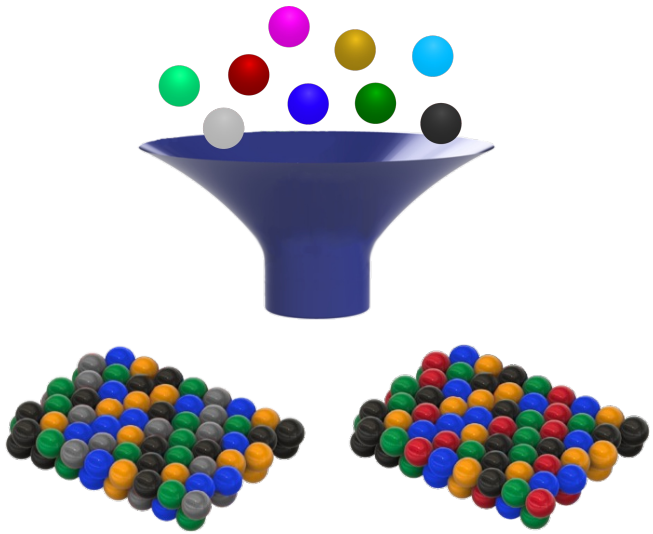

System selection

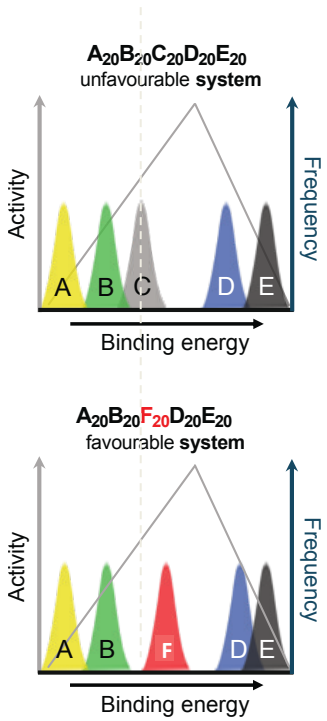

➞ **Identify most active SAA**
➞ **Maximise their number**

Composition optimisation

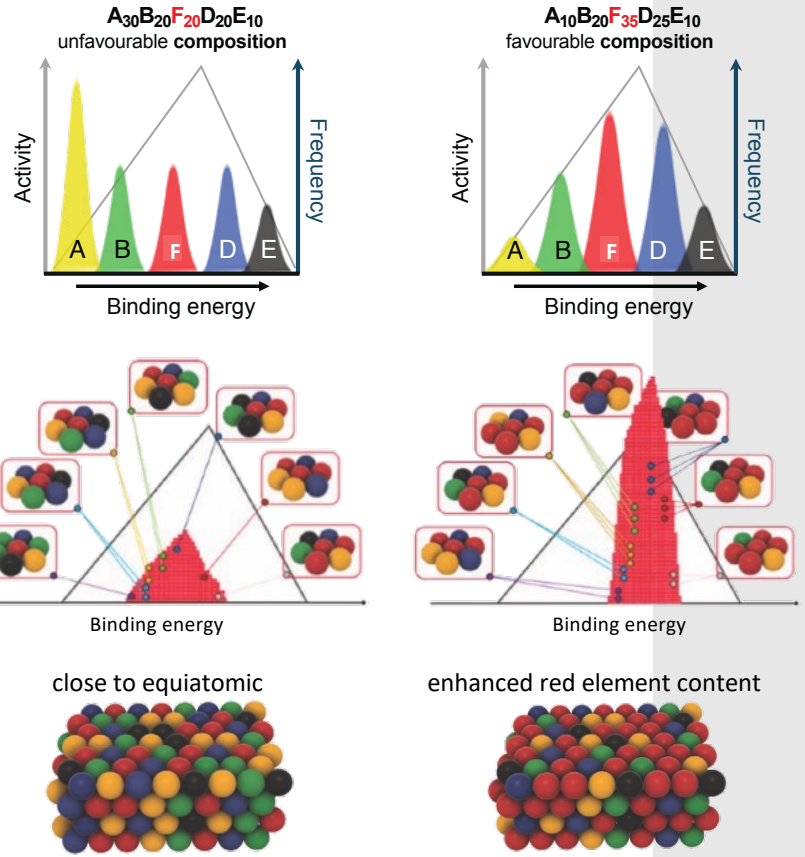

Elektrokatalytische Oberflächen

Theoretical basis for understanding and rational design of SAA

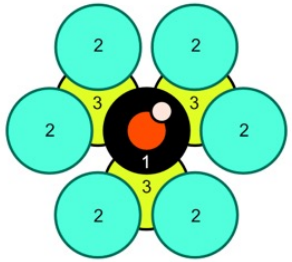

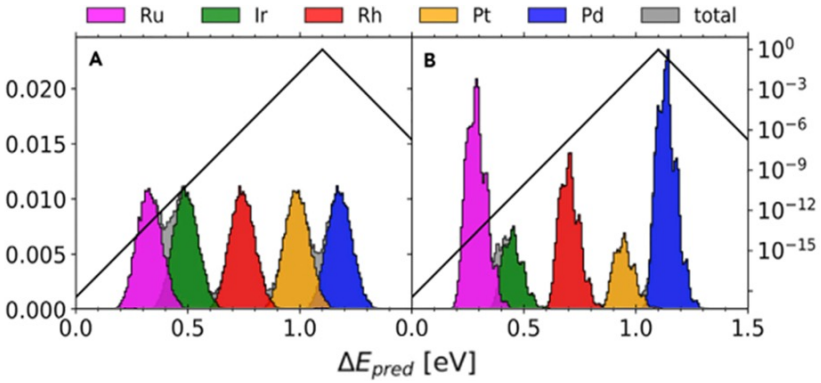

T. Batchelor, J. Pedersen, S. Winther, I. Castelli, K. Jacobsen, **J. Rossmeisl**, Joule, 2019, 3, 1

Adsorption energy regression procedure

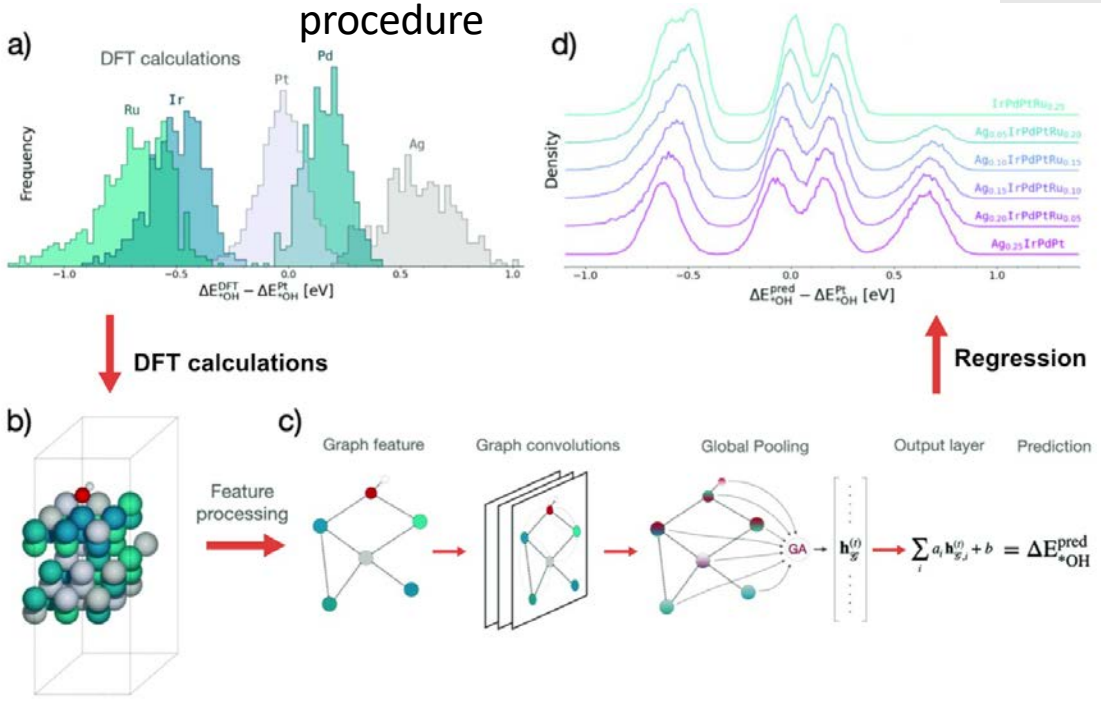

C.M. Clausen, M.L.S. Nielsen, J.K. Pedersen, **J. Rossmeisl** (2022) *Ab Initio to Activity: Machine Learning-Assisted Optimization of High-Entropy Alloy Catalytic Activity*, High Entropy Alloys & Materials

Elektrokatalytische Oberflächen

CRC 1625: A unique team to address the challenge

Scale-bridging approach integrating

- **theoretical prediction**
- **high-throughput and in-depth experiments**
- **data science**

Atomic-scale details
and
statistical abundance
of SAA

Deep collaboration
Sample and data lineage tracking

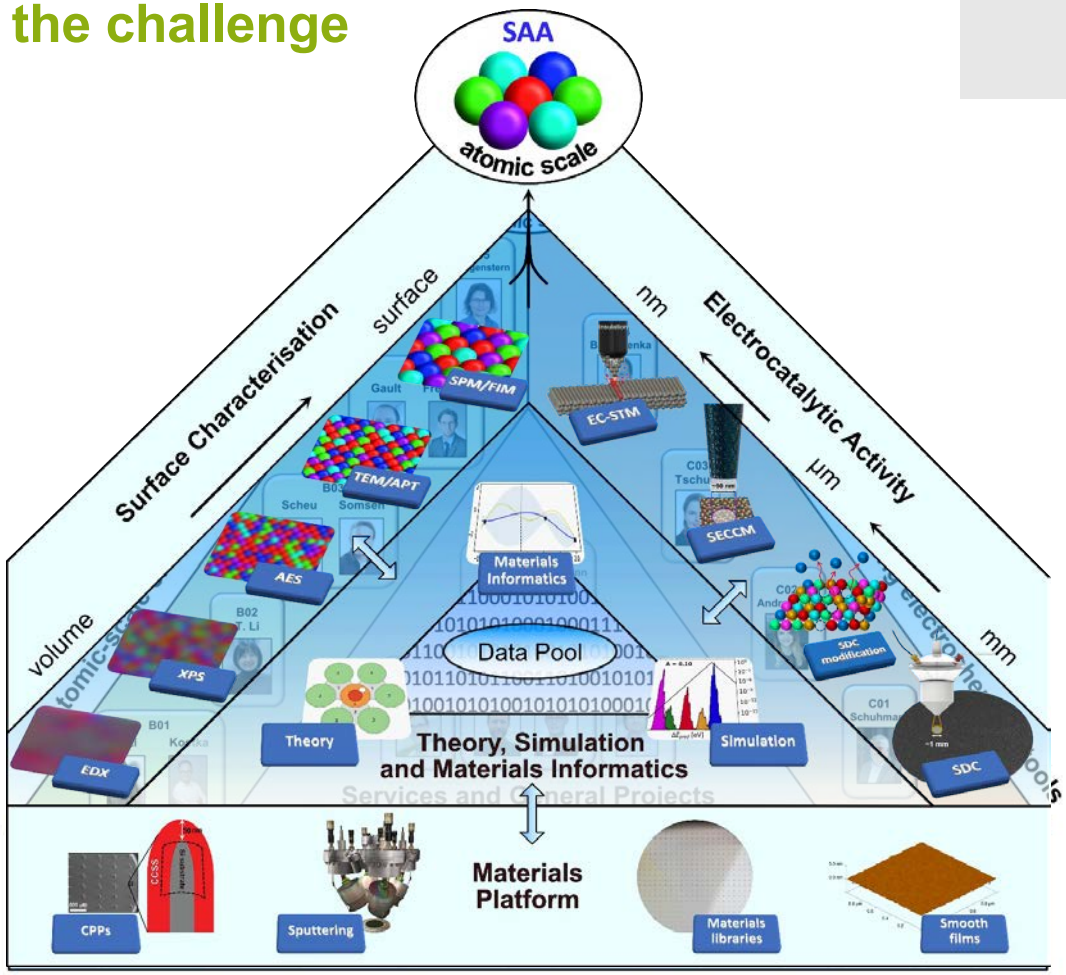

A: Theory, simulation, data-guided design and synthesis of CCSS surfaces

Advanced Materials Processing and Microfabrication

Elektrokatalytische Oberflächen

RUB

Exemplary workflow to identify SAA: Data-guided prediction-synthesis-characterisation

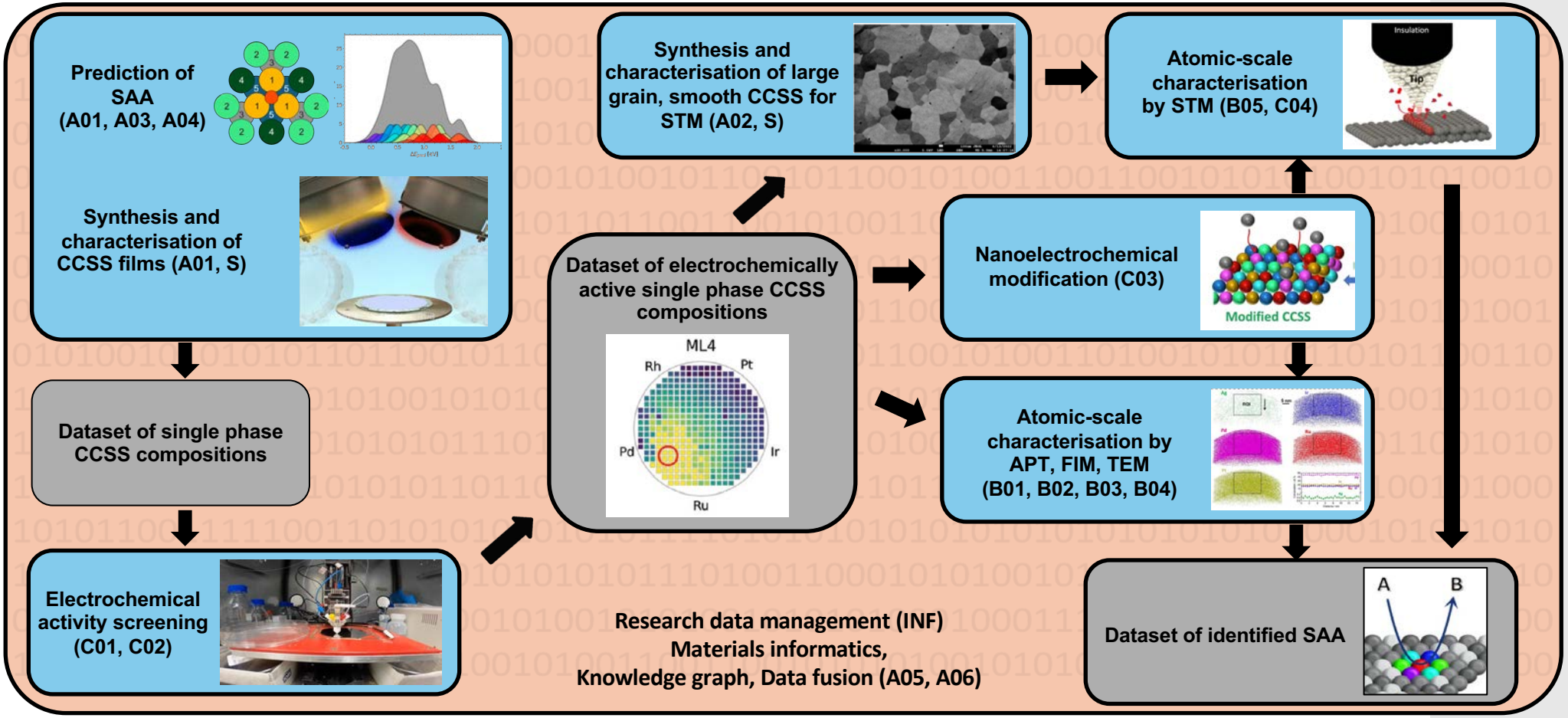

Ideale Werkstoffe und Oberflächen

Vom Idealkristall zum Realkristall

Was kommt dem Idealkristall am nächsten?

Gibt es perfekte Oberflächen?

Grundlegende Fragen

Können wir Werkstoffe mit atomarer Genauigkeit herstellen/analysieren?

Ist es möglich das Wachstum der Materialien in situ zu beobachten und zu kontrollieren?

Kristallzuchtverfahren

Kristallwachstum:

Keimbildungsgeschwindigkeit
Keimwachstum

Für Einkristalle:

- niedrige Keimbildungsgeschwindigkeit notwendig (sonst Polykristalle)
- niedrige Wachstumsgeschwindigkeit (sonst zu viele Defekte)

Kristallzucht:

- aus Lösungen
- aus Schmelze
- aus Gasphase

Einkristalle
(200 µm bis 500 µm)
werden z.B. für die Kristallstrukturbestimmung mittels Röntgenbeugung benötigt

Herstellung von Einkristallen aus Lösungen

- kristallisierende Substanz sollte geringe Löslichkeit in der Lösung aufweisen
- langsame Abkühlung von gesättigten Lösungen
- Vibrationen minimieren, erhöhte Temperaturen günstig (weniger Einbau von Lösungsmittel, Ausheilen von Kristallfehlern), Temperaturgradient günstig zur Erzeugung von Konvektion

- Kristallisation direkt bei der Reaktion zweier Lösungen
- Diffusionsmethode (reaktive Lösungen diffundieren ineinander)

- Hydrothermalmethode (Solvothermalmethode)
- bei schwer löslichen anorganischen Verbindungen
- meist wässrige Lösungsmittel
- Erhitzen der Lösung in einem Autoklaven erzeugt Drücke von einigen 100 bar. Bei diesen Bedingungen erhöhte Löslichkeit
- Beim langsamen Abkühlen kristallisieren Verbindungen aus
- wird auch zur Synthese von Verbindungen genutzt (Druck begünstigt Ordnung, gute Kristallqualitäten möglich)
- Bei Verwendung von ionischen Flüssigkeiten: Ionothermalsynthese

Quelle:
nach Massa

Advanced Materials Processing and Microfabrication

Hydrothermalsynthese

z.B. zur **Herstellung von SiO_2 Einkristallen (Quarz)** in wässrigen NaOH Lösungen

Hydrothermalsynthesen können oft bei niedrigeren Temperaturen ablaufen als vergleichbare Festkörperreaktionen

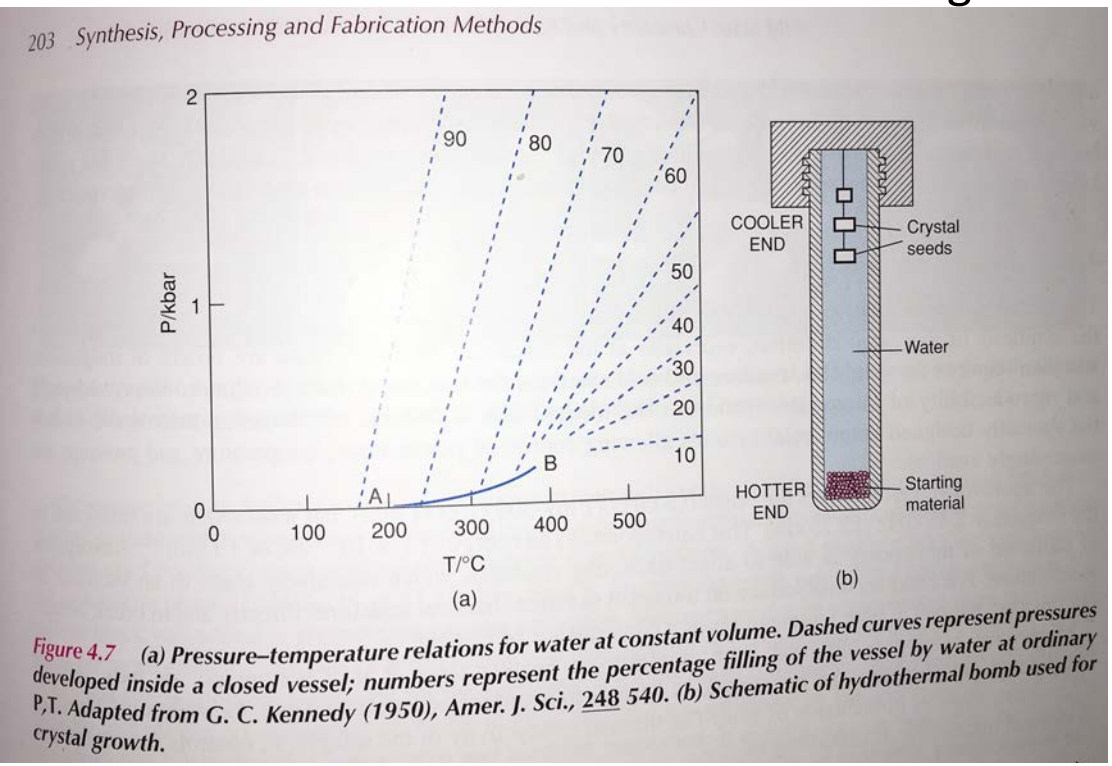

Figure 4.7 (a) Pressure–temperature relations for water at constant volume. Dashed curves represent pressures developed inside a closed vessel; numbers represent the percentage filling of the vessel by water at ordinary P,T. Adapted from G. C. Kennedy (1950), Amer. J. Sci., 248 540. (b) Schematic of hydrothermal bomb used for crystal growth.

Quelle: A. West

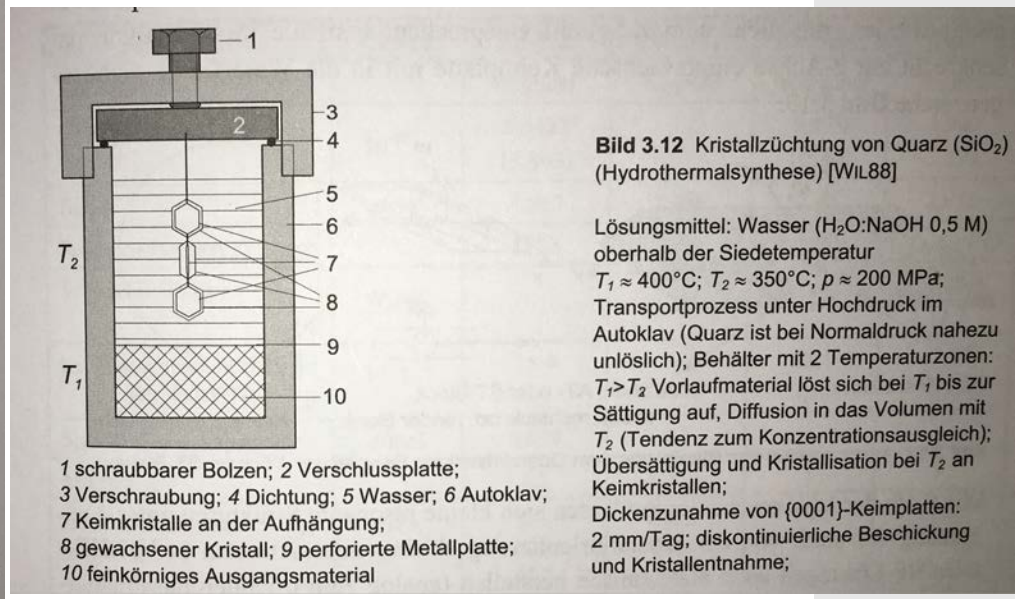

1 schraubbarer Bolzen; 2 Verschlussplatte; 3 Verschraubung; 4 Dichtung; 5 Wasser; 6 Autoklav; 7 Keimkristalle an der Aufhängung; 8 gewachsener Kristall; 9 perforierte Metallplatte; 10 feinkörniges Ausgangsmaterial

Bild 3.12 Kristallzüchtung von Quarz (SiO_2) (Hydrothermalsynthese) [WIL88]

Lösungsmittel: Wasser (H_2O:NaOH 0,5 M) oberhalb der Siedetemperatur
$T_1 \approx 400°C$; $T_2 \approx 350°C$; $p \approx 200$ MPa;
Transportprozess unter Hochdruck im Autoklav (Quarz ist bei Normaldruck nahezu unlöslich); Behälter mit 2 Temperaturzonen: $T_1 > T_2$ Vorlaufmaterial löst sich bei T_1 bis zur Sättigung auf, Diffusion in das Volumen mit T_2 (Tendenz zum Konzentrationsausgleich); Übersättigung und Kristallisation bei T_2 an Keimkristallen;
Dickenzunahme von {0001}-Keimplatten: 2 mm/Tag; diskontinuierliche Beschickung und Kristallentnahme;

Quelle: J. Frühauf

Herstellung von Einkristallen aus der Schmelze

- Verneuil Methode
- Czochralski Methode
- Bridgman Methode
- Zonenziehverfahren

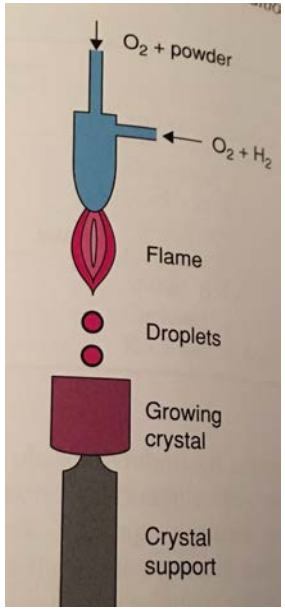

Herstellung von Einkristallen aus der Gasphase

- Sublimation
- chemischer Transport
- z.B. Chalkogenide, Halogenide

Quelle: nach Massa

Herstellung von Einkristallen:
Czochralski-Kristallziehverfahren

RUB

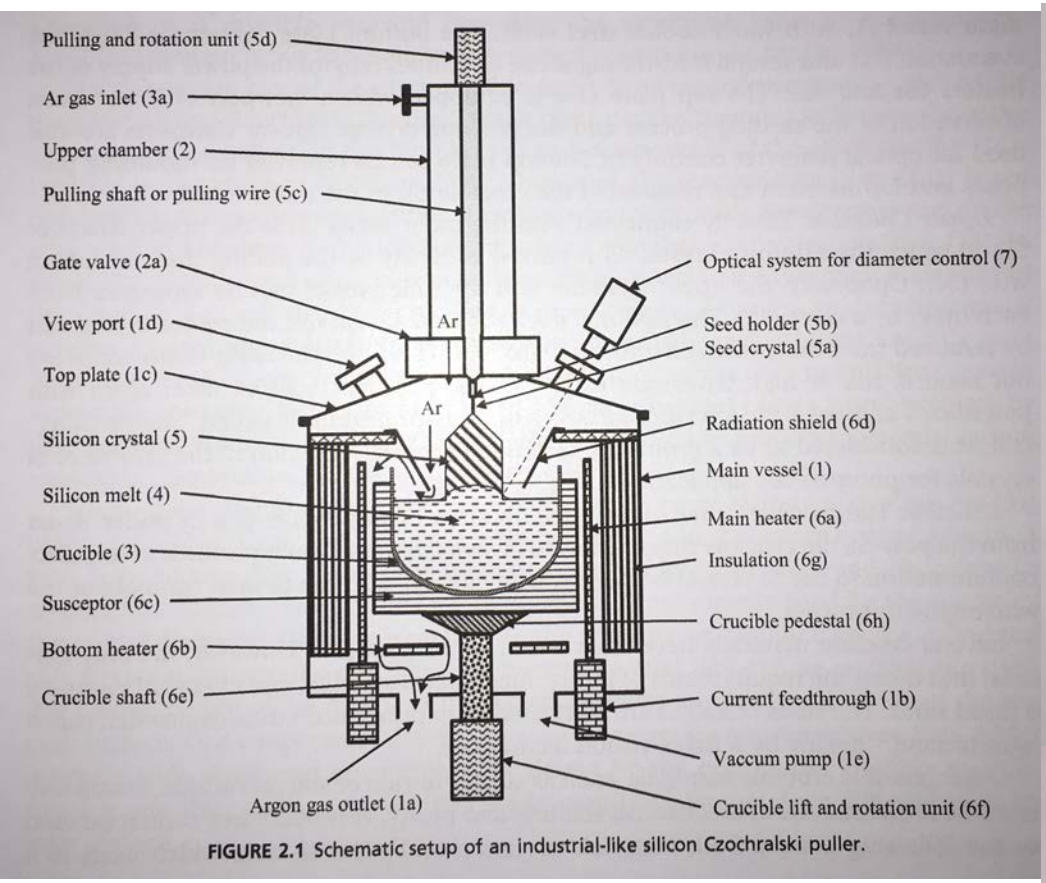

FIGURE 2.1 Schematic setup of an industrial-like silicon Czochralski puller.

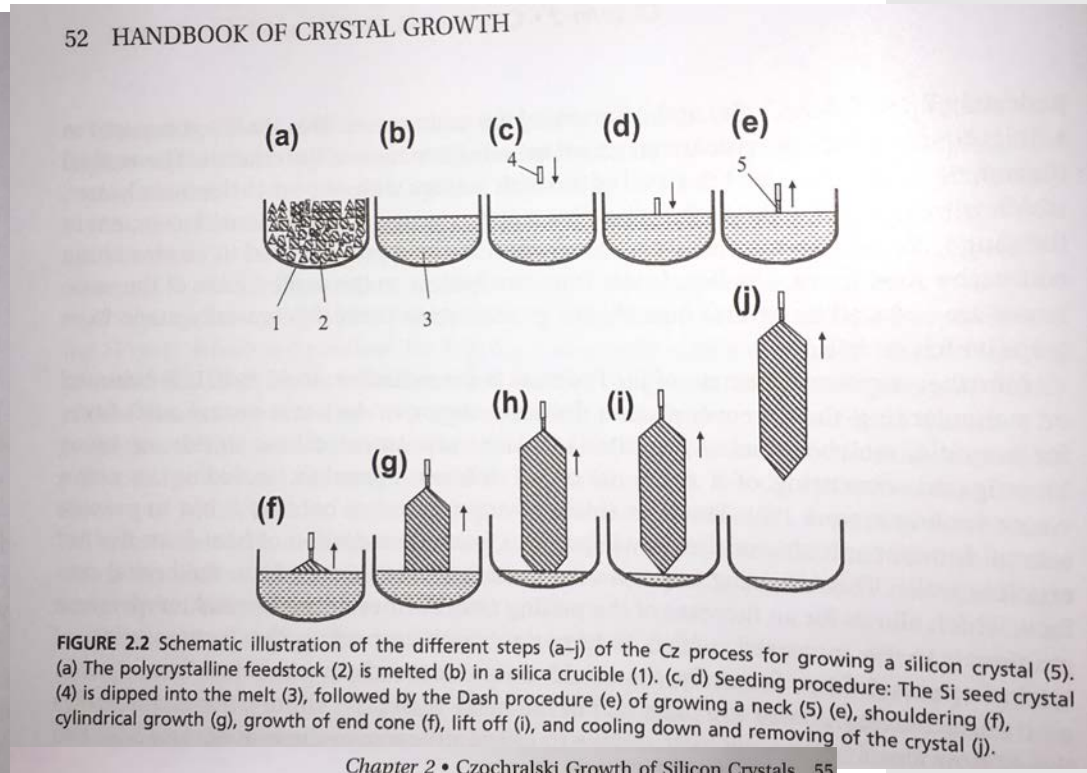

FIGURE 2.2 Schematic illustration of the different steps (a–j) of the Cz process for growing a silicon crystal (5). (a) The polycrystalline feedstock (2) is melted (b) in a silica crucible (1). (c, d) Seeding procedure: The Si seed crystal (4) is dipped into the melt (3), followed by the Dash procedure (e) of growing a neck (5) (e), shouldering (f), cylindrical growth (g), growth of end cone (f), lift off (i), and cooling down and removing of the crystal (j).

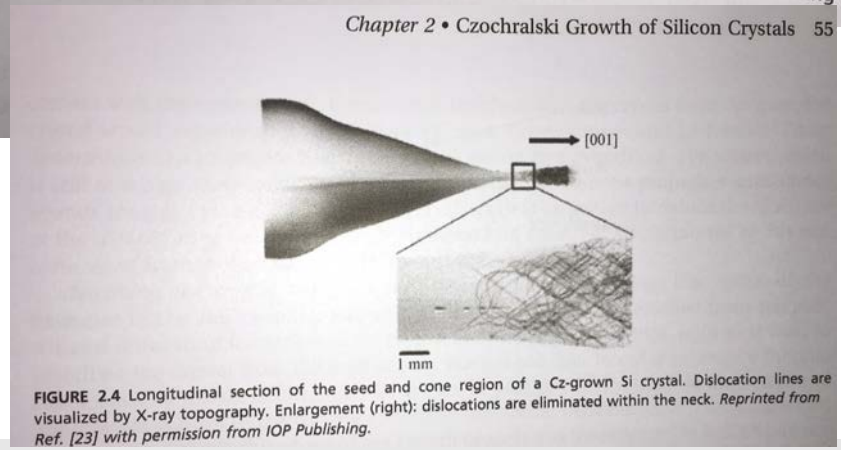

FIGURE 2.4 Longitudinal section of the seed and cone region of a Cz-grown Si crystal. Dislocation lines are visualized by X-ray topography. Enlargement (right): dislocations are eliminated within the neck. *Reprinted from Ref. [23] with permission from IOP Publishing.*

Quelle:
P. Rudolph

Herstellung von Einkristallen:
Czochralski-Kristallziehverfahren

RUB

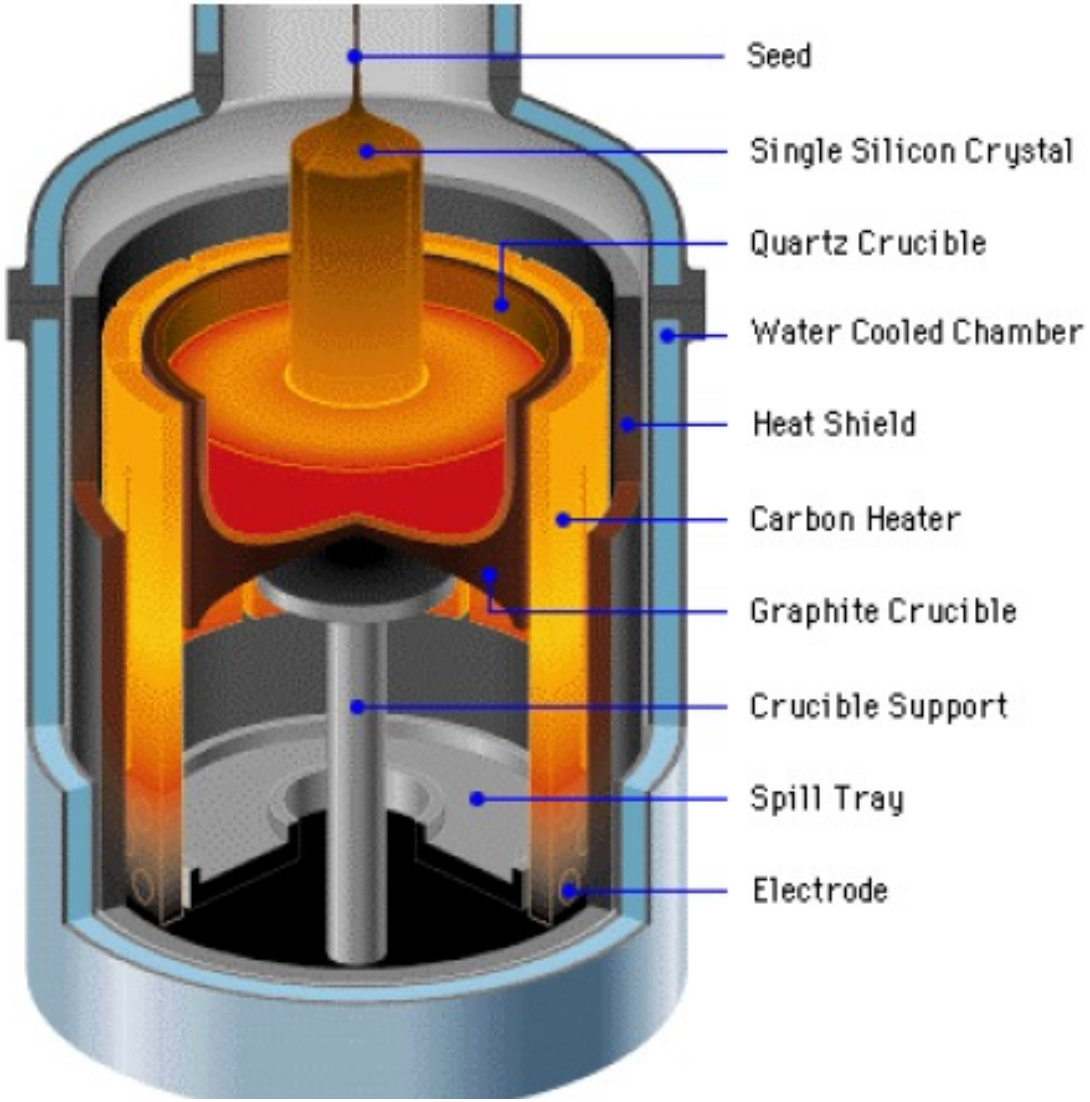

Czochralski- (Cz) oder Tiegelziehverfahren

In Quarztiegel wird polykristallines Si bei T > 1415°C unter Inertgas-atmosphäre (Ar) aufgeschmolzen.

Von einem Impfkristall ausgehend wird der Einkristall unter Rotation (Kristall, Tiegel) herausgezogen (bis 3 mm/min).

Dotierung während des Ziehens möglich.

Variation aus Ziehgeschwindigkeit und Temperatur bestimmt Durchmesser (max. 30 cm).

Vom Polykristall zum Einkristall: Czochralski-Kristallziehverfahren

Hohe Reinheitsanforderungen an Tiegelmaterial bei hoher Temperatur

SiO_2 aus Quarzglas-Tiegel (bis zu 1 m Durchmesser) geht über Dauer des Prozesses teilweise in Lösung

O-Atome wirken als Donator Störstellen ($N_O > 10^{17} cm^{-3}$), weitere Verunreinigung durch Graphittiegel (C)

Hochreines Quarzglas (Verunreinigungen 1 ppm) wird opak durch Luftbläschen im Glas, notwendig für Infrarot-Strahlungsheizung

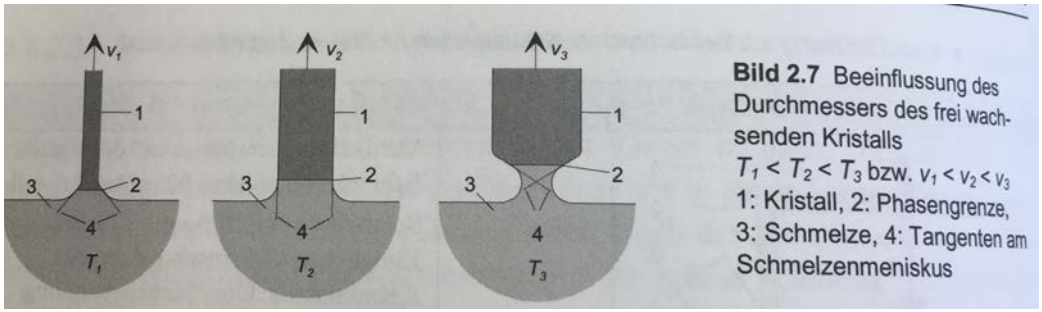

Bild 2.7 Beeinflussung des Durchmessers des frei wachsenden Kristalls
$T_1 < T_2 < T_3$ bzw. $v_1 < v_2 < v_3$
1: Kristall, 2: Phasengrenze, 3: Schmelze, 4: Tangenten am Schmelzenmeniskus

Quelle: Frühauf

Quelle: Glastechnik Band 4, Dt.Museum

Kristallziehverfahren:
Zonenziehverfahren

RUB

Auch: Floating Zone (FZ) Verfahren, im Hochvakuum oder in Inertgasatmosphäre.
Prozess zur Herstellung extrem reiner Si-Einkristalle (Segregation, s.u.).

Vorteil: Prozess ist wiederholbar, Reinheit höher als bei Cz-Verfahren
Nachteil: Prozess ist aufwändiger als Cz-Verfahren,
Durchmesser max. 20 cm

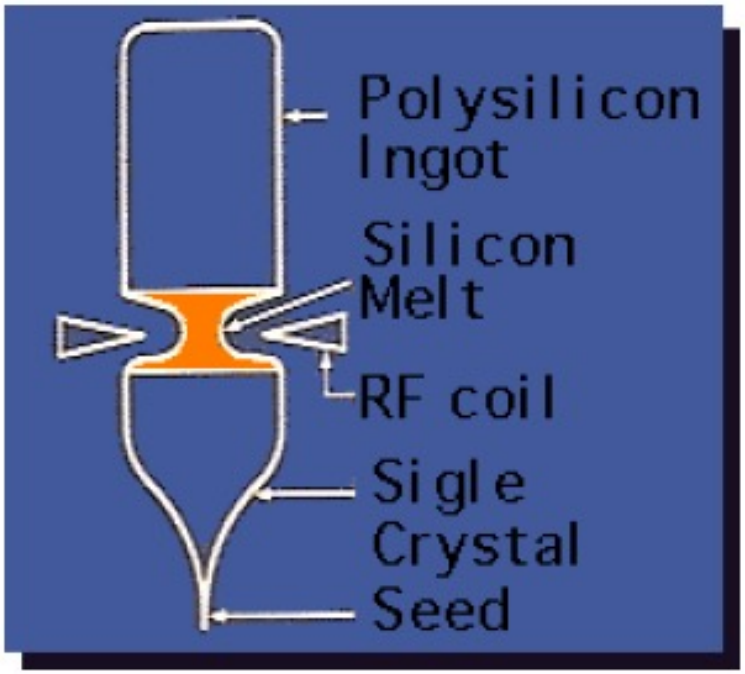

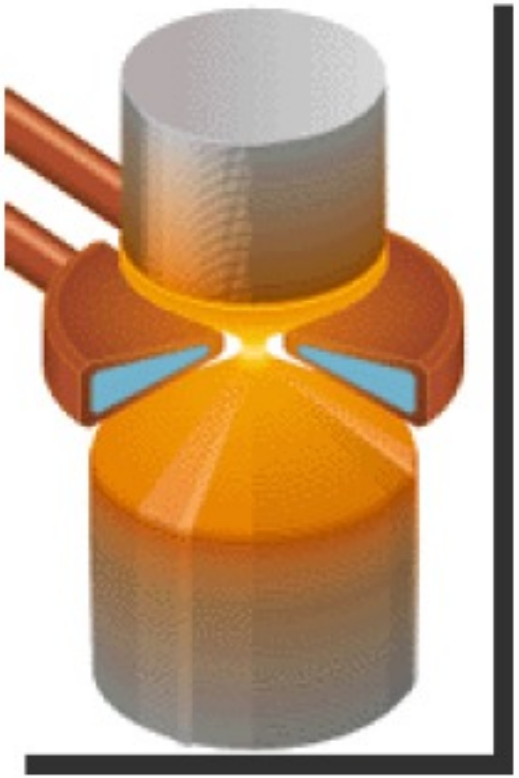

Zonenziehverfahren: Reinigung durch Segregation

Die Löslichkeit vieler Verunreinigungen in der flüssigen und in der festen Phase ist unterschiedlich.

Der Segregationskoeffizient k kann aus der atomaren Konzentration der Verunreinigungen in der festen Phase c_s und der atomaren Konzentration der Verunreinigungen in der flüssigen Phase c_l berechnet werden:

$$k=c_s/c_l$$

Ist k<1 sammeln sich die Verunreinigungen in der flüssigen Phase.

Si: k bei vielen Elementen <1, Ausnahme: Sauerstoff (k=1,25)

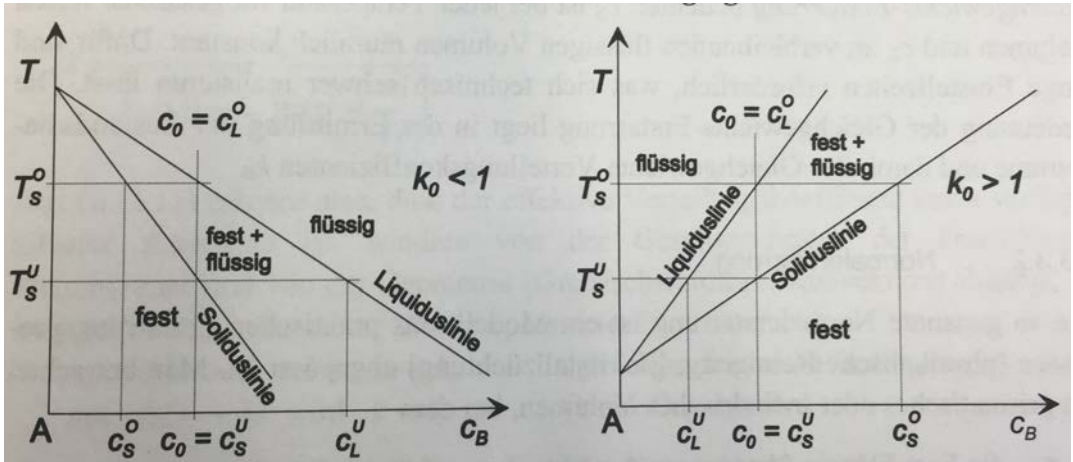

Bild 2.8 Varianten der Randbereiche von Zustandsdiagrammen binärer Stoffsysteme (S und U bezeichnen die oberen bzw. unteren Grenzen des Erstarrungsintervalls)

Quelle: Frühauf

Einkristalle:

Kristallzucht mittels Bridgmanverfahren

Verfahren zur Herstellung von Einkristallen:
Horizontales Bridgman-Verfahren (HB) und *Vertikales Bridgman-Verfahren* (VB)
Material wird in Schiffchen bzw. Ampulle horizontal bzw. vertikal durch einen Ofen bewegt. Dabei wird das Material aufgeschmolzen und kristallisiert beim Abkühlen. Steuerung der Abkühlung notwendig für Einkristalle.

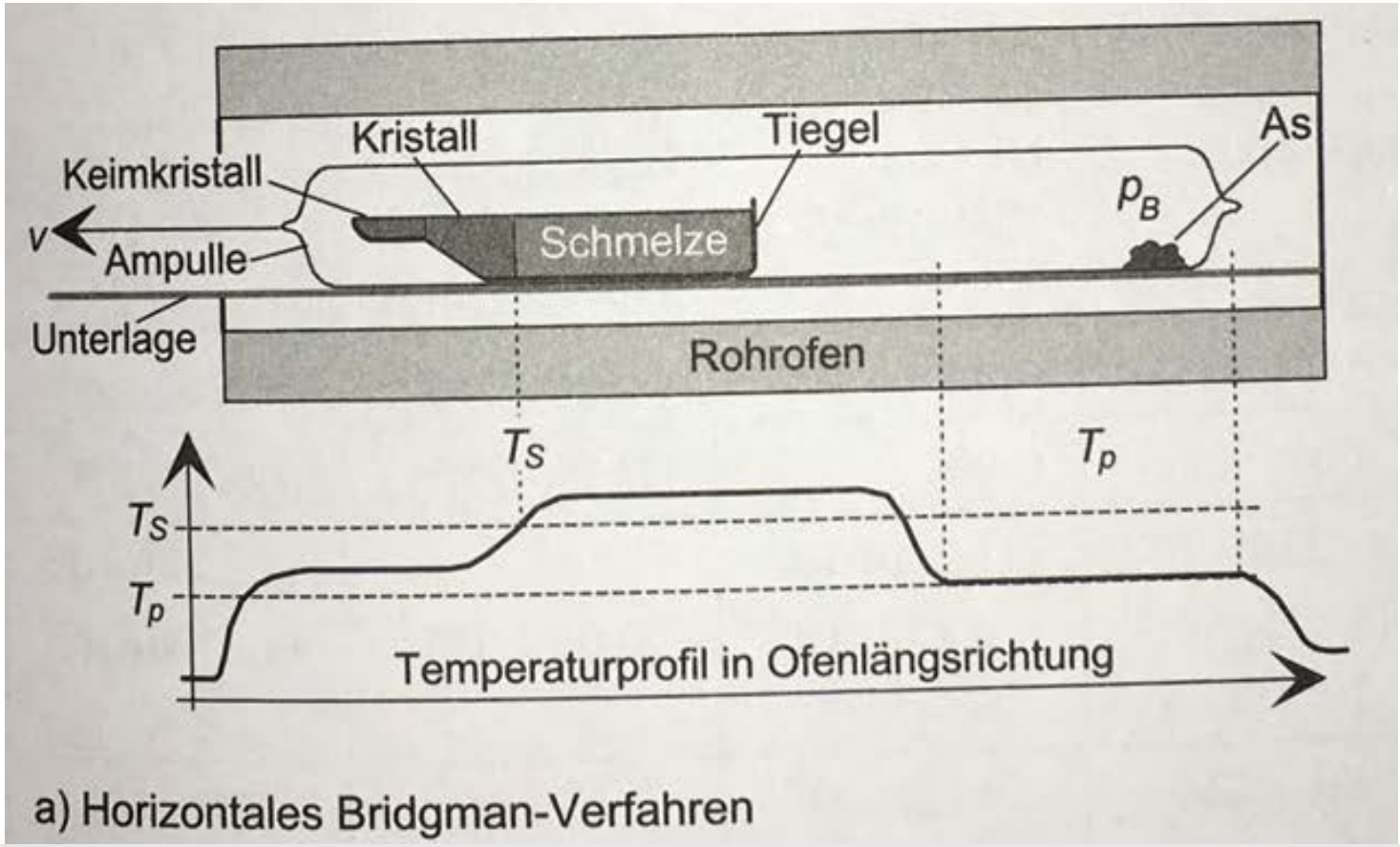

Quelle: Wikipedia, Frühauf

Einkristalle:

Kristallzucht mittels Bridgmanverfahren

Weiterentwicklung des vertikalen Verfahrens:

Bridgman-Stockbarger-Methode

Mehrzonenofen mit unterschiedlichen Temperaturzonen

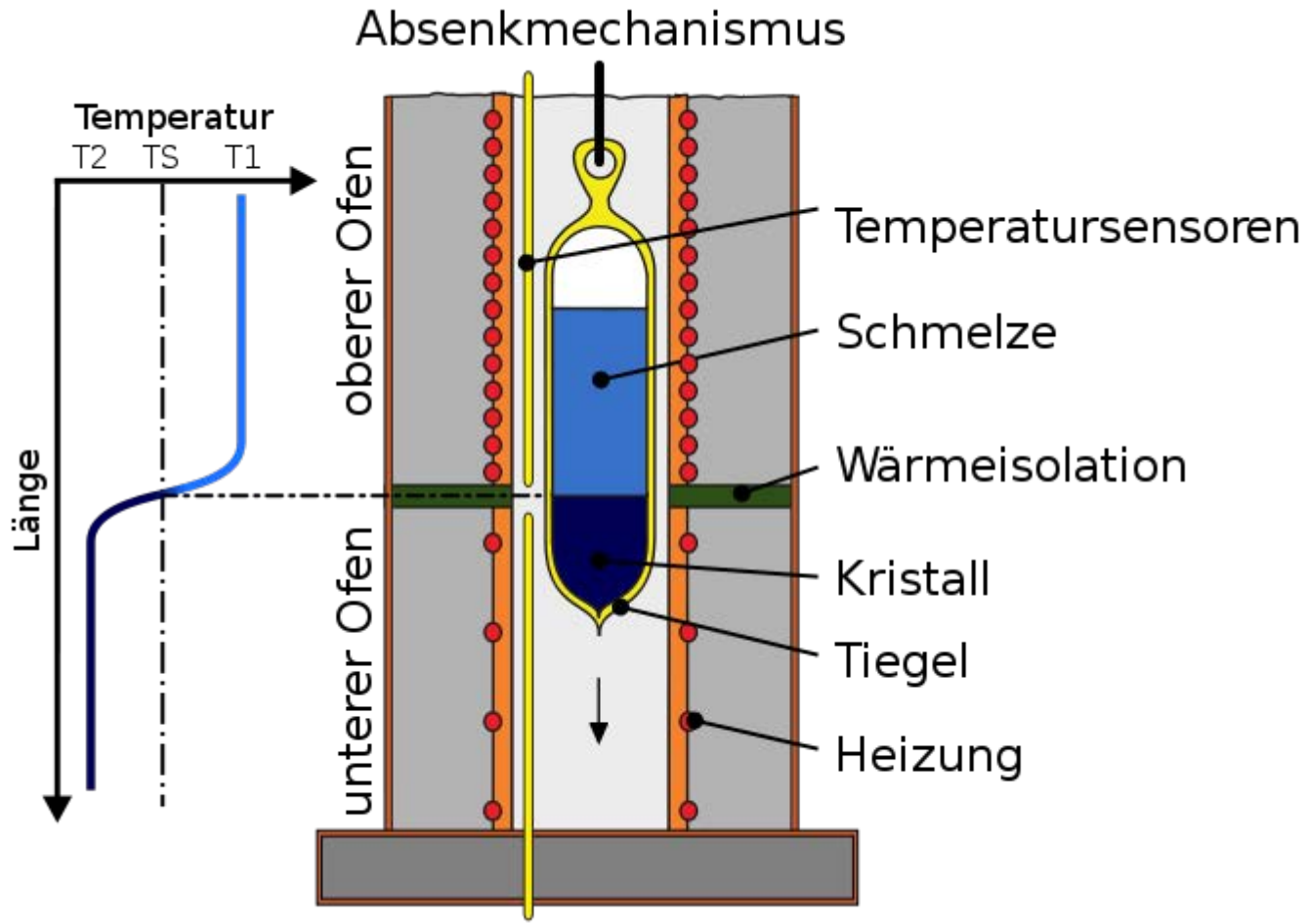

Einkristalle:

Kristallzucht von Verbindungen: GaAs (Verbindungshalbleiter)

Synthese aus Ga und As oder aus der GaAs-Schmelze, Problem: hoher Dampfdruck von As
As-Verarmung bzw. Ga+GaAs Zweiphasengemisch
Gegenmaßnahme: Aufbau eines ausreichend hohen As-Partialdrucks oder
Abdeckung der Schmelze durch inerte Schutzschicht (B_2O_3)

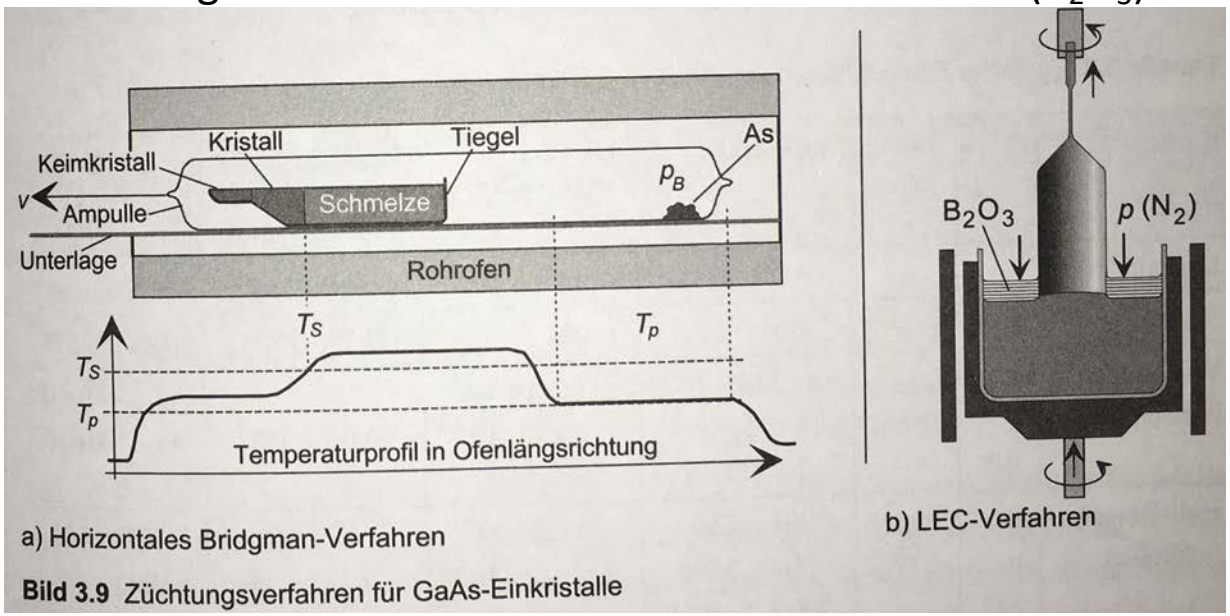

Bild 3.9 Züchtungsverfahren für GaAs-Einkristalle

LEC: liquid encapsulated Czochralski; effizient, aber Versetzungsdichte > 10^4 cm^{-2}
z.B. für LEDs (dotiertes GaAs, z.B. Zn, Si, Te)
weitere Möglichkeit: VGF, vertikales „gradient-freezing“ Verfahren
VGF und HB Versetzungsdichte < 10^3 cm^{-2} , z.B. für Laserdioden

Einkristalle:

Kristallzucht von Verbindungen

SiC, Sublimation

SiC lässt sich nicht aus der Schmelze herstellen,
da sich die Verbindung bei hoher Temperatur zersetzt.
Daher Züchtung aus der Gasphase durch Sublimation aus dem polykristallinen SiC Pulver und Kondensation am Keimkristall, der bei einer niedrigeren Temperatur gehalten wird.

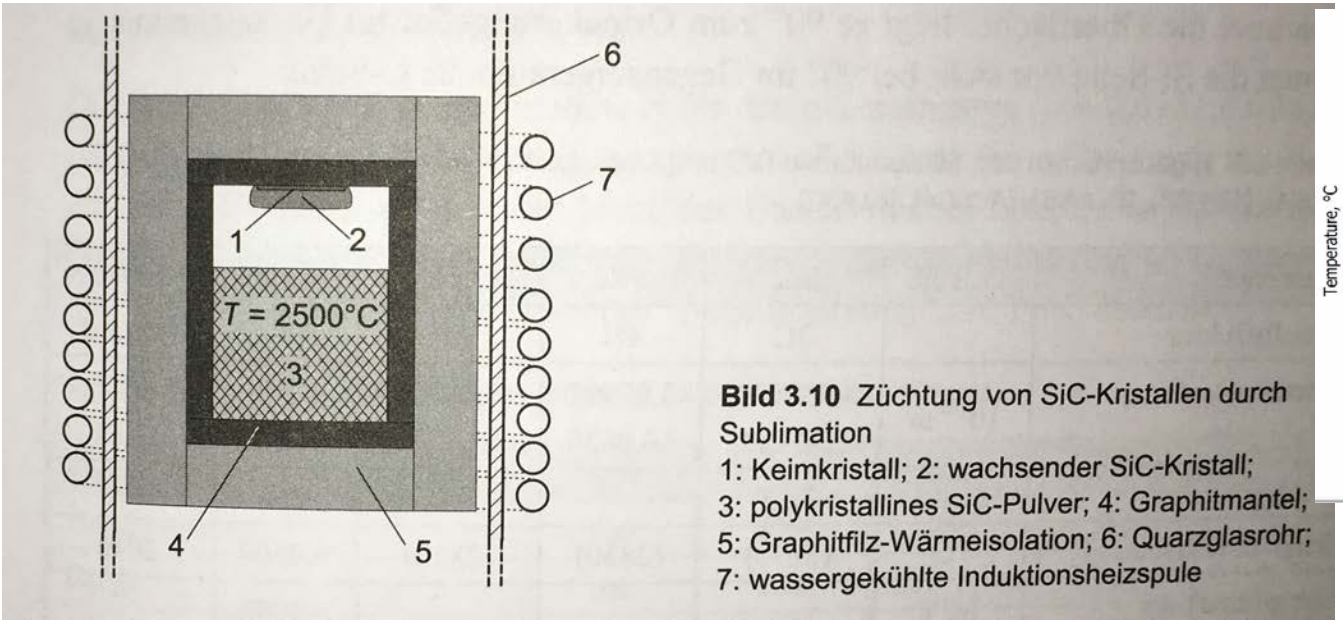

Bild 3.10 Züchtung von SiC-Kristallen durch Sublimation
1: Keimkristall; 2: wachsender SiC-Kristall;
3: polykristallines SiC-Pulver; 4: Graphitmantel;
5: Graphitfilz-Wärmeisolation; 6: Quarzglasrohr;
7: wassergekühlte Induktionsheizspule

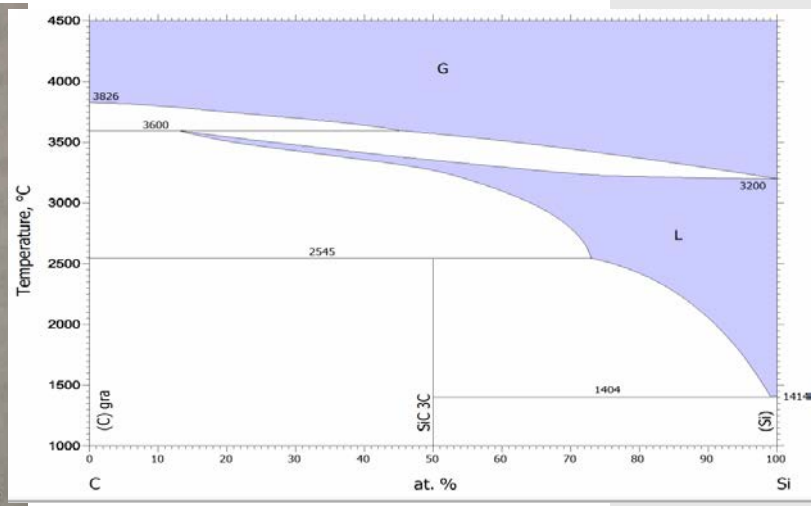

GaN lässt sich ebenfalls nicht aus der Schmelze als Einkristall herstellen:
Daher Gasphasenverfahren

Herstellung von einkristallinen Oberflächen

Epitaxieverfahren

Verfahren, bei dem die einkristalline Struktur eines Substrates durch Beschichtungsverfahren, die bei hoher Temperatur ablaufen, weiter fortgesetzt wird.

Homo-Epitaxie

- Aufwachsen von Schichten aus dem gleichen Material wie das Substrat (abgesehen von unterschiedlicher Dotierung)
- Anlagerung der Atome geschieht zuerst an Keimstellen auf der Oberfläche (Ecken und Kanten von unvollendeten Kristallebenen)

→ zunächst werden unvollständige Kristallebenen durch Anlagerung ergänzt

→ gleichmäßiges Aufwachsen einer einkristallinen Epitaxieschicht

Hetereo-Epitaxie

Aufwachsen von Schichten mit einer zum Substrat unterschiedlichen einkristallinen Schicht (die Gitterkonstante beider Materialien muss etwa gleich groß sein)

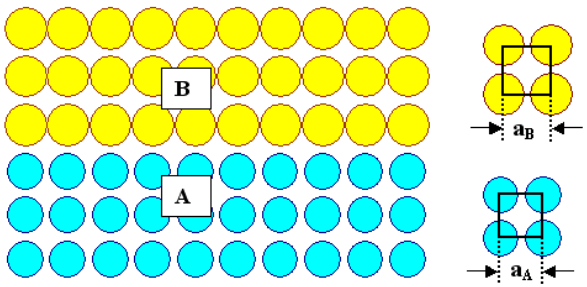

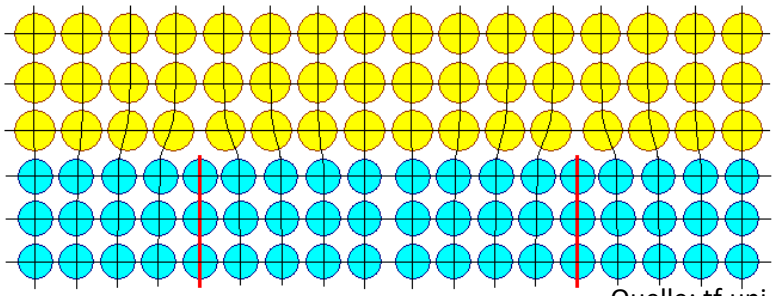

Quelle: tf.uni-kiel.de

Molekularstrahlepitaxie

(MBE, engl.: *molecular beam epitaxy*)

Ultrahochvakuum (UHV)

Quelle: directindustry.com

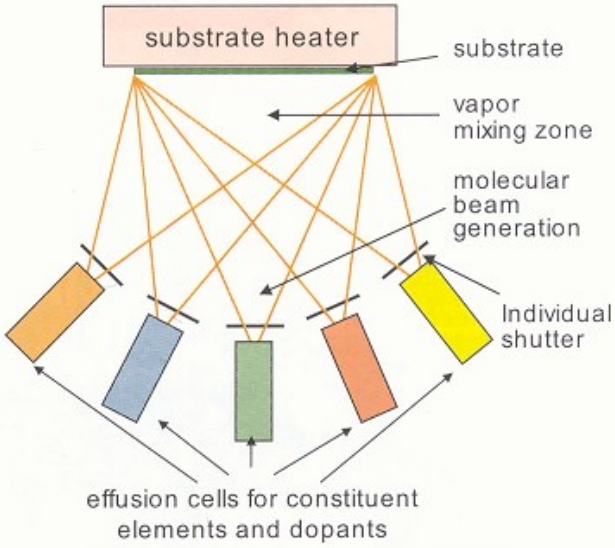

Figure 12: Schematic view of a MBE system for the growth of multi-element compound films.

Quelle: Waser

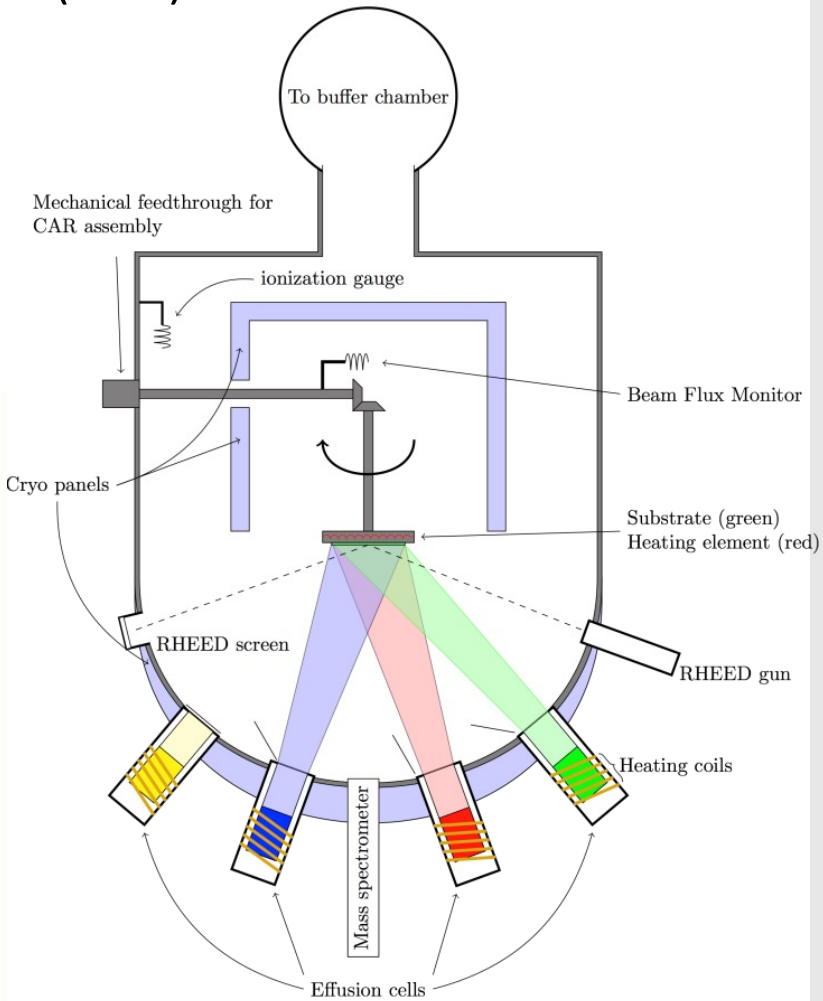

Schematic diagram of a typical MBE growth chamber

Quelle: k-space.com

Epitaxie mittels MBE

- Verdampfen molekularer (z.B. As_4) und/oder atomarer (z.B. Ga) Spezies aus geeigneten Quellen (z.B. Knudsen-Zelle)
- in situ Messung von Beschichtungsraten:

  z.B. Quarzkristallmonitor (Mikrowaage, Messung von Resonanzfrequenzänderungen während der Beschichtung)
- z.B. für Verbindungshalbleiter in opto-elektronischen Anwendungen (hohe Reinheit und kristalline Perfektion notwendig), wie Galliumarsenid (GaAs), Indiumphosphid (InP), GaInNAs, Galliumantimonid (GaSb)

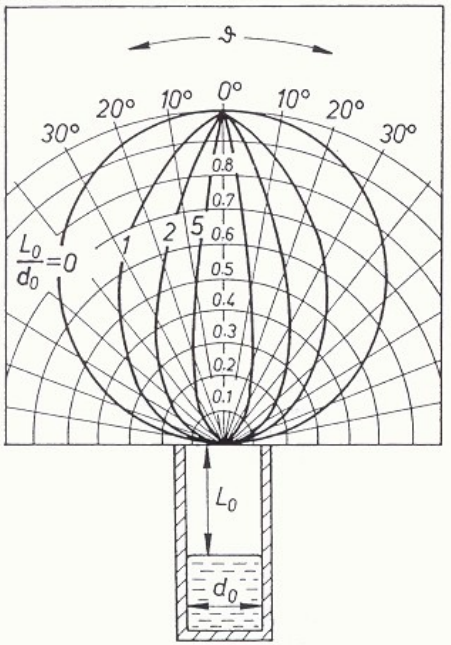

Figure 13: Schematics of a Knudsen cell and the distribution of the vapour beam intensity [7]. The distribution depends on the ratio L_0/d_0 and consequently on the filling level of the cell.

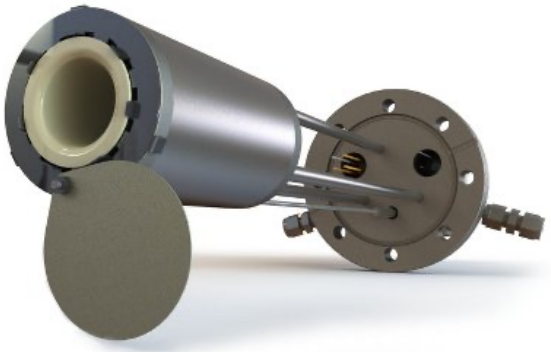

Quelle: mantisdeposition.de

MBE und RHEED
(reflection high energy electron diffraction)

RUB

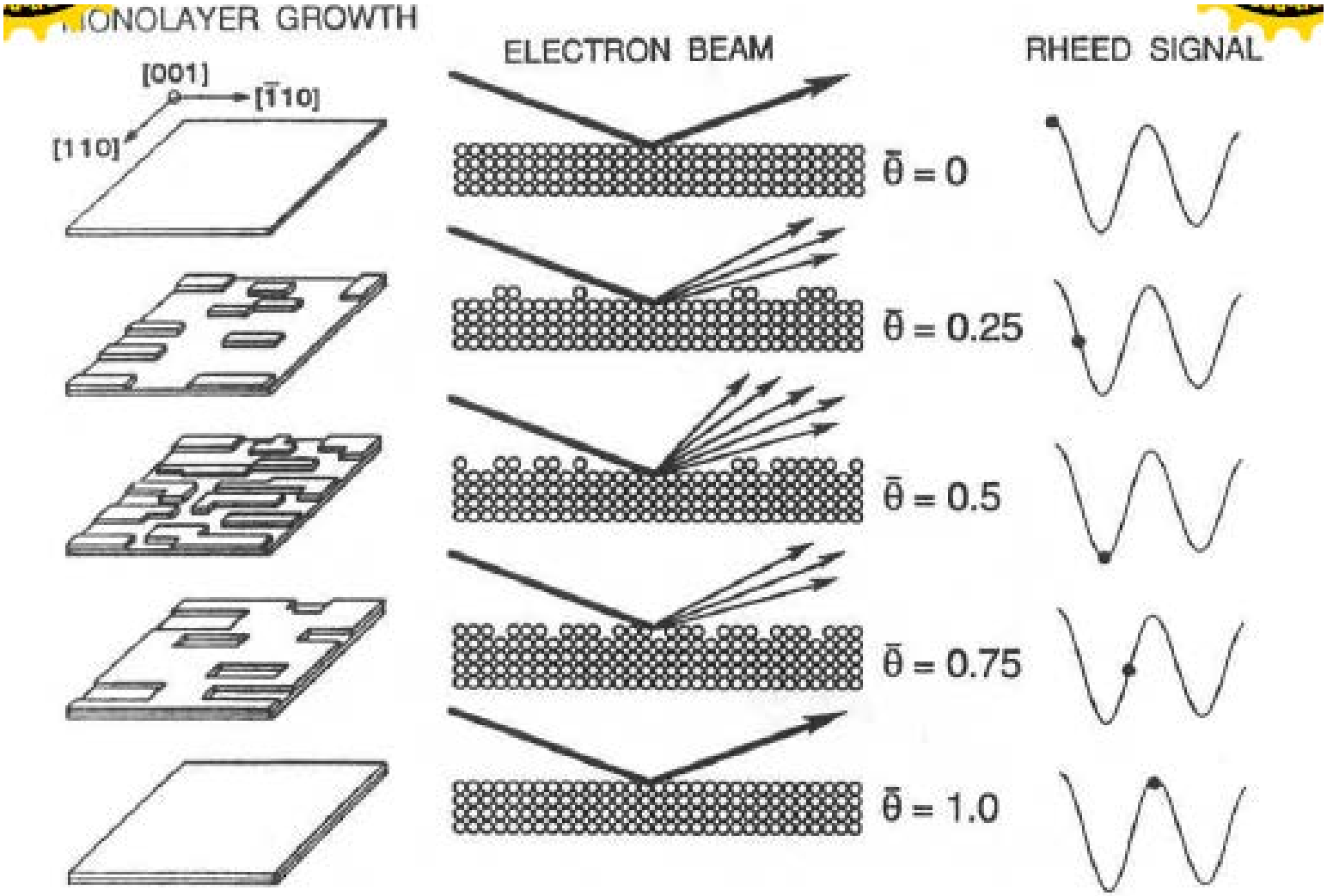

Figure 8-36 Real space representation of the formation of a single complete monolayer. $\bar{\theta}$ is the fractional layer coverage. Corresponding RHEED oscillation signal is shown.

Epitaxie mittels MBE: in situ Charakterisierungsmethoden

in situ Charakterisierung der Struktur und Kristallinität der wachsenden Schicht, z.B. mittels **RHEED**

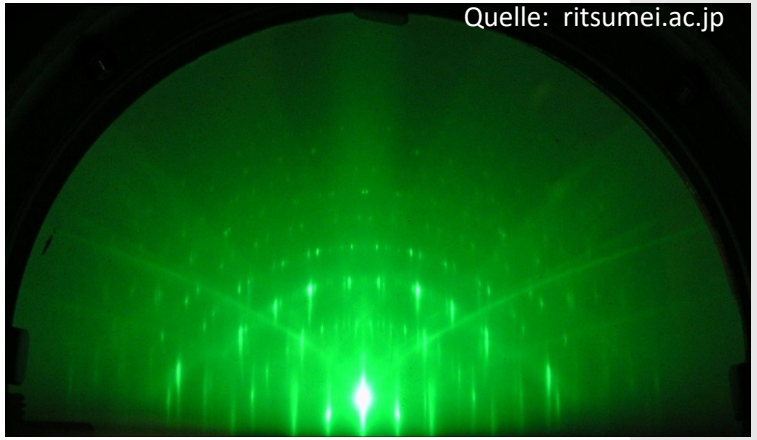

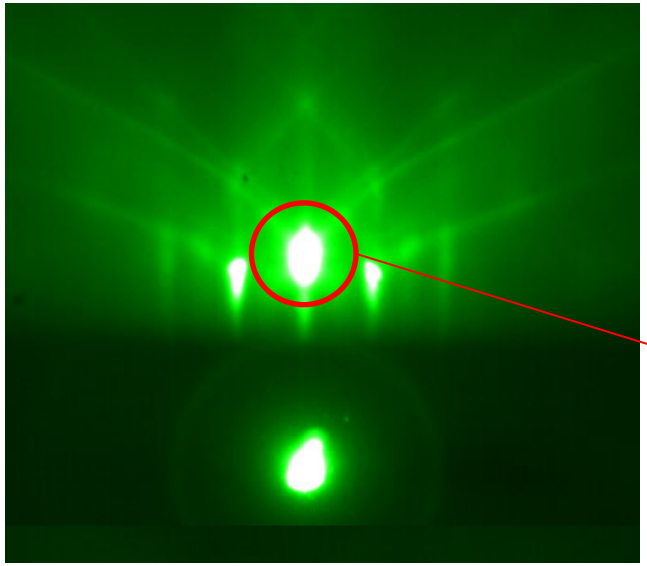

RHEED: $SrTiO_3$ Oberfläche

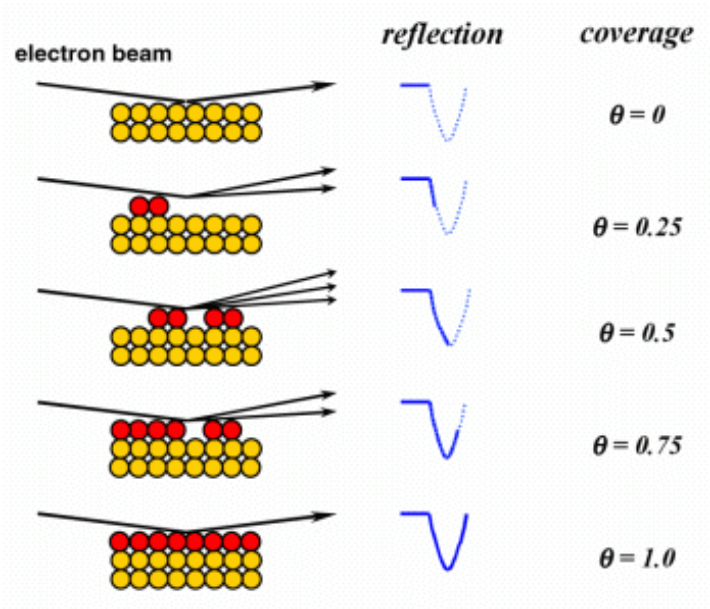

Quelle: material.tohoku.ac.jp

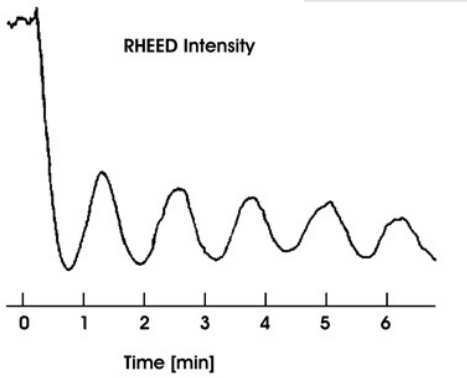

Quelle: MBE-Komponenten.de

http://www.youtube.com/watch?v=YyBJFDqeW2Y
(ab 2. Minute)

Epitaxie: TEM Querschnittsaufnahme

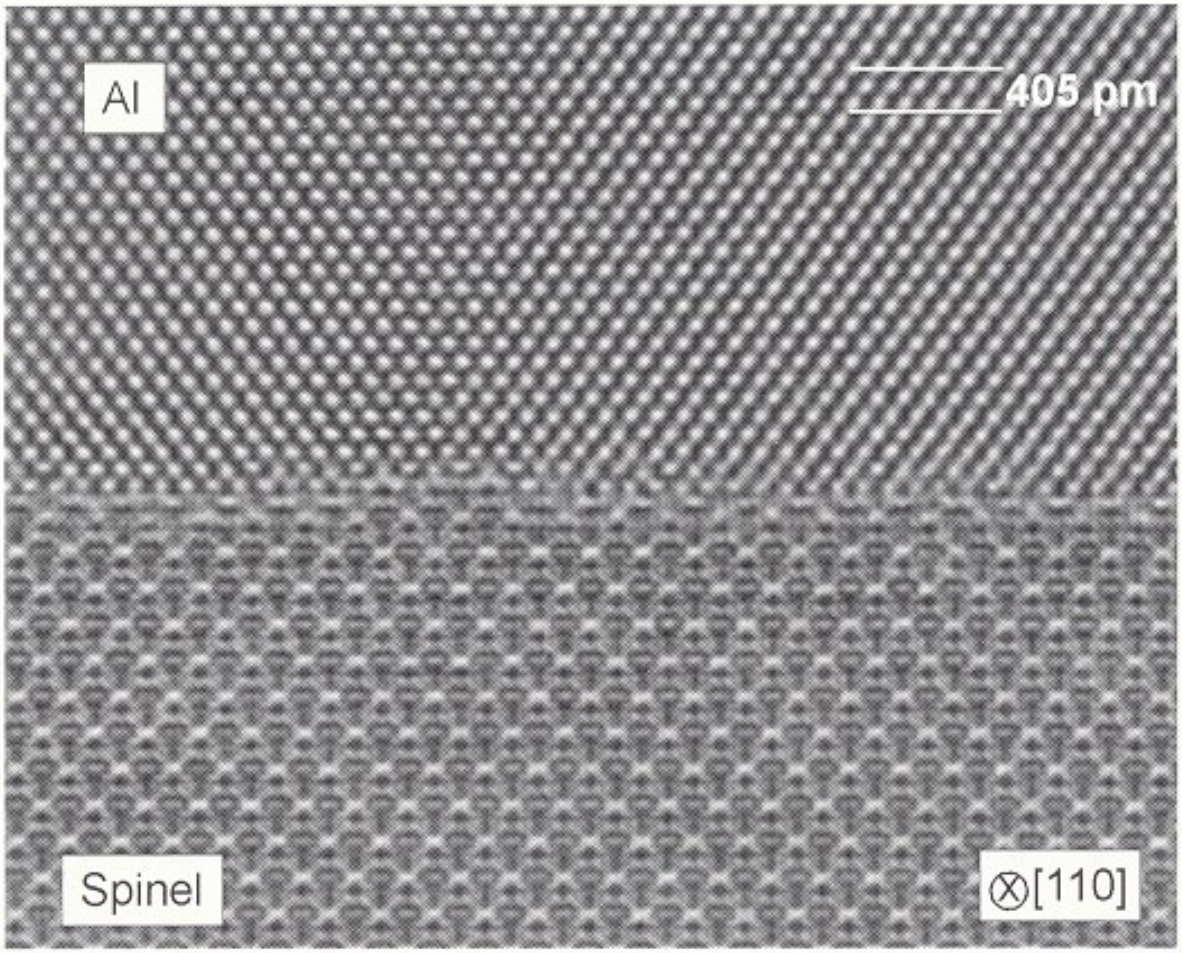

Fig. 1.15. A HRTEM image showing the [110] cross-sectional view of a coherent interface that develops with no interface defects during the epitaxial growth of an Al film on a $MgAl_2O_4(001)$ substrate. (Courtesy of M. Rühle, Max-Planck Institut für Metallforschung, Stuttgart, Germany. Reproduced with permission.)

Source: Freund-Suresh

MBE

Superlattice: epitaktische Viellagenschichten

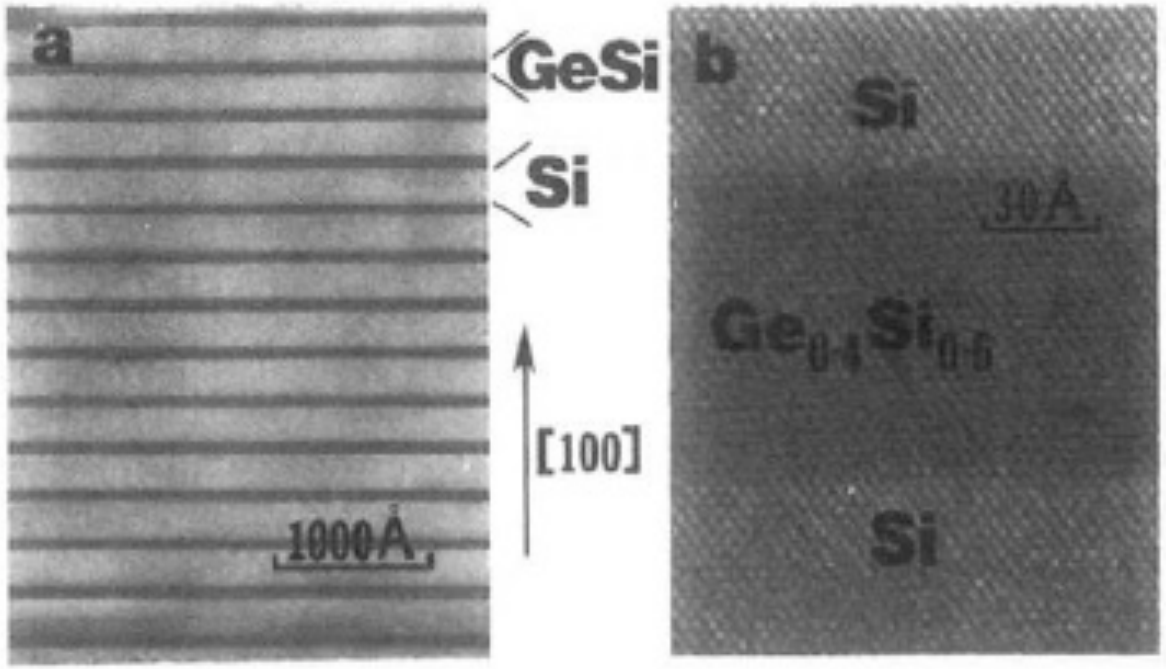

Figure 8-29 (a) Cross-sectional TEM image of $Ge_{0.4}Si_{0.6}$–Si strained-layer superlattice. (b) High-resolution lattice image. (Courtesy of J. C. Bean and R. Hull, AT&T Bell Laboratories.)

Wichtige Anwendung:
Epitaktische Verbindungshalbleiter-Viellagenschichten

Quelle: Ohring

Viellagenschichten: größenabhängige Phasenstabilitätskontrolle

Sequential deposition techniques such as molecular beam epitaxy, atomic layer deposition, physical vapor deposition, and chemical vapor deposition, and solution methods are powerful approaches to create heterostructures by stacking two or more chemically different layers along a given stacking direction. Many of the unique and interesting properties of heterostructures result from the finite thicknesses of the individual layers and the resulting interfacial states between each constituent. These approaches are powerful because they create designed artificial structures that are inaccessible by bulk synthesis techniques, as exemplified by the synthesis of a family of ordered materials consisting of intergrowth layers of SnSe and $MoSe_2$ (Figure 12).[14] These studies confirm that the structure, order, and thickness of the constituent layers can be controlled by matching structures with that of their precursors.

Conceptually, heterostructures provide both experimentalists and theorists with reasonably well-defined targets, in which the interleaved layers are very likely to be at least local free energy minima. Furthermore, these structures enable theorists to explore the expected properties of currently unknown materials with reasonable assurance that the structures could be made. For experimentalists, the challenge is to control the reaction pathway, avoiding more thermodynamically stable atomic arrangements and allowing atoms to diffuse as the desired interleaved structure forms.

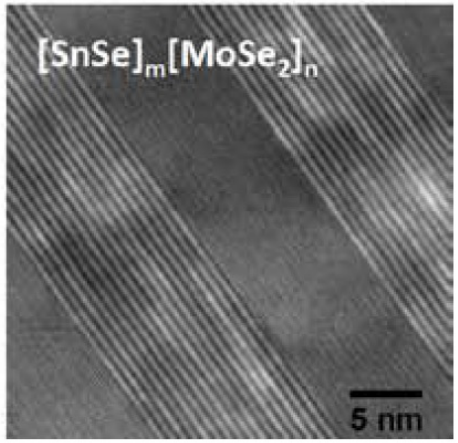

Figure 12. Alternating SnSe/$MoSe_2$ layers define a new phase deposited by a physical vapor deposition method. A bulk composition of layered Sn-Mo-Se phase has not been reported.[14] *| Reprinted with permission from M. Beekman et al., "Controlling Size-Induced Phase Transformations Using Chemically Designed Nanolaminates." Angewandte Chemie International Edition 52(50), 13211–14 (2013). DOI: 10.1002/anie.201305377. © 2013 John Wiley and Sons.*

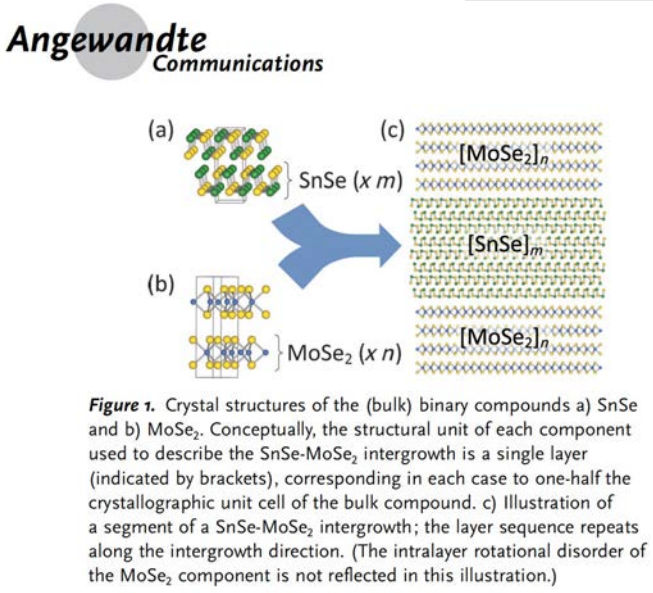

Figure 1. Crystal structures of the (bulk) binary compounds a) SnSe and b) $MoSe_2$. Conceptually, the structural unit of each component used to describe the SnSe-$MoSe_2$ intergrowth is a single layer (indicated by brackets), corresponding in each case to one-half the crystallographic unit cell of the bulk compound. c) Illustration of a segment of a SnSe-$MoSe_2$ intergrowth; the layer sequence repeats along the intergrowth direction. (The intralayer rotational disorder of the $MoSe_2$ component is not reflected in this illustration.)

Quelle: Basic Research Needs for Synthesis Science, Angewandte Chemie 2013

Materialsynthese: In situ Charakterisierungsmethoden

RUB

in situ Charakterisierung der Struktur und Kristallinität mittels **Synchrotronstrahlung** oder **Neutronenstrahlung**

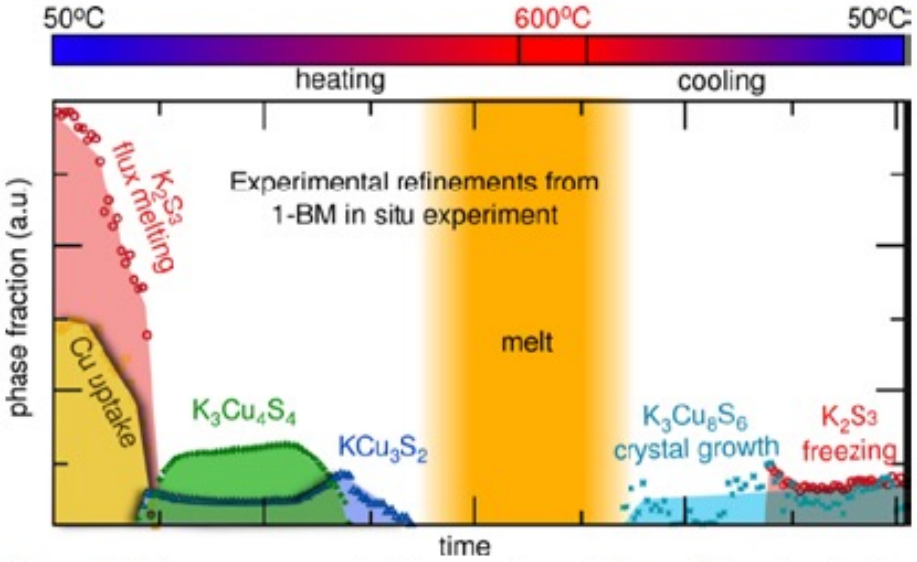

Figure 16. Time sequence in the reaction of Cu + K_2S_3 using in situ synchrotron radiation. The in situ diffraction data reveal that, on heating, the $K_3Cu_4S_4$ and KCu_3S_2 materials form, maximize their yield, and disappear as the temperature increases. When the molten temperature is reached, all phases dissolve; and when the cooling begins, the only compound forming is $K_3Cu_8S_6$, the sole reaction product.[45] | *Reprinted by permission from D. P. Shoemaker et al. "In Situ Studies of a Platform for Metastable Inorganic Crystal Growth and Materials Discovery." PNAS 111[30]: 10922–27. DOI: 10.1073/pnas.1406211111.*

Basic Research Needs for Synthesis Science

Modern advances toward in situ diagnostics promise to revolutionize our understanding and practice of crystal growth and synthesis. For example, in situ, real-time neutron imaging (Figure 45) is being developed to provide direct observation of large-scale Bridgman crystal growth.[99] When deployed, neutron imaging will enable growers to directly "see" the phase change occurring in processes that have heretofore been carried out blindly. Such developments are synergistic with the computational models mentioned earlier for validation and interpretation, offering a means for feedback, optimization, and on-the-fly changes to parameters to control crystal growth in target compounds that require the most stringent control of purity, homogeneity, or other characteristics. This style of active monitoring with feedback can be extended to other crystal synthesis techniques, such as hydrothermal synthesis, to achieve the goal of optimized synthesis conditions in a complex parameter space.

Finally, solution growth of crystals has historically relied on a set of "usual suspect"

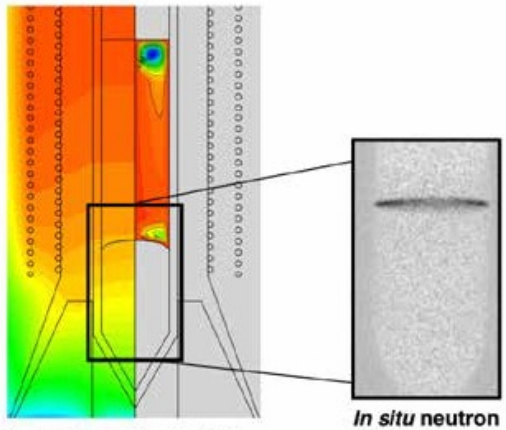

Figure 45. Continuum models of heat and mass flow during Bridgman growth (left) can be monitored in situ using neutron imaging, which shows the melt interface. In the future, feedback control of growth is envisioned. *Image courtesy of J. Derby.* | *Reprinted with the permission of Nature Publishing Group from A. S. Tremsin et al. 2017. "Real-Time Crystal Growth Visualization and Quantification by Energy-Resolved Neutron Imaging." Scientific Reports 7 [46275]. DOI: 10.1038/srep46275. Distributed under the terms of the Creative Commons Attribution 4.0 International [CC BY 4.0] License.*

Quelle: Basic Research Needs for Synthesis Science

Advanced Materials Processing and Microfabrication

Dünne Schichten und Oberflächen im Maschinenbau

Oberflächenprozessierung

Durch Oberflächenprozessierung werden Werkstoffe mit makroskopischen Abmessungen („bulk“) **funktionalisiert**, d.h. zusätzliche Funktionen durch Herstellung und Modifikation von Grenzflächen im Nanometer- bis Mikrometerbereich.

Oberflächenmodifikation

z.B. Dotieren, Oxidieren

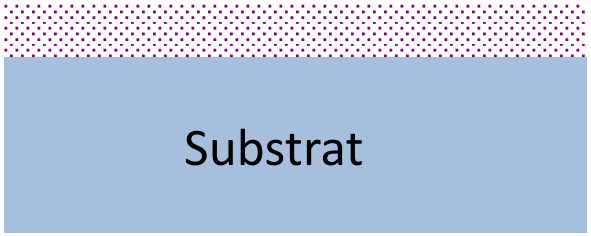

Schichtaufbringung und -strukturierung:

Schicht-Substrat-Verbunde

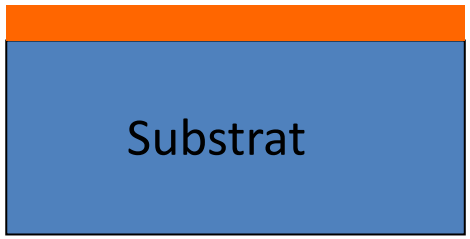

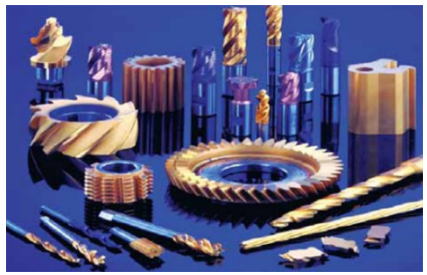

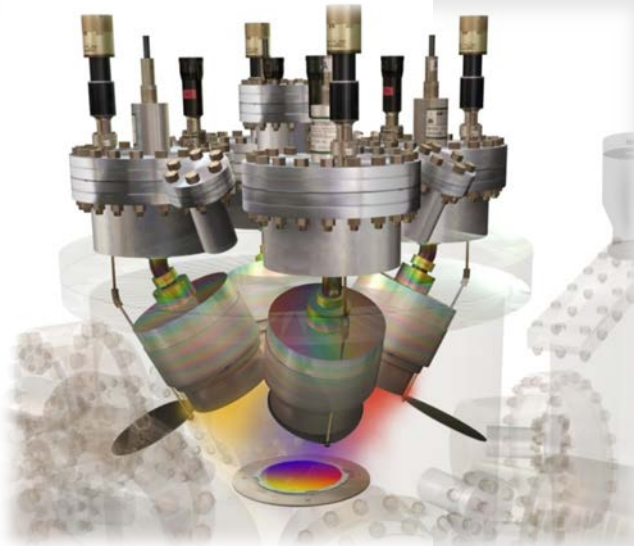

Dünne Schichten

Wozu dünne Schichten?

RUB

Anwendungen in Industrie und Forschung

- Gezielte Änderung der Oberflächeneigenschaft(en)
- Zusätzliche Eigenschaften, die im Grund-Volumenkörper nicht vorhanden oder möglich sind
- Effiziente Untersuchung von Materialeigenschaften (weniger Materialvolumen)
- Untersuchung von neuen Materialeigenschaften die nur in dünnen Schichten möglich sind Dünnschicht und „bulk“-Eigenschaften sind oft unterschiedlich

Eigenschaften

- Mechanisch: Härte, tribologische Eigenschaften, Reibung, Verschleiß
- Chemisch: Korrosion, Katalyse
- Elektrisch: Leitfähigkeit (Metall, Halbleiter, Isolator
- Optisch: Transmission, Reflektion, Absorption, Farbe
- Magnetisch: Speicherfähigkeit, Abschirmung
- Biologisch: Biokompatibiltät, Benetzungseigenschaften
- Barriereschichten: Lebensmittelverpackungen

Dünne Schichten

Beispiel Spiegel

Historisch:
Polierte Metallplatten (Cu, Ag),
Amalgamschichten (Hg, Sn)
1835 J. von Liebig: „[…] wenn man Aldehyd mit einer Silbernitratlösung mischt und erhitzt, scheidet sich Silber auf der Wand des Glases ab und es entsteht ein brillanter Spiegel.“

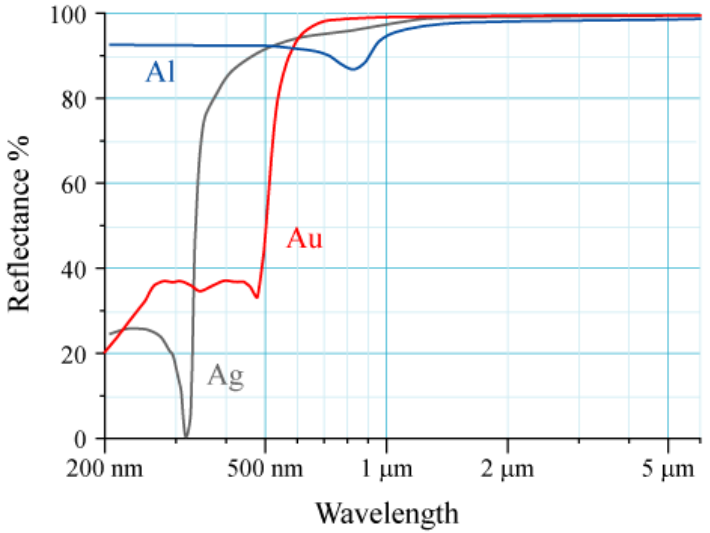

Quelle: Wikipedia

heute Glas + Al-Schicht

Aber auch nichtdurchsichtige glatte Körper können beschichtet werden und als Spiegel genutzt werden.

Grundkonzept: Veredelung eines günstigen Grundkörpers durch Beschichtung

Schichtherstellungstechnologien

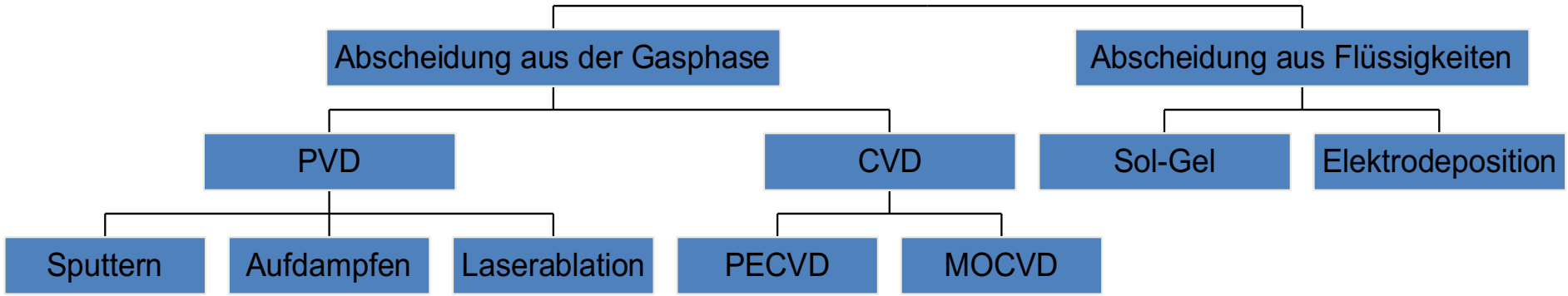

PVD: Physical Vapor Deposition
CVD: Chemical Vapor Deposition
PECVD: Plasma Enhanced CVD
MOCVD: Metal Organic CVD

Dünne Schichten
Anwendungen

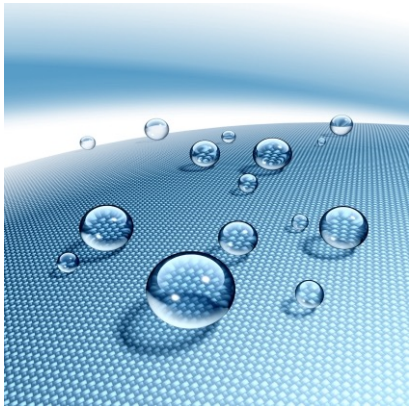

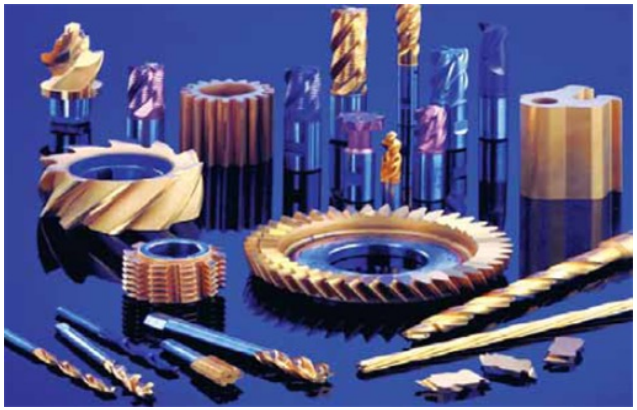

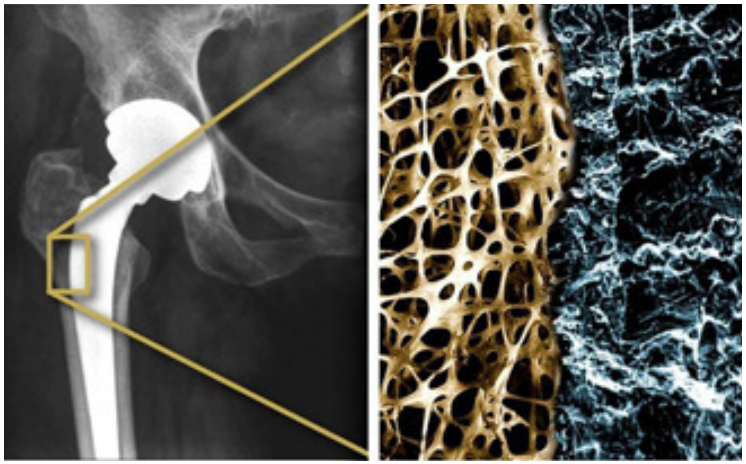

Oberbach, Mathys Orthopädie GmbH

➢ Tribologische Beschichtungen

- verschleißfeste Hartstoff-/Schutzschichten
- Passivierung
- Antihaftbeschichtung
- Haftvermittlung
- Erhöhung der chemischen Beständigkeit
- ...

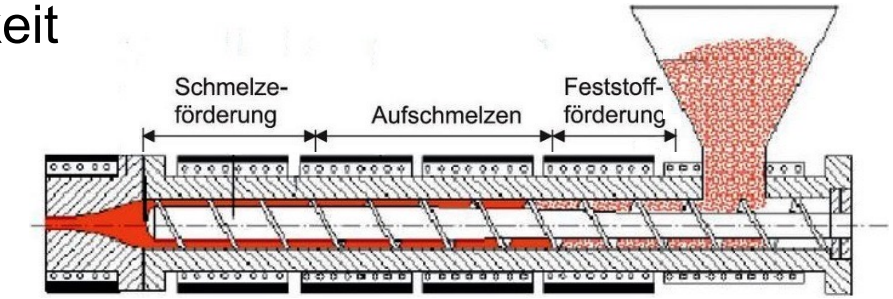

Advanced Materials Processing and Microfabrication

Dünne Schichten und Oberflächen im Maschinenbau

- Beschichtungstechnologien (Galvanik, PVD, CVD)
- Beispiele für wichtige Schichtsysteme
  - Schutzschichtsysteme (TiN, TiAlN, CrAlN)
  - thermische Barriereschichten
  - …

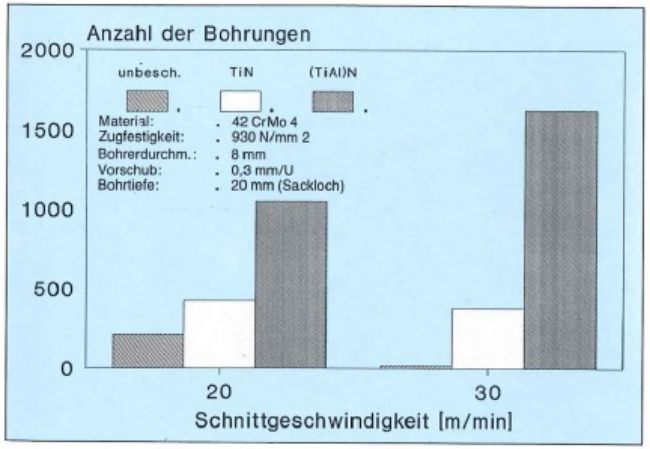

Vorlesung Beschichtungstechnik RUB
Prof. Dr. R. Vaßen

TiN beschichteter Wälzfräs
und Bohrer

Oberflächentechnik,
Verlag Moderne Industrie

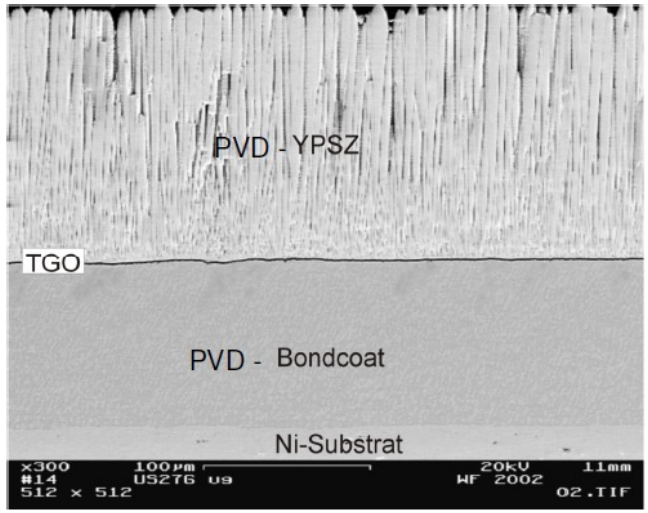

U. Schulz,
DLR Köln

Vorlesung Beschichtungstechnik RUB
Prof. Dr. R. Vaßen

Hartstoffschichtsysteme: TiN und TiAlN, Diamant

- TiN: NaCl-Struktur
  - hohe Härte
  - Diffusionsbarriere
  - elektrische Leitfähigkeit
  - optische Eigenschaften
- Ti-Al-N
- Diamant

Stukturzonendiagramm für das Aufdampfen (Movchan & Deminishin)

Prozessparameter beeinflussen Gefüge der Schichten,

hier: **Substrattemperatur**

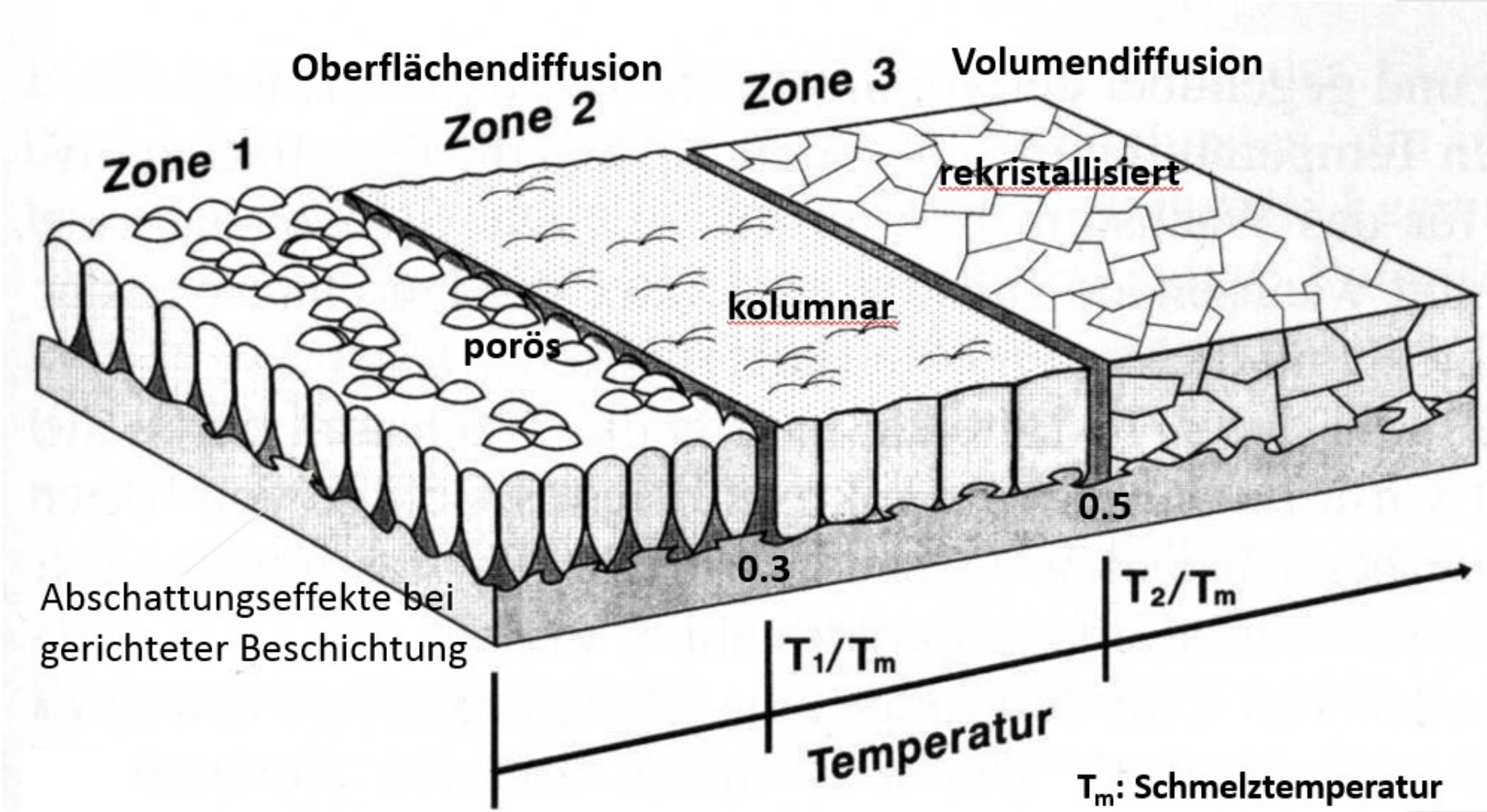

Abschattungseffekte bei gerichteter Beschichtung

RUB

Advanced Materials Processing and Microfabrication

Einige spezielle Material-Synthesemethoden

Advanced Materials Processing and Microfabrication

Festkörperreaktionen (solid state reactions)

Synthese anorganischer Festkörper durch Reaktion von Pulvern bei erhöhter Temperatur

Langsamer Prozess, aufgrund nötiger Diffusionswege (Pulver sind nicht auf atomarer Ebene gemischt)

Beispiel: Reaktion von MgO und Al_2O_3 zu Spinell $MgAl_2O_4$

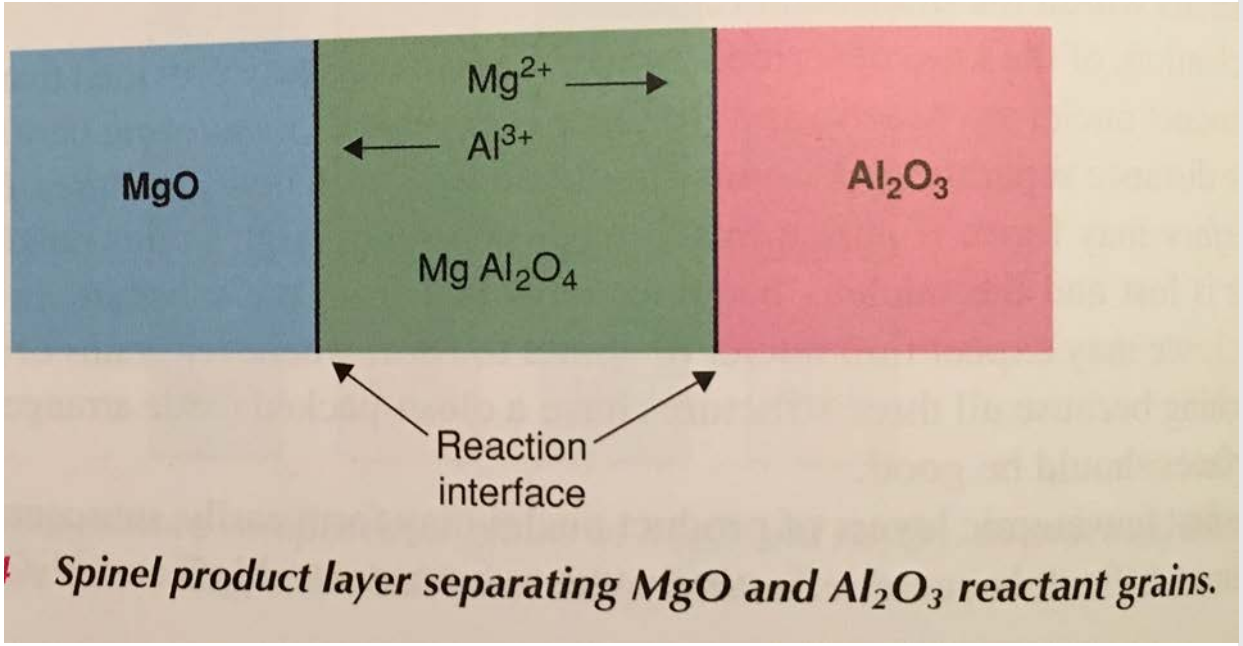

Spinel product layer separating MgO and Al_2O_3 reactant grains.

Quelle: A. West

Herstellung von amorphen metallischen Systemen

amorphe Metalle:
„Metglas“
typ.: $(Fe\text{-}Co)_{80}(B\text{-}Si\text{-}C)_{20}$

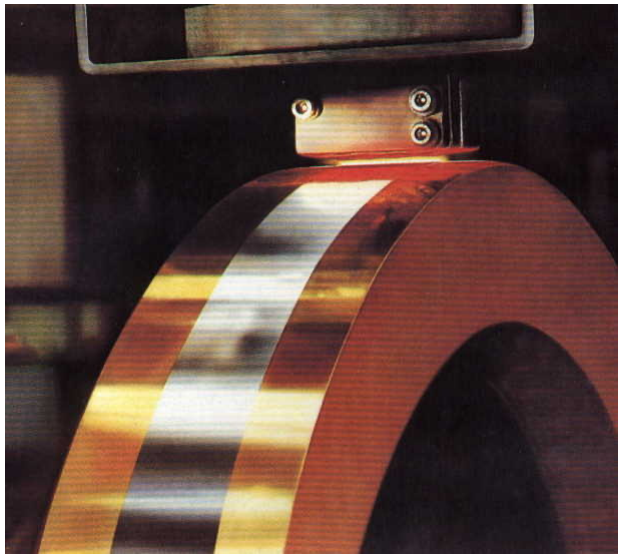

Sputtern

Melt-Spinning

Herstellung von amorphen Bändern

Abkühlgeschwindigkeit:
10.000 – 1.000.000 K/s

Bulk metallic glases

http://www.youtube.com/watch?v=L00HbH8Vla8

Advanced Materials Processing and Microfabrication

Hochdruckphasen: Charakterisierung in der Diamant-Stempelzelle

In kleinen Probenvolumina können extreme Drücke (> 100 GPa) erreicht werden

„diamond anvil cell“ (1958), zwei geschliffene Diamanten, abgeschlossener Raum, hydraulische Übertragung. Kleine Abmessungen ermögliche optischen Zugang durch transparente Diamanten für in situ Messungen. Heizen und elektrische Messungen der Probe sind auch möglich.

<u>Optisches Messverfahren</u>
zur Bestimmung des Druckes (Rubin-Fluoreszenz, druckabhängige Verschiebung der Fluoreszenzlinien), Vergleich mit Rubin Referenzprobe die 1% des Probenvolumens einnimmt.

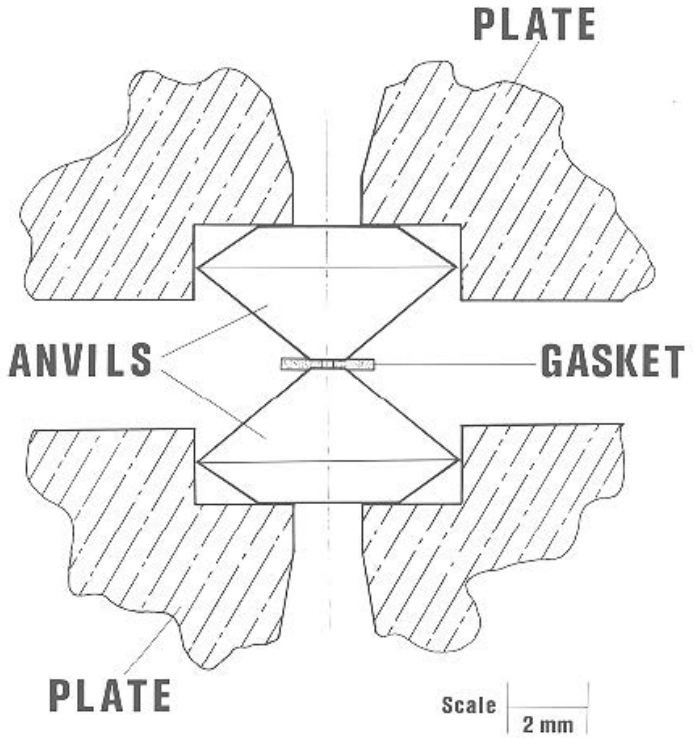

Fig. 4. A schematic diagram of the opposed diamond anvil assembly to illustrate the 180° optical transmission characteristics and the concept of Bridgman opposed anvils. A thin metal gasket containing a 250 μm diameter hole for encapsulating a sample (liquid or solid or both) is squeezed between the two anvils.

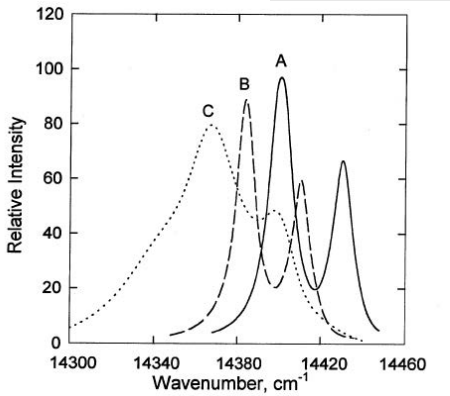

Fig. 6. The R-line luminescence spectrum of ruby in the DAC: curve A, ruby at ambient atmospheric pressure; curve B, ruby in a mixture of ices VI and VII at about 2.2 GPa; curve C, ruby in a nonhydrostatic mixture of CCl_4 III and IV at about 4 GPa.

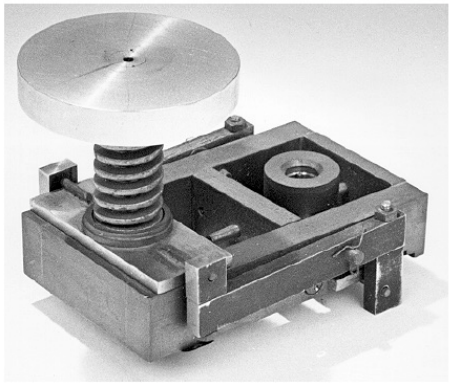

Fig. 1. The original DAC, on display in the NIST Museum.

http://nvlpubs.nist.gov/nistpubs/sp958-lide/100-103.pdf

Hochdruckphasen: Charakterisierung in der Diamant-Hochdruckzelle

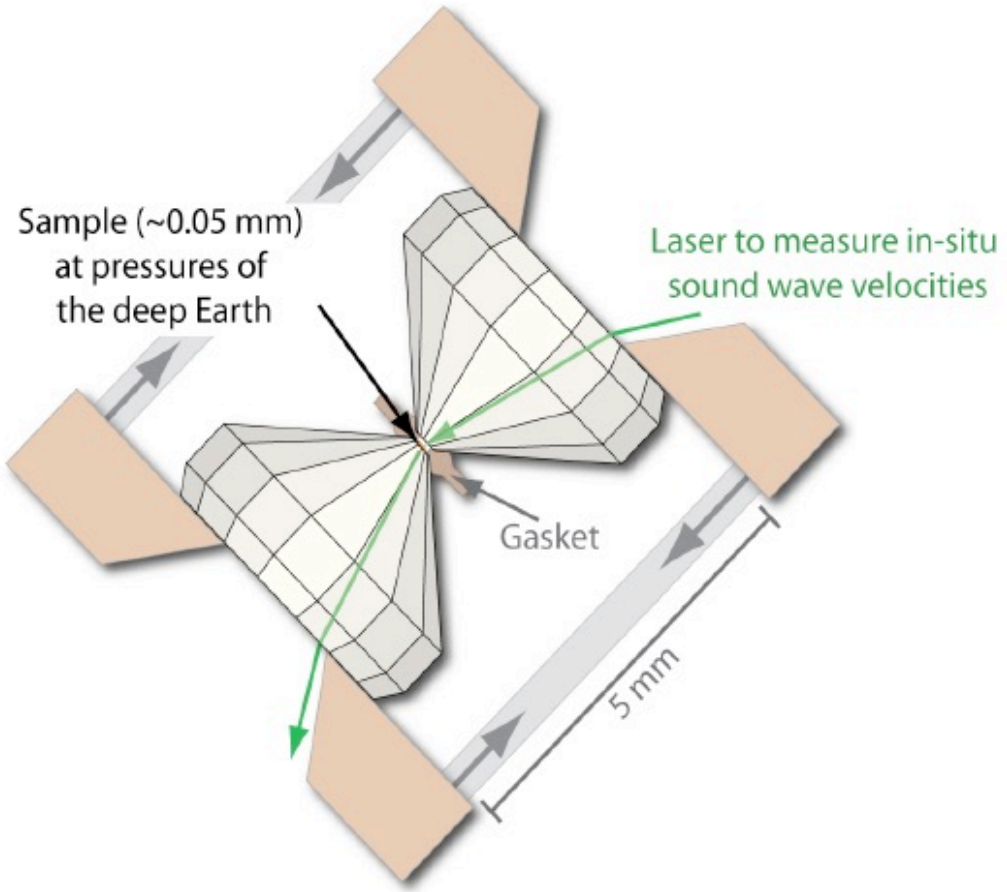

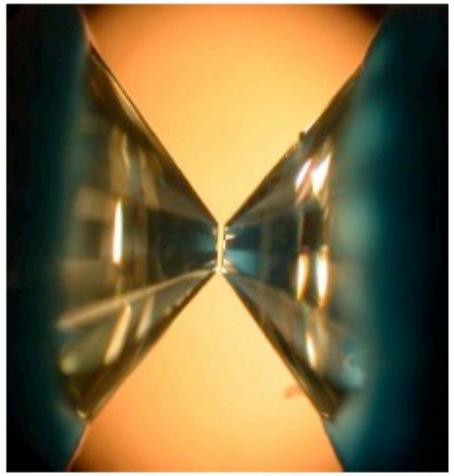

GFZ Helmholtz-Zentrum Potsdam

HELMHOLTZ GEMEINSCHAFT

Hochdruckphasen: Synthese und Charakterisierung in der Diamant-Hochdruckzelle

ACS central science

Research Article

http://pubs.acs.org/journal/acscii

Discovery of $FeBi_2$

James P. S. Walsh,[†] Samantha M. Clarke,[†] Yue Meng,[‡] Steven D. Jacobsen,[§] and Danna E. Freedman*

[†]Department of Chemistry, Northwestern University, Evanston, Illinois 60208, United States
[‡]HPCAT, Geophysical Laboratory, Carnegie Institution of Washington, Argonne, Illinois 60439, United States
[§]Department of Earth and Planetary Sciences, Northwestern University, Evanston, Illinois 60208, United States

Supporting Information

ABSTRACT: Recent advances in high-pressure techniques offer chemists access to vast regions of uncharted synthetic phase space, expanding our experimental reach to pressures comparable to the core of the Earth. These newfound capabilities enable us to revisit simple binary systems in search of compounds that for decades have remained elusive. The most tantalizing of these targets are systems in which the two elements in question do not interact even as molten liquids—so-called immiscible systems. As a prominent example, immiscibility between iron and bismuth is so severe that no material containing Fe–Bi bonds is known to exist. The elusiveness of Fe–Bi bonds has a myriad of consequences; crucially, it precludes completing the iron pnictide superconductor series. Herein we report the first iron–bismuth binary compound, $FeBi_2$, featuring the first Fe–Bi bond in the solid state. We employed geologically relevant pressures, similar to the core of Mars, to access $FeBi_2$, which we synthesized at 30 GPa and 1500 K. The compound crystallizes in the Al_2Cu structure type (space group $I4/mcm$) with a = 6.3121(3) Å and c = 5.4211(4) Å. The new binary intermetallic phase persists from its formation pressure of 30 GPa down to 3 GPa. The existence of this phase at low pressures suggests that it might be quenchable to ambient pressure at low temperatures. These results offer a pathway toward the realization of new exotic materials.

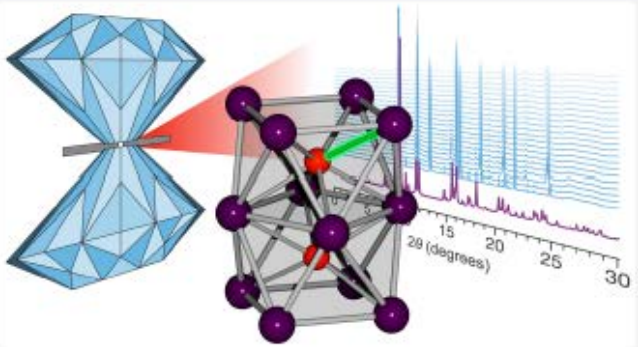

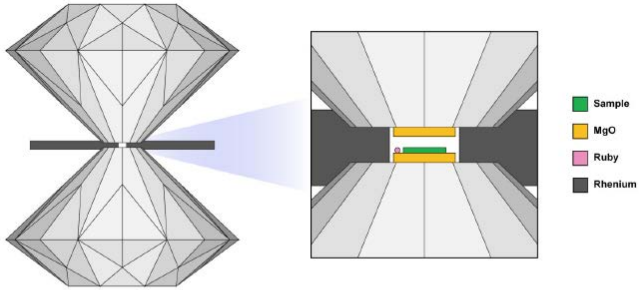

Figure S2 | Side-view schematic of the DAC after closing the cell and before the initial pressurization. MgO discs are placed on the center of the upper and lower diamond culets. The MgO acts simultaneously as the pressure medium, the pressure calibrant, and the thermal insulation between the sample and the diamonds. The sample, which is a pressed flake of iron and bismuth with a thickness of around 10 μm, is placed on top of the lower MgO piece along with a ruby sphere. The top diamond is lowered carefully into place so that it settles into the indentation and delivers the upper MgO disc to the sample chamber. Upon compression, the sample chamber collapses so that the MgO fills the volume, holding the sample flake and ruby in the center of the chamber.

http://pubs.acs.org/doi/suppl/10.1021/acscentsci.6b00287/suppl_file/oc6b00287_si_001.pdf

http://pubs.acs.org/doi/abs/10.1021/acscentsci.6b00287

RUB

Advanced Materials Processing and Microfabrication

Microfabrication

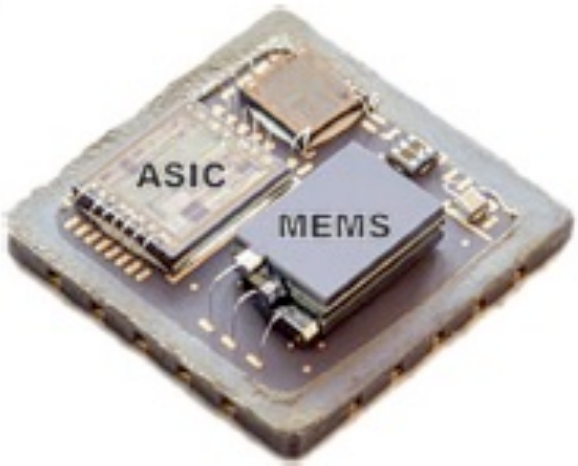

Technologien und Werkstoffe

Mikrosystem:
Mikroelektronik
+
Mikrosensoren
Mikroaktoren
Hilfsstrukturen

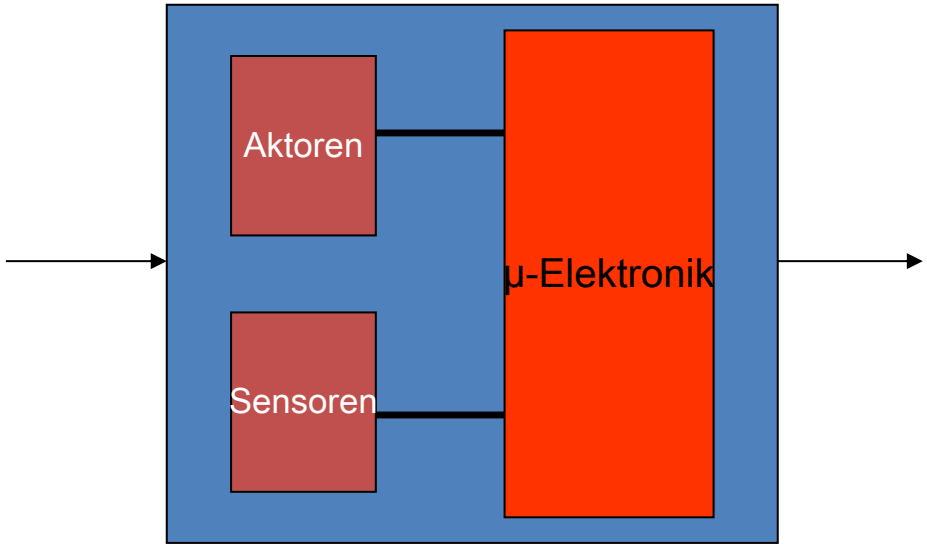

- Photolithographie
- LIGA, Si-Micromachining
- Dünnschichttechnik (PVD,CVD, Ätzen)
- Aufbau- + Verbindungstechnik

+

- Strukturwerkstoffe
- Funktionswerkstoffe
- Hilfswerkstoffe

Konzepte und Besonderheiten der Mikrosystemtechnik

RUB

Mikrostrukturierung:

eine oder mehrere Dimensionen im Mikrometerbereich

Matrixanordnung von Sensoren und Aktoren (Arrays):

z.B. Sensor-Array mit abgestuften Empfindlichkeiten

Batchherstellung:

Fertigungsverfahren zur parallelen Herstellung einer großen Bauteilanzahl auf einem Wafer, bzw. parallele Bearbeitung mehrerer Wafer in einem Prozeßschritt

Genauigkeit:

Reproduzierbare Herstellung von Strukturen mit Abmessungen um 1 µm, z.B. mittels Photolithographie

Erzeugung von Mikrostrukturen durch Photolithographie und weitere Prozessschritte

Photolithographie

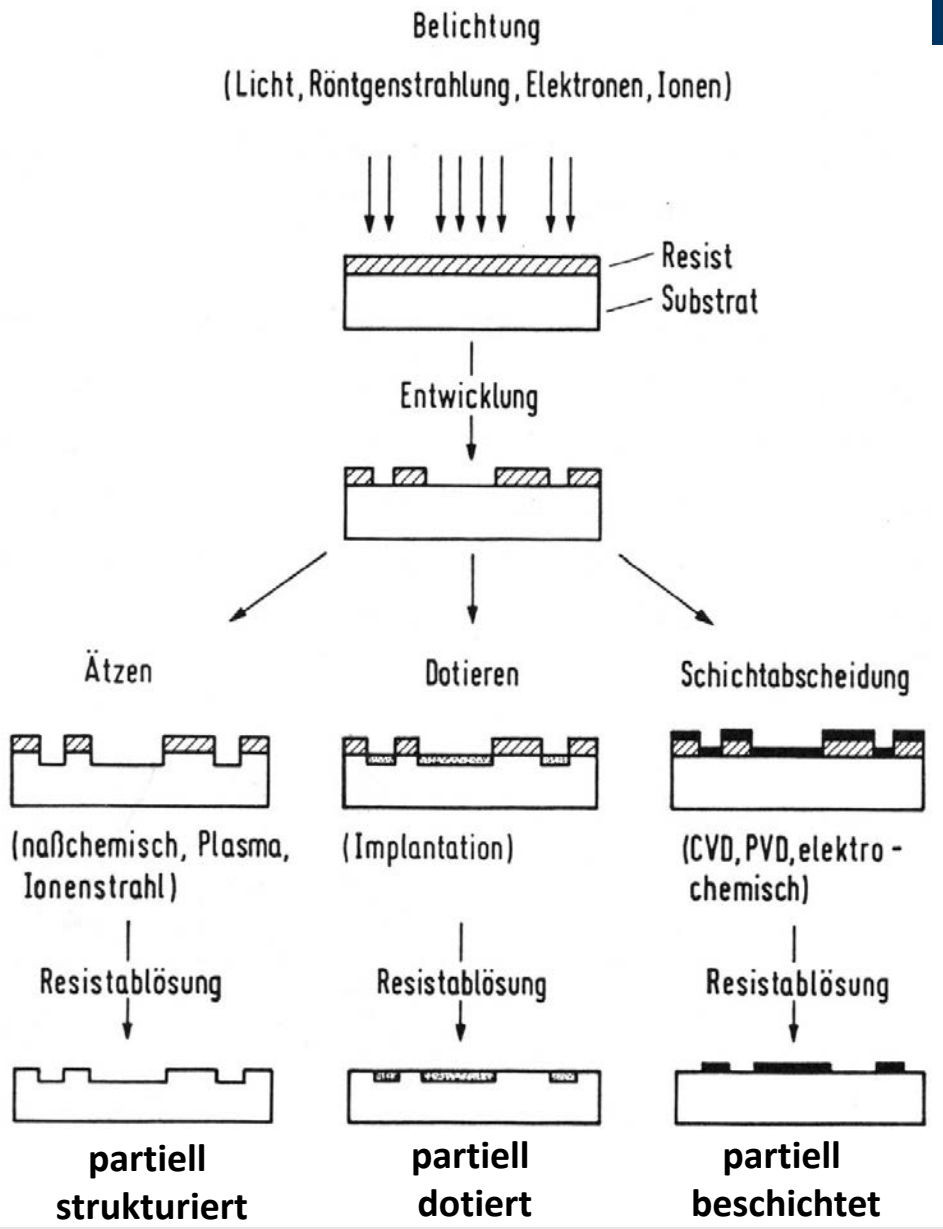

Strukturübertragung

Resist muss gegenüber dem Strukturübertragungsprozess widerstandsfähig (resistent) sein

$T_{Prozess}$< 200°C (Polymer)

Quelle:Büttgenbach

Advanced Materials Processing and Microfabrication

Photolithographie

Photolithographie → Maskierung

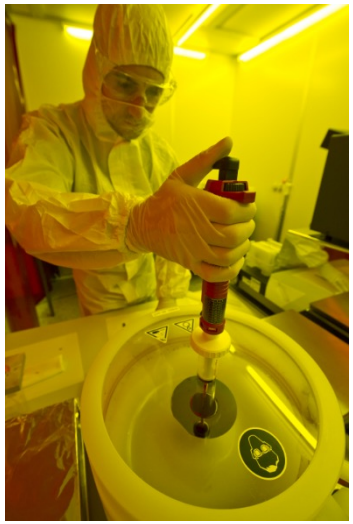

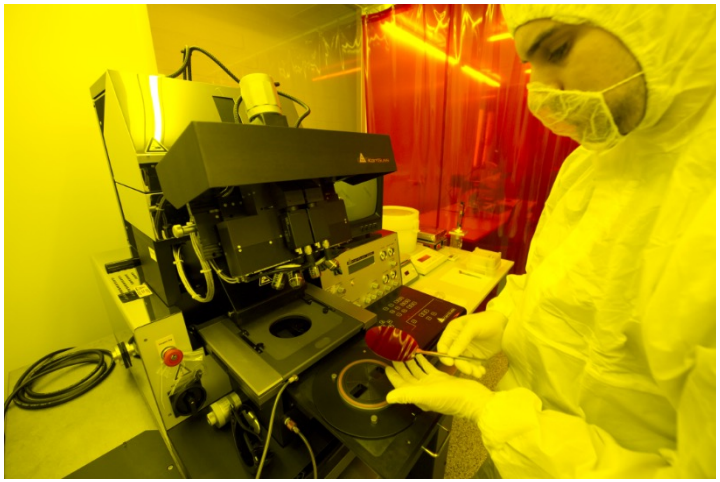

- Strukturierung durch UV Licht
- Schlüsseltechnologie für Mikroelektronik und Mikrosystemtechnik
- großflächige Belichtung
- Auflösung < 1 µm

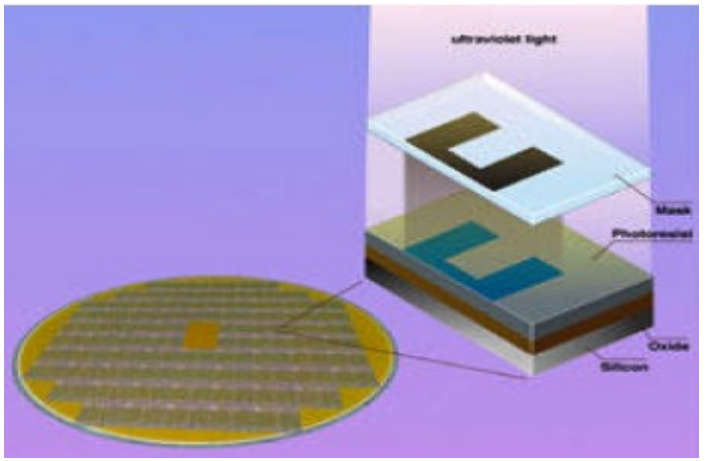

Photolithographie

- positive Resists: belichtete Flächen werden entwickelt
- negative Resists: belichtete Flächen werden unlöslich

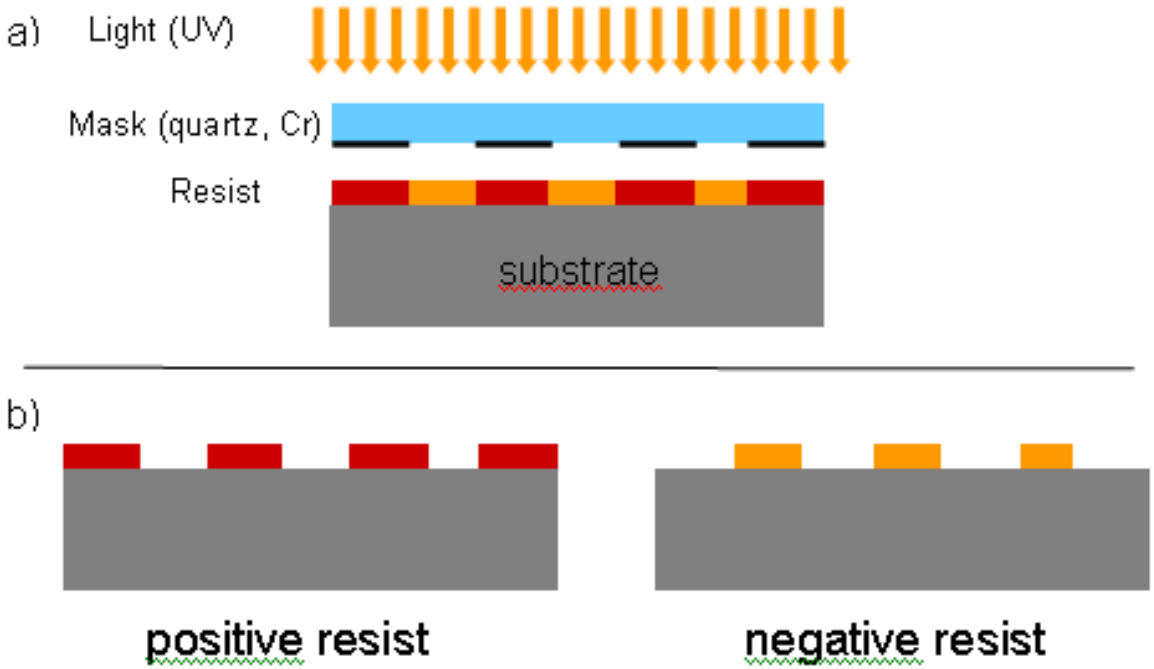

Advanced Materials Processing and Microfabrication

Si-Ätztechnik

Si-Oberflächenmikrotechnik

Si-Volumenmikrotechnik

Advanced Si Etching (ASE)

MEMS und Nanotechnologie

Mikrotechnik als „Werkzeug“ für die Materialforschung

RUB

Mikroheizer

zur in situ kontrollierten Prozessierung von dünnen Schichten

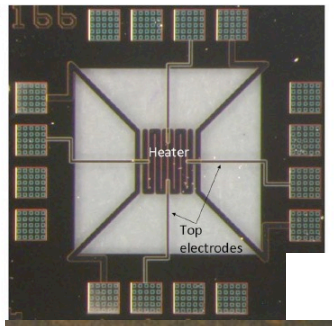

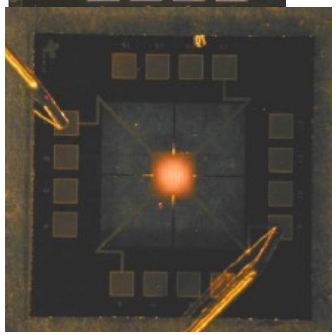

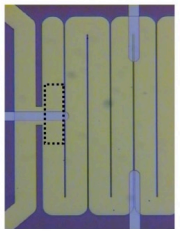

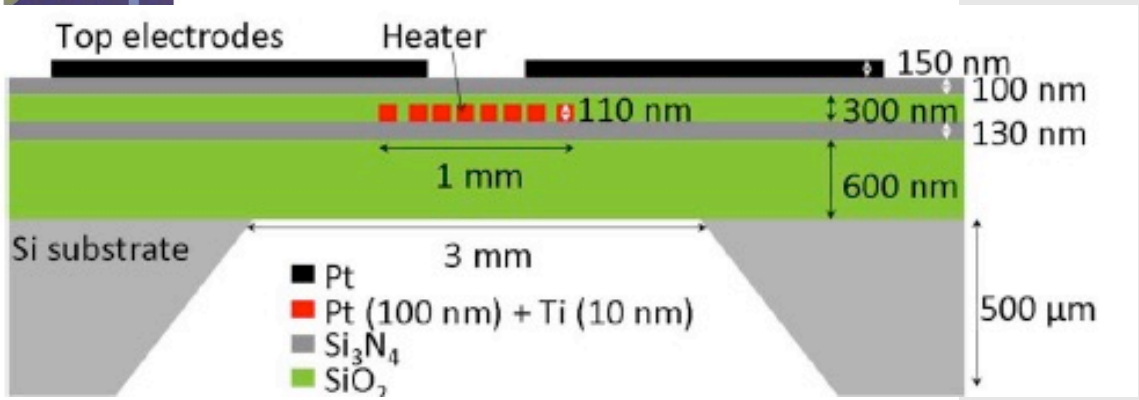

Mikrostrukturierte Systeme für in situ TEM

a) Membranen
b-c) Plattformen für in situ Messungen

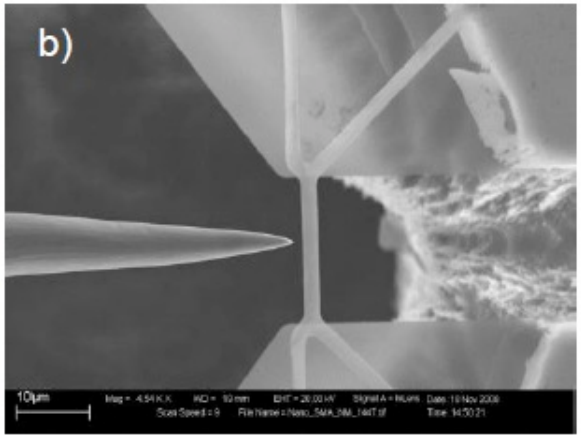

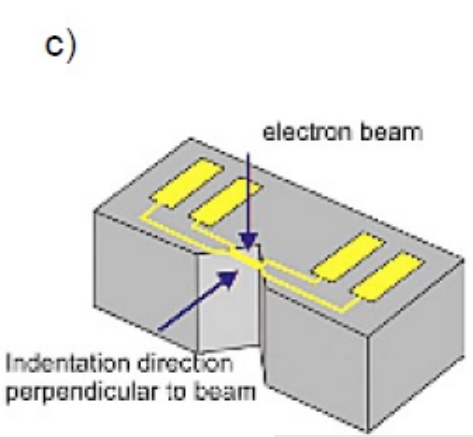

Ludwig et al. (2008) Sensors and Actuators A, 147, 576
Ludwig et al. (2010) JMEMS19 (5), 1264

MEMS und Nanotechnologie

Mikrotechnik als Werkzeug für die Nanotechnologie

Beispiel:

Scanning Probe Microscopy

AFM Spitzen

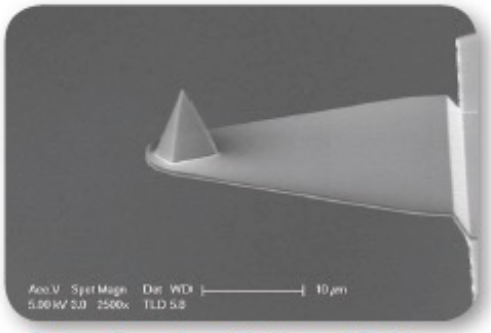

Bruker Broadband™ Air and Fluid Cantilevers.

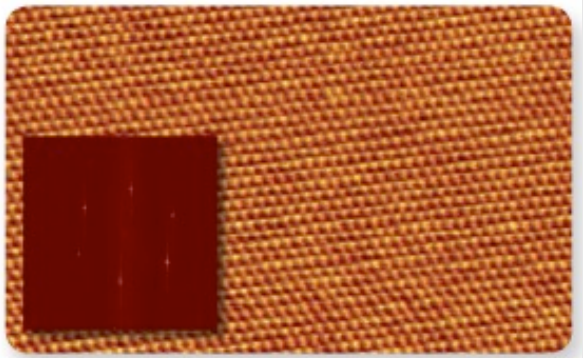

Atomically resolved lattice of mica imaged in contact mode at 0.6Hz.

Beispiel:

Atomsondentomographie

Spitzen

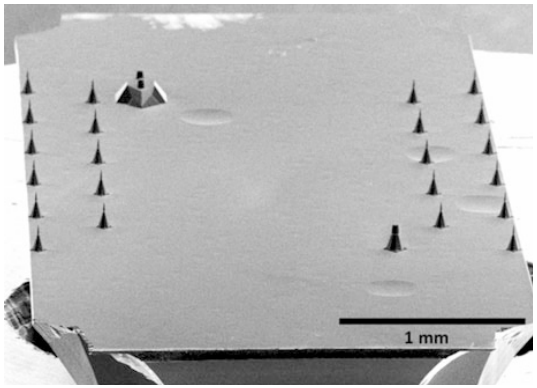

REM Bild eines Mikrospitzenarrays für APT. Ätzmasken für die Spitzenätzung werden durch RIE hergestellt. (Larson et al., Local Electrode Atom Probe Tomography 2011)

Mikrosysteme für die Materialforschung: Miniaturisierte Zugversuche im REM und TEM

In-situ Tensile Testing of Nano-scale Specimens in SEM and TEM

by M. A. Haque and M. T. A. Saif

ABSTRACT—We present a new experimental method for the mechanical characterization of freestanding thin films with thickness on the order of nanometers to micrometers. The method allows, for the first time, in-situ SEM and TEM observation of materials response under uniaxial tension, with measurements of both stresses and strains under a wide variety of environmental conditions such as temperature and humidity. The materials that can be tested include metals, dielectrics, and multi-layer composites that can be deposited/grown on a silicon substrate. The method involves lithography and bulk micromachining techniques to pattern the specimen of desired geometry, release the specimen from the substrate, and co-fabricate a force sensor with the specimen. Co-fabrication provides perfect alignment and gripping. The tensile testing fits an existing TEM straining stage, and a SEM stage. We demonstrate the proposed methodology by fabricating a 200 nm thick, 23.5 μm wide, and 185 μm long freestanding sputter deposited aluminum specimen. The testing was done in-situ inside an environmental SEM chamber. The stress–strain diagram of the specimen shows a linear elastic regime up to the yield stress σ_y = 330 MPa, with an elastic modulus E = 74.6 GPa.

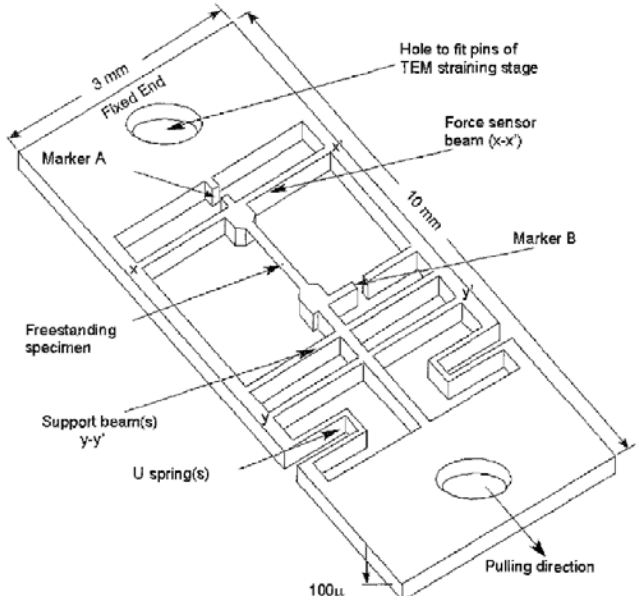

l—Schematic diagram of the tensile testing chip

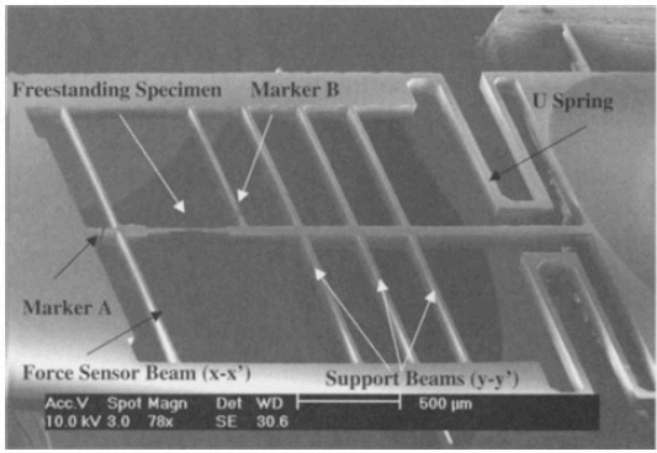

Fig. 4—SEM image of the tensile test chip

Haque, M.A.; Saif, M.T.A. Experimental Mechanics (2002) 42: 123. doi:10.1007/BF02411059

Mikrosysteme für die Materialforschung: Miniaturisierte Zugversuche im REM und TEM

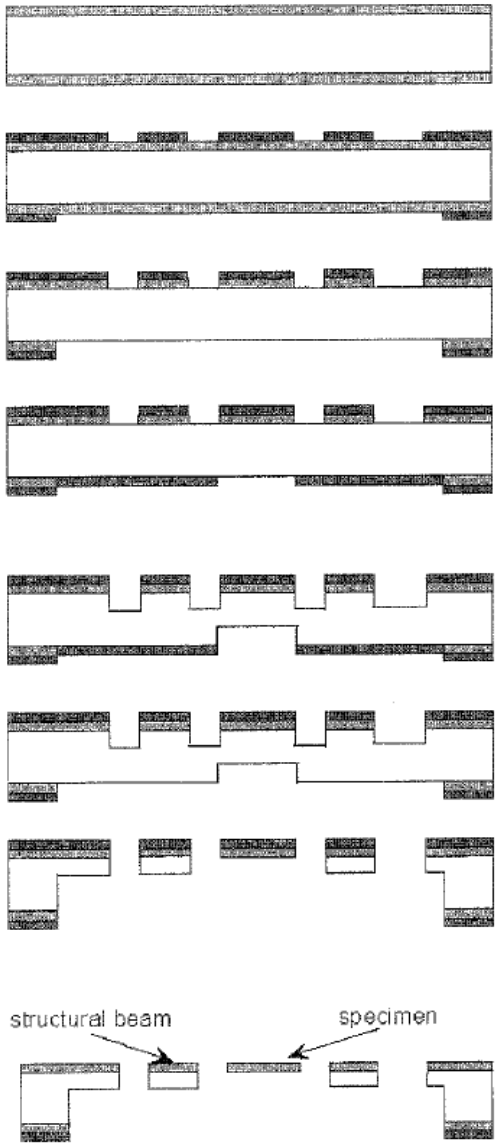

Sputter deposition of Aluminum on both sides of wafer

Pattern the test chip on the front side, and etch mask on the backside of the wafer

Etching of Aluminum on both sides of wafer.

Pattern etch-mask on the backside side, aligned to cover exactly the gauge length portion of the specimen.

Etch 100 microns by Deep Reactive Ion Etching (DRIE) process[13]

Remove the photoresist on the backside by O_2 plasma.

Through the wafer etch from backside to release gauge length, and produce the structural beams.

Remove the remaining layer of photoresist from the front side of the wafer.

—Tensile testing chip fabrication process schematic

Haque, M.A.; Saif, M.T.A. Experimental Mechanics (2002) 42: 123. doi:10.1007/BF02411059

Advanced Materials Processing and Microfabrication

Mikrosysteme für die Materialforschung

small
Nanowires

In Situ Electron Microscopy Four-Point Electromechanical Characterization of Freestanding Metallic and Semiconducting Nanowires

*Rodrigo A. Bernal, Tobin Filleter, Justin G. Connell, Kwonnam Sohn, Jiaxing Huang, Lincoln J. Lauhon, and Horacio D. Espinosa**

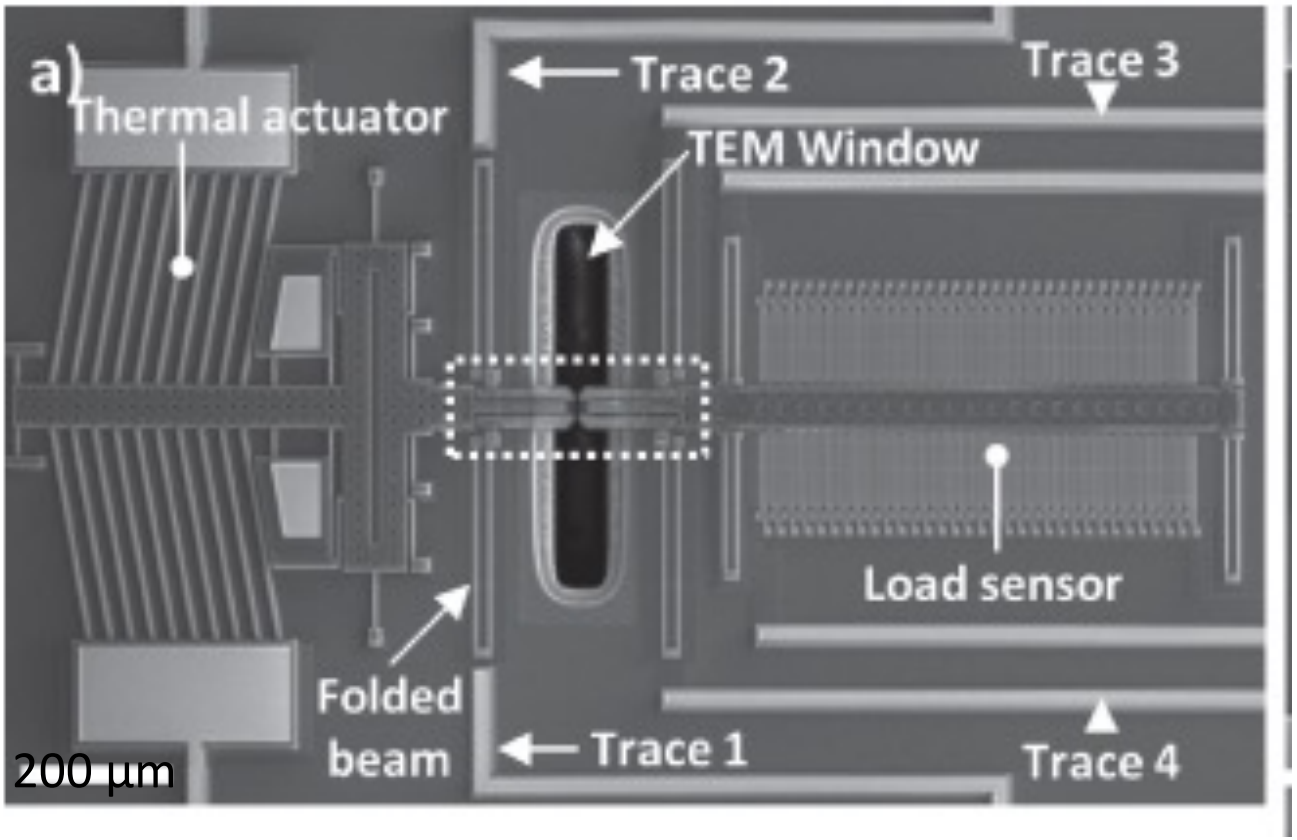

Mikrosysteme für die Materialforschung

Four Point Electromechanical Characterization of Freestanding Nanowires

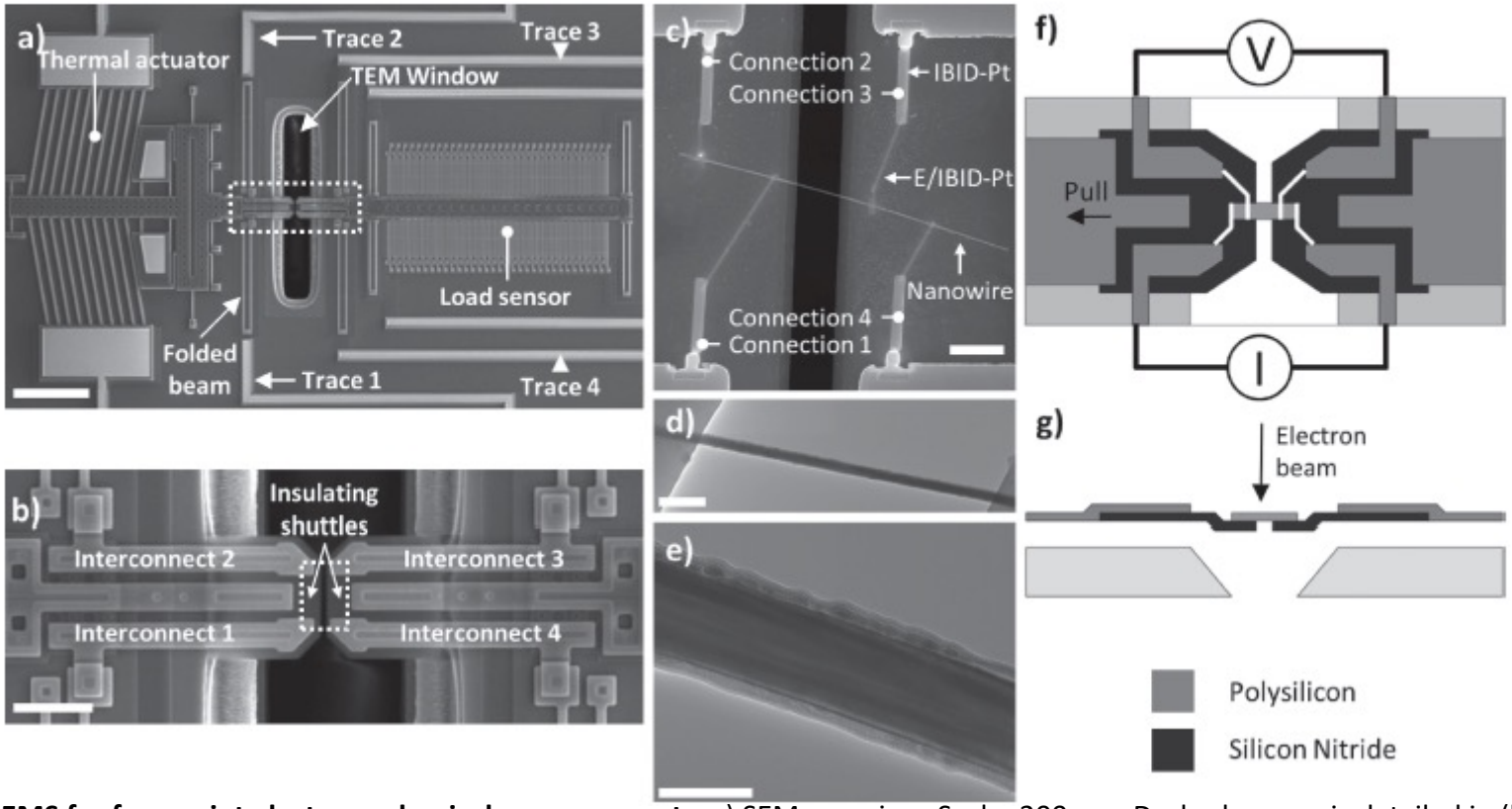

MEMS for four-point electromechanical measurements. a) SEM overview. Scale: 200 µm. Dashed square is detailed in (b). The folded beams (u-shaped) shown in (a) provide electrical connections, extend on top of silicon nitride shuttles and come close to where the specimen is placed. The platforms ensure insulation among the 4 specimen connections and between other signals used to operate the device. Scale bar: 40 µm. A detail of the dashed square is provided in (c) where a nanowire laid on the insulating shuttle and connected in four-point configuration is shown. Scale bar: 4 µm. d,e) TEM images, as viewed through the TEM window, of the same nanowire in (c) are shown (300 nm and 100 nm scale bar, respectively). f) Top-view schematic of the device operation for four-point measurements. g) Cross-section of the device.

Advanced Materials Processing and Microfabrication

Mikrosysteme für die Materialforschung

TEM Anwendungen

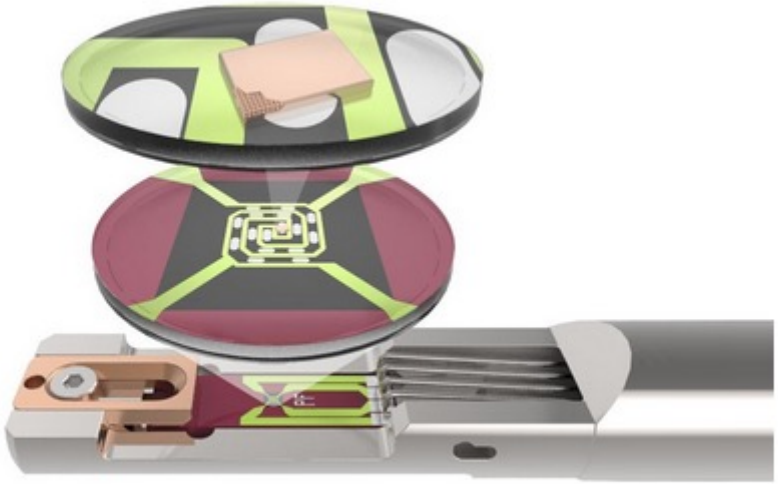

DENS chips

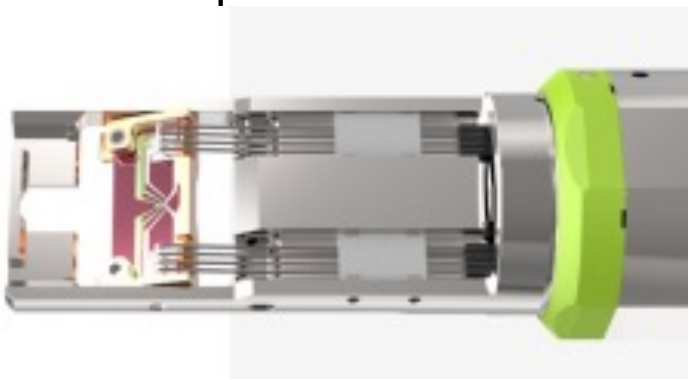

http://www.denssolutions.com/products/gas/nano-reactor/

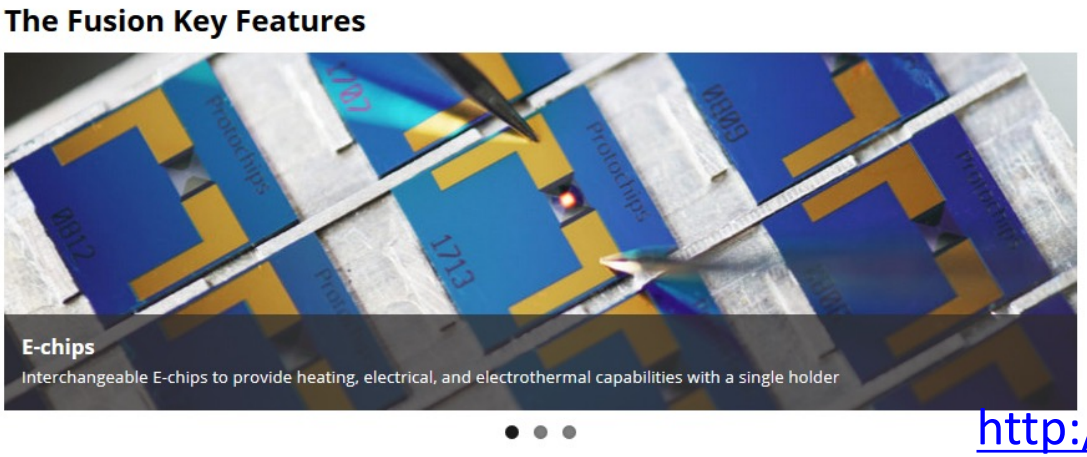

http://protochips.com/products/fusion/

Advanced Materials Processing and Microfabrication

Mikrosysteme für die Materialforschung

RUB

Processed /etched/ silicon is widely applied in micro devices that are further applied in material science. Recently, the demand for advanced solutions for in-situ electron microscopy is rising. New applications push the development of the Si-based mems chips into advanced level. Few, well recognizable companies share the market

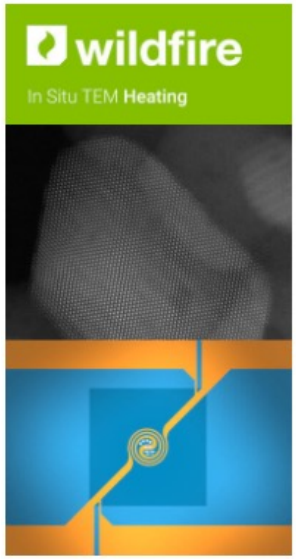

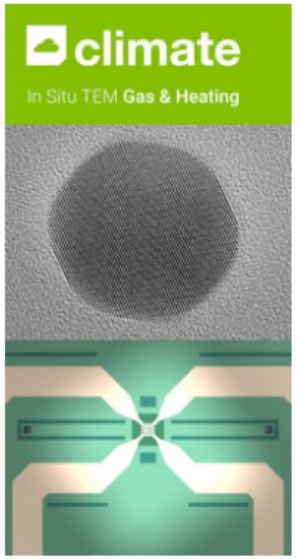

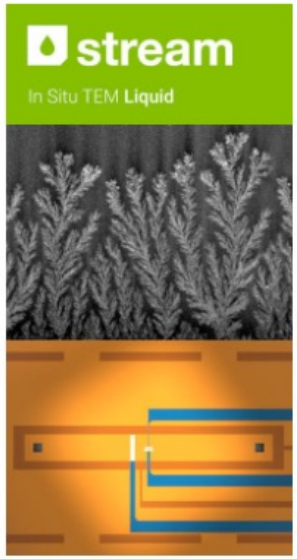

Protochips

HUMMINGBIRD SCIENTIFIC

DENS solutions

Lightning Nano-chip

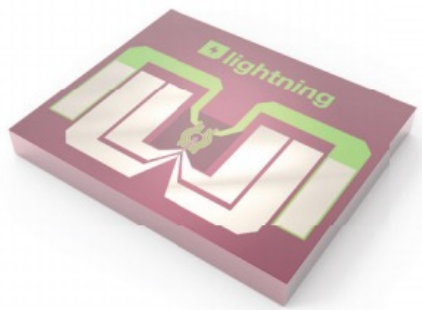

https://denssolutions.com

Advanced Materials Processing and Microfabrication

Mikrosysteme für die Materialforschung

RUB

TEM Anwendungen,
Hysitron,
nanofactory

- Patented Miniature and MEMS transducers provide electrostatic actuation and capacitive displacement sensing

(B)

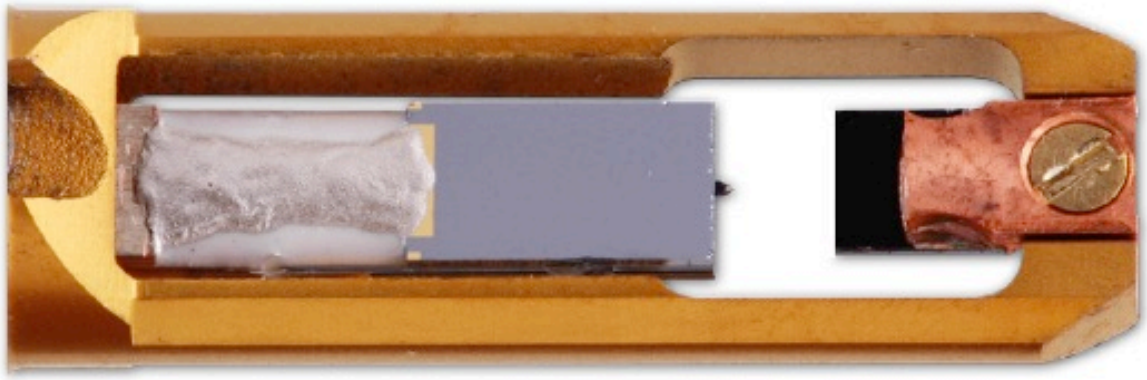

Specifications	Miniature Transducer	MEMS Transducer
Maximum Force (μN)	1500	1000
Maximum Displacement (nm)	5000	2000
Resonance Frequency (Hz)	~110	~1800

Holder detail: by positioning the indenter tip directly opposite the sample and perpendicular to the electron beam, the deformation event can be viewed *in situ*.
(A) JEOL compatible front-end
(B) FEI/Hitachi/Zeiss compatible front-end with MEMS transducer

https://www.hysitron.com/media/1579/pi95ss_sam-0073-a.pdf

Advanced Materials Processing and Microfabrication

Mikrosysteme für die Materialforschung

TEM Anwendungen,
Hysitron,
nanofactory

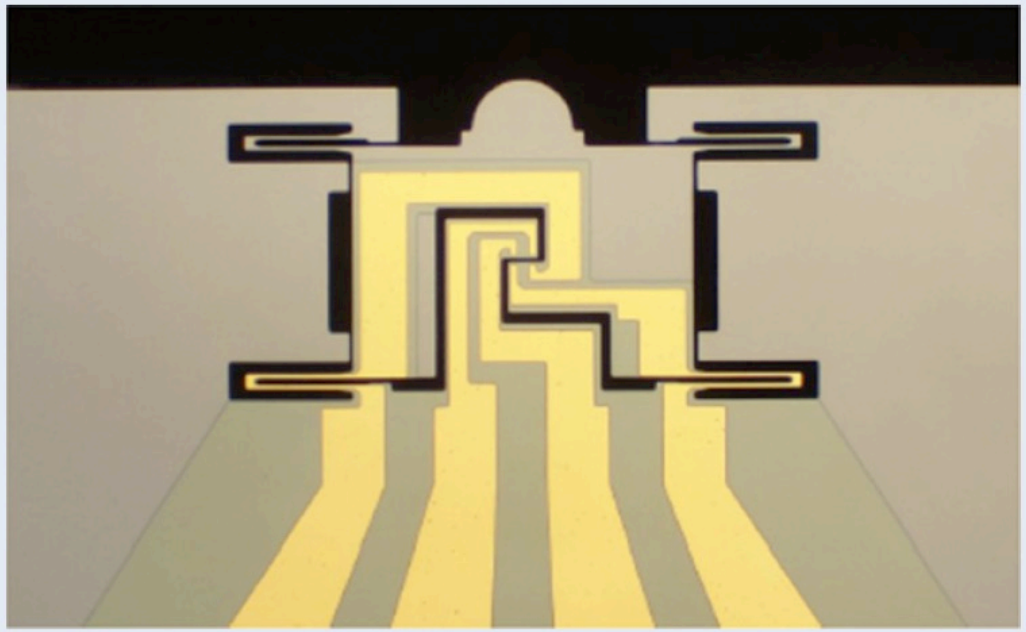

Figure 3: Optical image of Electrical Push-to-Pull (E-PTP) device.

https://www.hysitron.com/media/1557/picoindenterou-r1f.pdf

Advanced Materials Processing and Microfabrication

Mikrosysteme für die Materialforschung

TEM Anwendungen,
Hysitron,
nanofactory

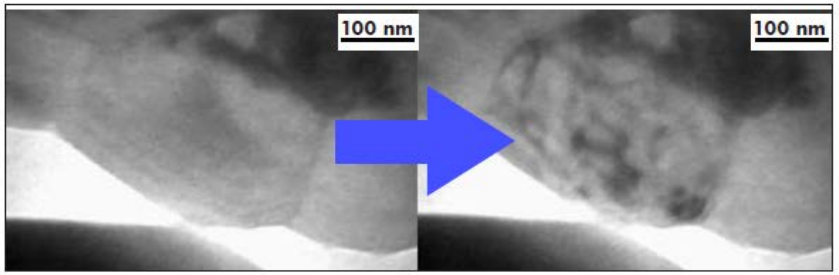

Indentation: Consecutive video frames illustrating the onset of dislocation plasticity in an initially dislocation-free grain of Al.
Nature Materials **5**, 697-702 (2006)

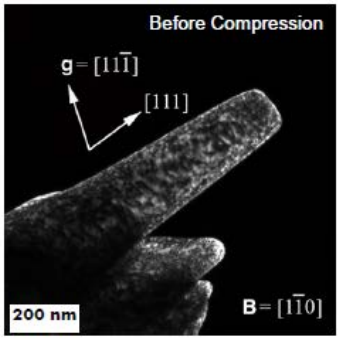

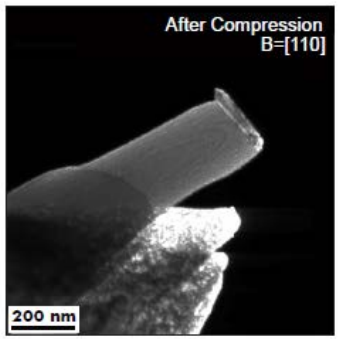

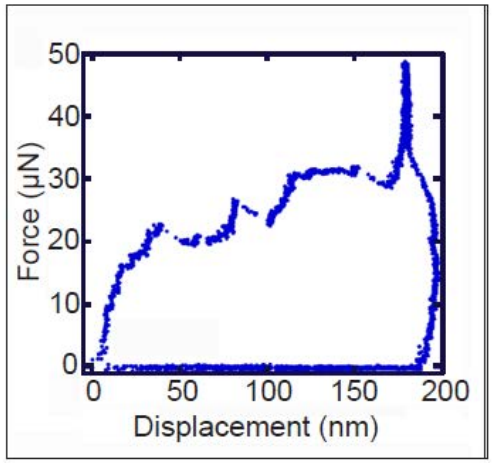

Nanopillar Compression: Dark-field TEM images of a Ni nanopillar before and after compression. The high dislocation density initially observed in the pillar has disappeared upon compression.
Nature Materials **7**, 115-119 (2007)

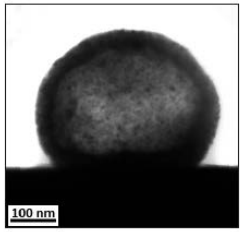

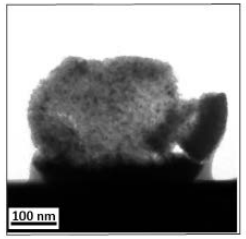

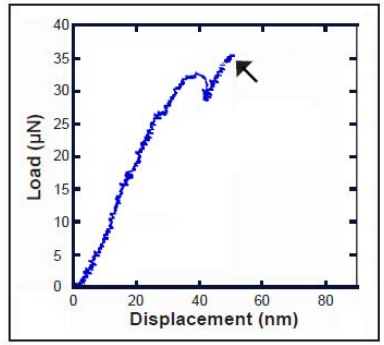

Nanoparticle Compression: Bright-field TEM images of a hollow CdS nanosphere before and after *in situ* compression, and the corresponding load-displacement curve showing catastrophic fracture.
See also: *Nature Materials* **7**, 947-952 (2008)

https://www.hysitron.com/media/1579/pi95ss_sam-0073-a.pdf

Nature Materials Schroers

ARTICLES

PUBLISHED ONLINE: 13 APRIL 2014 | DOI: 10.1038/NMAT3939

nature materials

Combinatorial development of bulk metallic glasses

Shiyan Ding[1,2†], Yanhui Liu[1,2†], Yanglin Li[1,2], Ze Liu[1,2], Sungwoo Sohn[1,2], Fred J. Walker[2,3] and Jan Schroers[1,2*]

The identification of multicomponent alloys out of a vast compositional space is a daunting task, especially for bulk metallic glasses composed of three or more elements. Despite an increasing theoretical understanding of glass formation, bulk metallic glasses are predominantly developed through a sequential and time-consuming trial-and-error approach. Even for binary systems, accurate quantum mechanical approaches are still many orders of magnitude away from being able to simulate the relatively slow kinetics of glass formation. Here, we present a high-throughput strategy where ~3,000 alloy compositions are fabricated simultaneously and characterized for thermoplastic formability through parallel blow forming. Using this approach, we identified the composition with the highest thermoplastic formability in the glass-forming system Mg–Cu–Y. The method provides a versatile toolbox for unveiling complex correlations of material properties and glass formation, and should facilitate a drastic increase in the discovery rate of metallic glasses.

Mikrosysteme für die Materialforschung

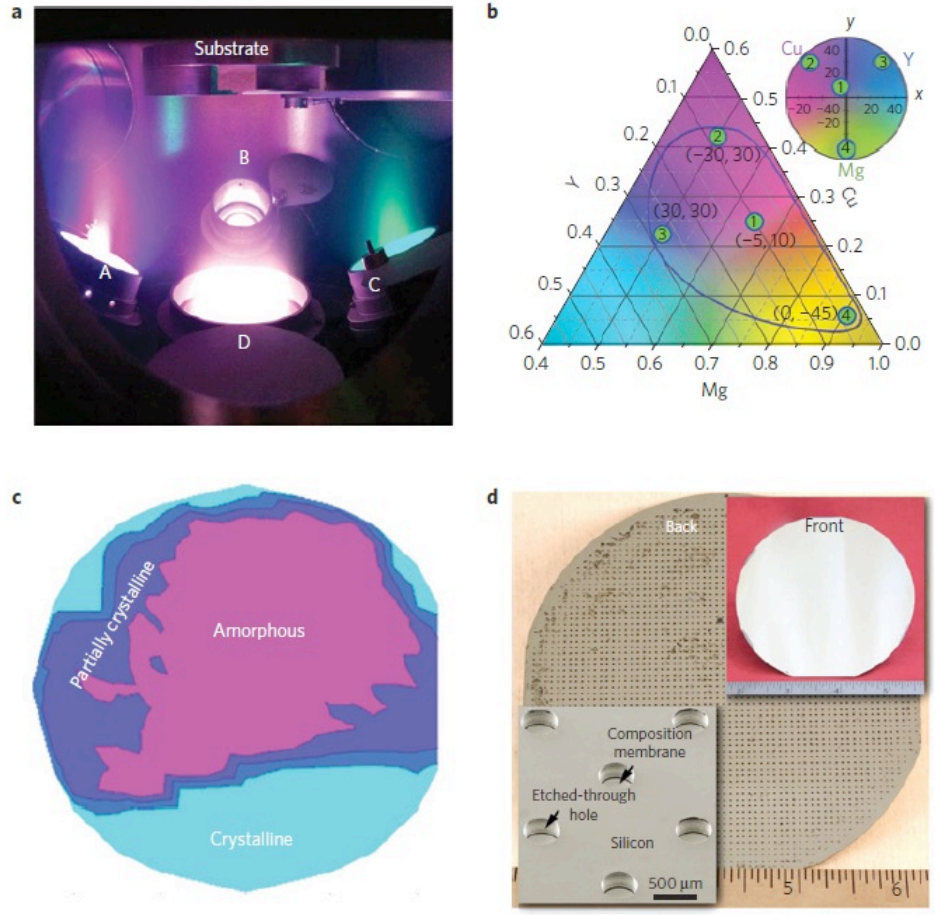

Figure 2 | Compositional library of approximately 3,000 samples synthesized through confocal magnetron co-sputtering and silicon micromachining. **a**, A d.c. magnetron co-sputtering system equipped with three 5 cm targets arranged in a tetrahedral symmetry is used to synthesize the compositional library. A further sputtering target located directly underneath the substrate and 10 cm in diameter can be used to add an additional element with constant composition. **b**, Compositional mapping obtained by EDX analysis and its correlation with the *x*, *y* coordinates of the Mg–Cu–Y library deposited on a 10-cm-diameter wafer. **c**, X-ray diffraction mapping of the peak width reveals that the majority of the film is amorphous as deposited (42–82% Mg, 10–46% Cu and 3–32% Y), and only a fraction is crystalline. **d**, Back side and front side (main image and upper-right inset) of the compositional library on a Si wafer after backside etching. Lower-left inset: Deep reactive ion etching releases the film to create membranes of 500 µm in diameter and 2 µm in thickness, which are the samples of the library.

Nature Materials Schroers

Advanced Materials Processing and Microfabrication

Mikrosysteme für die Materialforschung

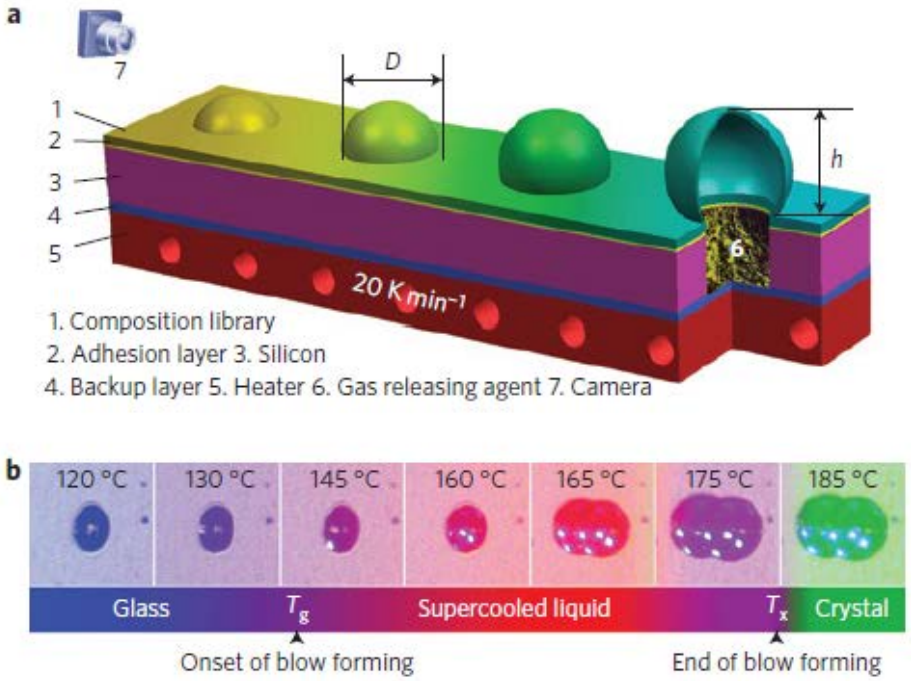

Figure 3 | Parallel blow-forming set-up of compositional membranes and its realization. a, Schematics of the parallel blow-forming set-up. The relative TPF is given by the final height of the membrane after deformation. **b**, Evaluation of the deformation with temperature during blow forming of the $Mg_{70}Cu_{20}Y_{10}$ membrane. At the glass transition temperature, the viscosity of the alloy decreases to the point that blow forming occurs through plastic deformation. Deformation continues with an increasing rate until crystallization sets in. Crystallization terminates the deformation and conserves the maximum height of the blow-formed dome. The apparent dual-hemisphere above 160 °C is an artefact originating from the reflection of the blow moulded dome from the undeformed film surrounding

Nature Materials Schroers

Advanced Materials Processing and Microfabrication

Mikrosysteme für die Materialforschung

RUB

Möglichkeiten zur in situ kontrollierten Prozessierung von Materialien
z.B. Mikroheizplatten

Sensors and Actuators A 147 (2008) 576–582

Contents lists available at ScienceDirect

Sensors and Actuators A: Physical

journal homepage: www.elsevier.com/locate/sna

Micro-hotplates for high-throughput thin film processing and *in situ* phase transformation characterization

S. Hamann[a,b], M. Ehmann[a], S. Thienhaus[a,b], A. Savan[a], A. Ludwig[a,b,*]

[a] Combinatorial Materials Science Group, Center of Advanced European Studies and Research (caesar), Ludwig-Erhard-Allee 2, 53175 Bonn, Germany
[b] Institute of Materials, Faculty of Mechanical Engineering, Ruhr-University Bochum, 44780 Bochum, Germany

ARTICLE INFO

Article history:
Received 1 January 2008
Received in revised form 13 March 2008
Accepted 4 May 2008
Available online 14 May 2008

Keywords:
Micro-hotplates
High-throughput
processing/characterization
Quenching
In situ characterization

ABSTRACT

This paper presents the use of micro-hotplates (MHPs) as thermal processing and *in situ* characterization platforms for phase transformations in thin films. MHPs are fabricated by microsystem technology processes and consist of a SiO_2/Si_3N_4 membrane (app. 1 μm) supported by a bulk Si frame. Several embedded Pt thin films serve as heater and electrical measurement electrodes. It is shown that the MHPs have unique properties for the controlled annealing of thin film materials (up to 1270 K), as the annealing temperature and heating/cooling rates can be precisely controlled by *in situ* measurements. These rates can be extremely high (up to 10^4 K/s), due to the low thermal mass of MHPs. The high cooling rates are especially useful for the fabrication of metastable phases (e.g. $Fe_{70}Pd_{30}$) by quenching. By measuring the resistivity of a thin film under test *in situ* as a function of the MHP temperature, microstructural changes (e.g. phase transformations) can be detected during heating and cooling cycles. In this paper, examples are presented for the determination of phase transitions in thin films using MHPs: the solid–liquid–gas phase transition (Al), the ferromagnetic–paramagnetic phase transition (Fe–Pt) and martensitic transformations (Ni–Ti–Cu, Fe–Pd). Furthermore, it is demonstrated that crystallization processes from amorphous to crystalline (Ni–Ti–Cu) can be detected with this method. Finally the application of MHPs in thin film combinatorial materials science and high-throughput experimentation is described.

Advanced Materials Processing and Microfabrication

Mikroheizplatten

Möglichkeiten zur in situ kontrollierten Prozessierung von Materialien

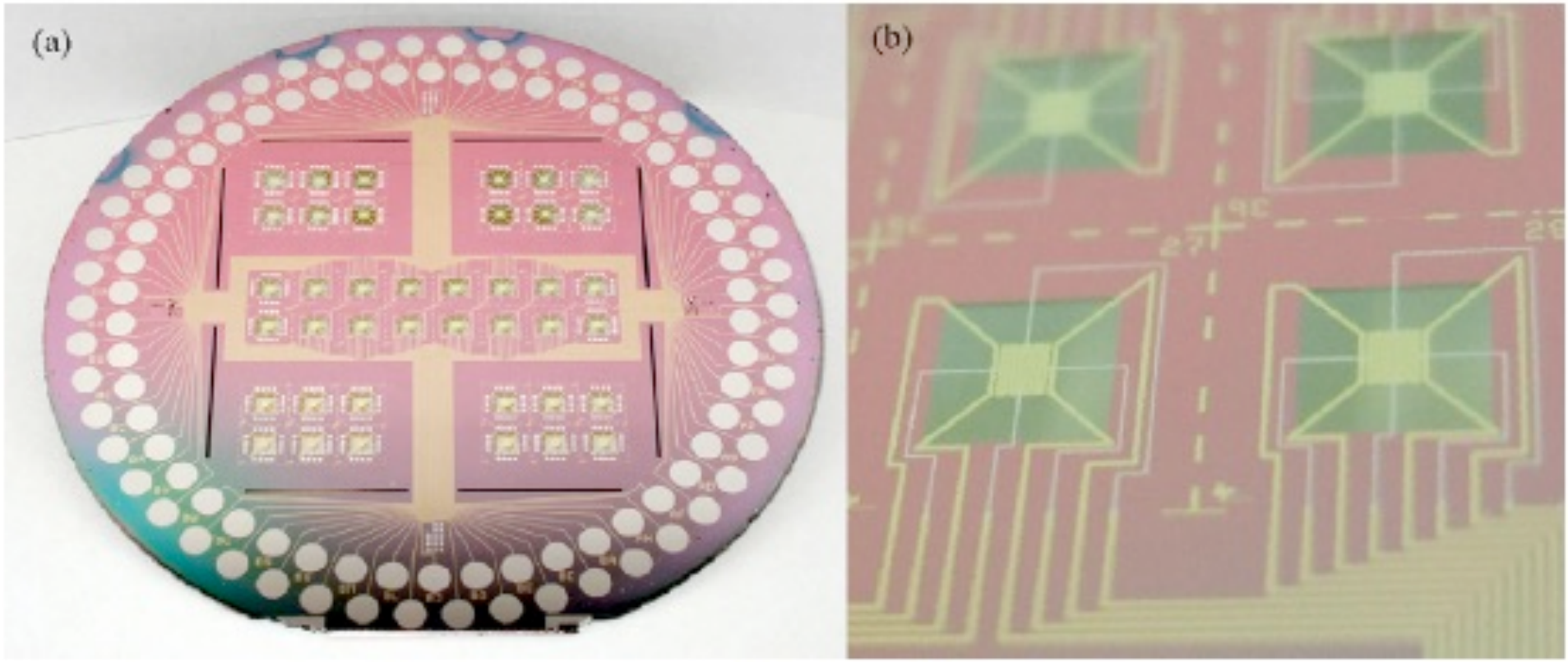

Fig. 2. (a) MHP array on a 4 in. wafer; (b) zoom of MHPs with electrical connections.

Advanced Materials Processing and Microfabrication

Mikroheizplatten

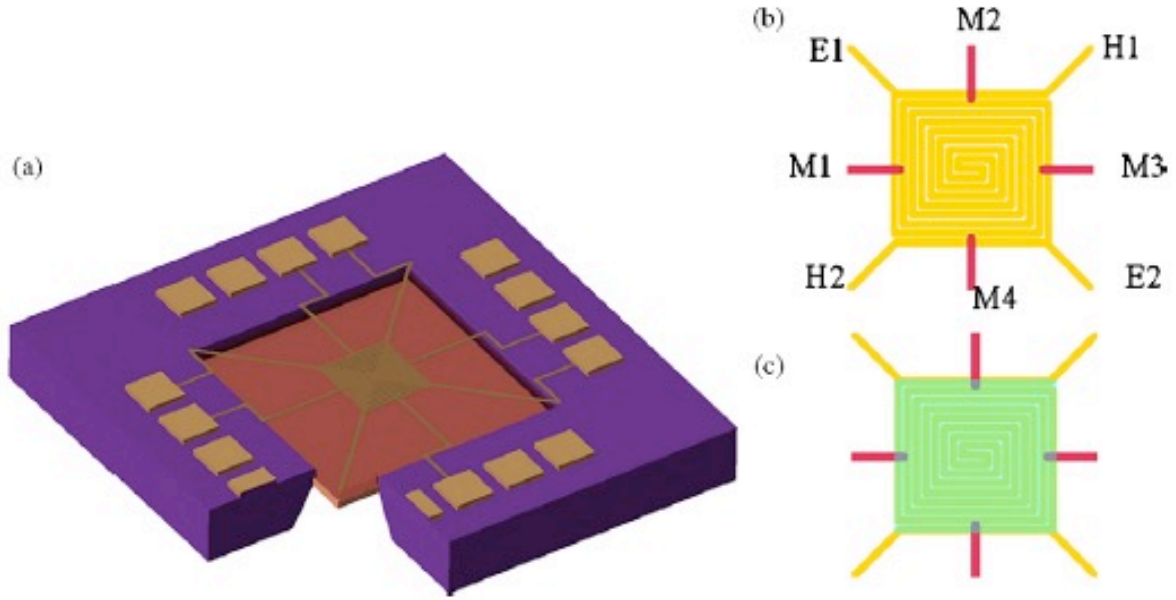

Fig. 1. (a) Schematic of a single MHP chip consisting of a suspended membrane with integrated electrodes for heating and *in situ* resistivity measurements; (b) electrodes of the heater area: H1, H2—heater current, E1, E2—additional electrodes to determine the heater temperature via resistivity by 4-point measurement method, M1–M4—electrodes for the *in situ* measurement of the thin film resistivity; (c) thin film deposited on the heater area on top of the measurement electrodes (M1–M4).

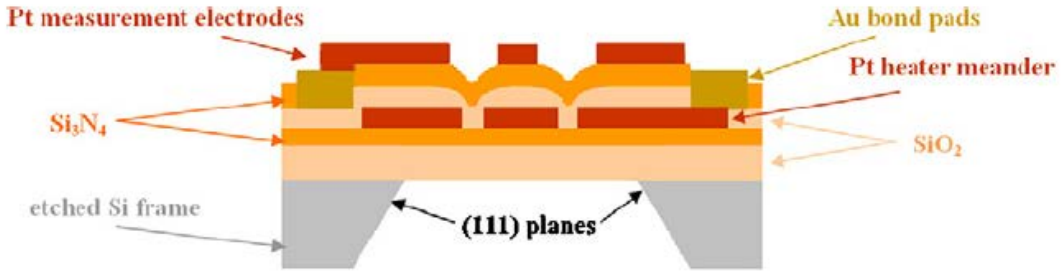

Fig. 3. Schematic cross section of a MHP (not to scale).

Advanced Materials Processing and Microfabrication

Mikroheizplatten

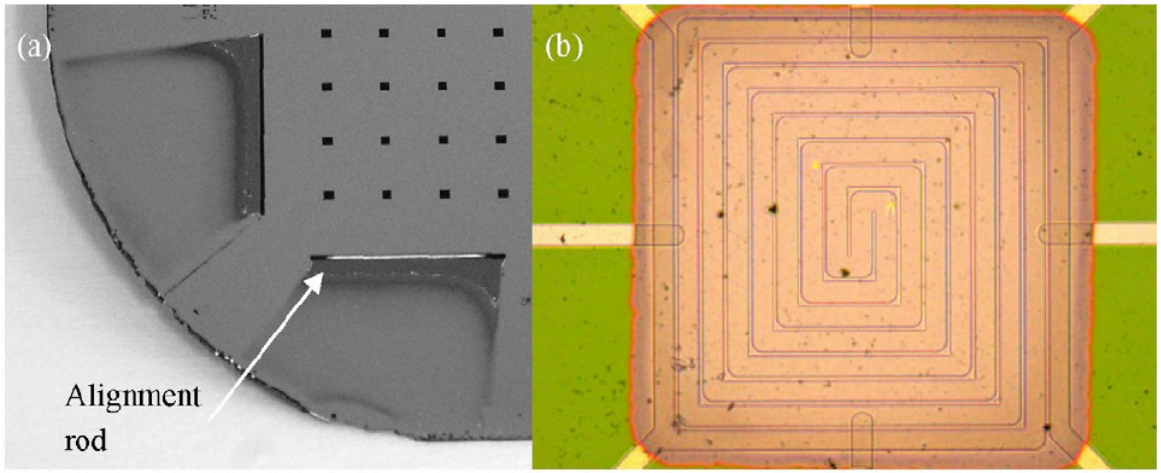

Fig. 4. (a) Close up section of a Si shadow mask with rod for alignment on the MHP-wafer. (b) Thin film deposited on the heating plane of a MHP using a Si shadow mask.

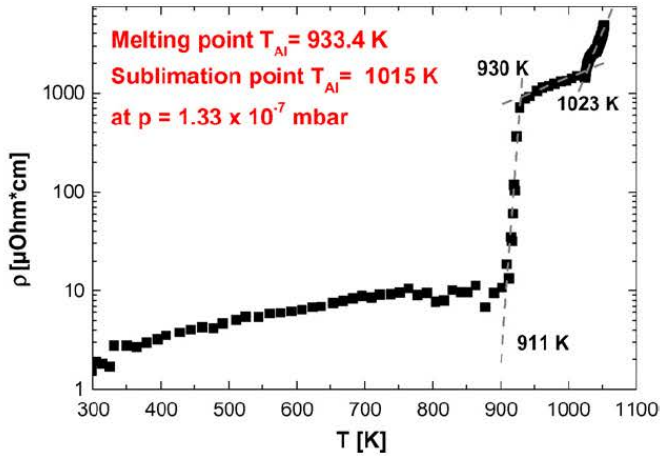

Fig. 7. *In situ* resistivity measurement of an Al thin film as a function of temperature.

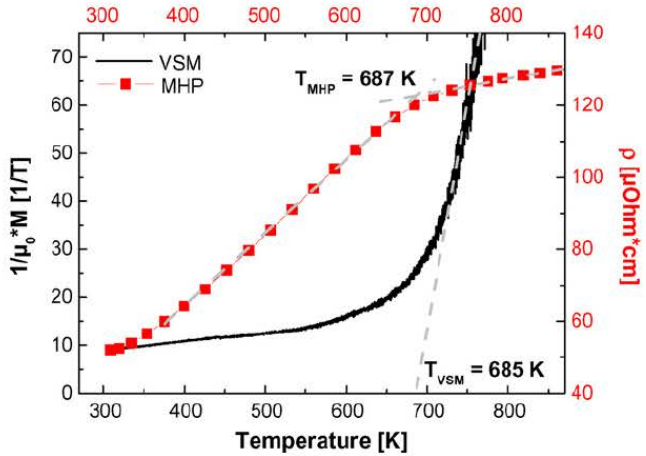

Fig. 8. Comparison of $\rho(T)$ and magnetization measurement cooling curve to determine the Curie temperature of a $Fe_{56}Pt_{44}$ thin film.

Advanced Materials Processing and Microfabrication

Mikroheizplatten: in situ Prozessierung und Charakterisierung

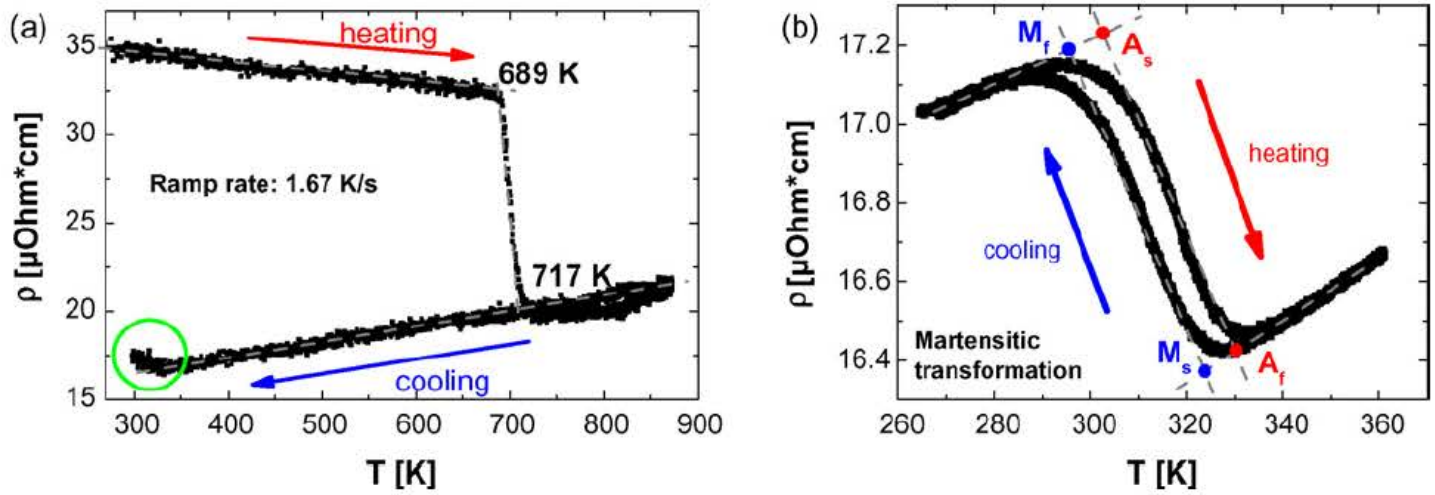

Fig. 9. (a) Resistance-temperature behaviour of an as-deposited $Ni_{30}Ti_{55}Cu_{15}$ thin film upon first annealing; (b) resistance-temperature behaviour of the same thin film after annealing showing the reversible martensitic transformation with small hysteresis width of 7 K.

TEM chips

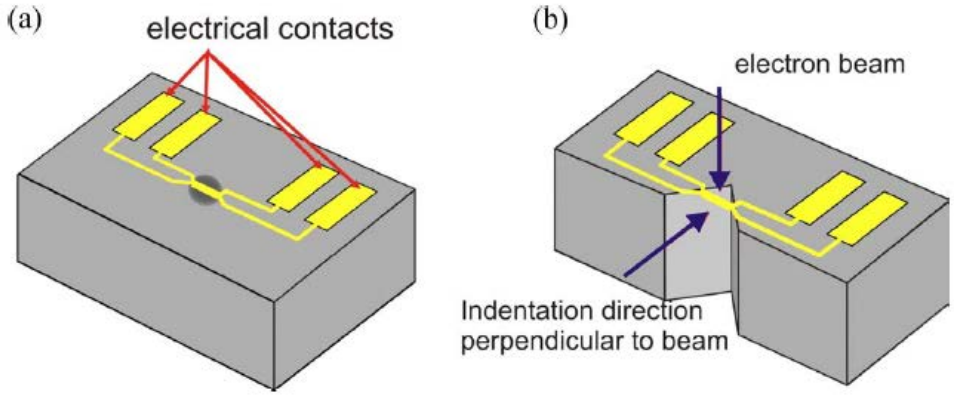

Fig. 1. Design of micromachined test platforms. Electrical contacts (same material as the microbridges) allowing for R(T) measurements are shown in yellow. (a) Sample testing device with accessibility from the top exhibiting a small etch groove under the microbridge (TAD). (b) Testing device with accessibility from top and side (LAD). This device is designed for *in situ* TEM nanoindentation with the indenter coming from the side and the electron beam coming from the top, perpendicular to the indentation direction.

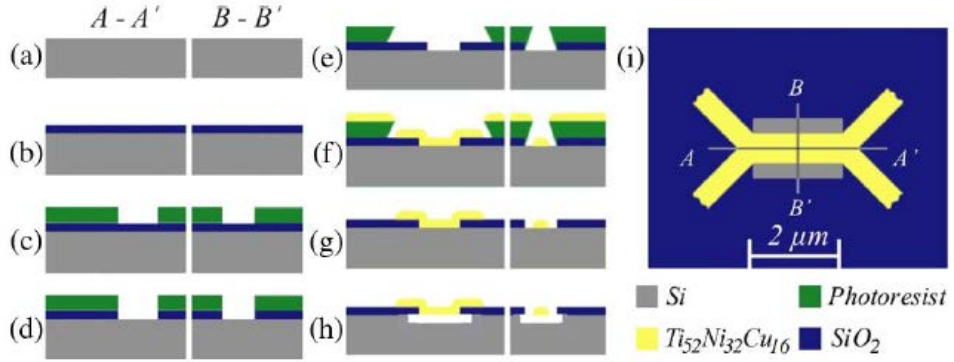

Fig. 2. Schematic process flow for (a)–(h) the fabrication of the freestanding thin-film structures. (i) Top view of the TAD indicating lines $A-A'$ and $B-B'$ for which the process flow is shown.

TEM chips

Möglichkeiten zur in situ kontrollierten Prozessierung von Materialien
z.B.

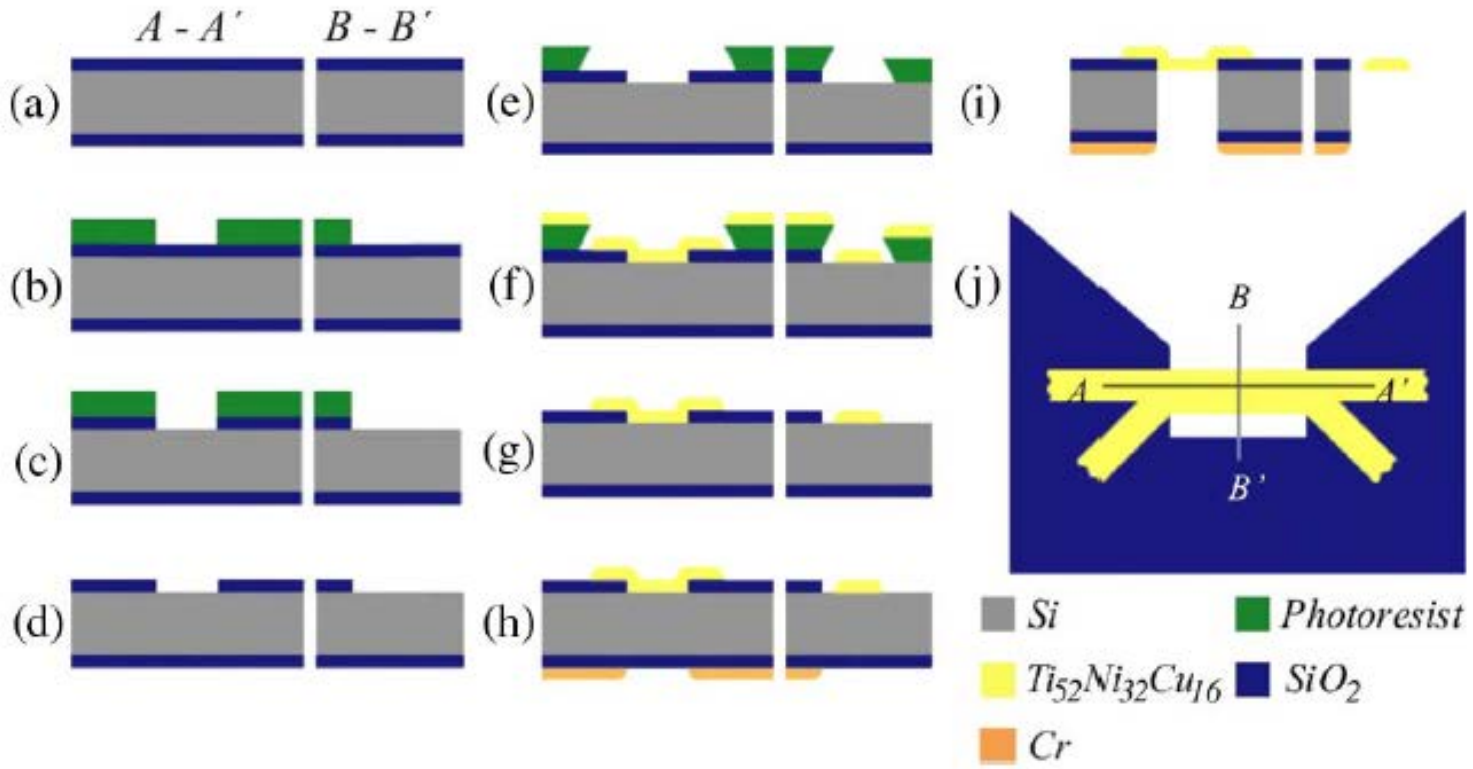

Fig. 3. Schematic process flow for (a)–(i) the fabrication of the freestanding thin-film structures (LAD). (j) Top view of the LAD indicating lines $A-A'$ and $B-B'$ for which the process flow is shown.

TEM chips

Möglichkeiten zur in situ kontrollierten Prozessierung von Materialien

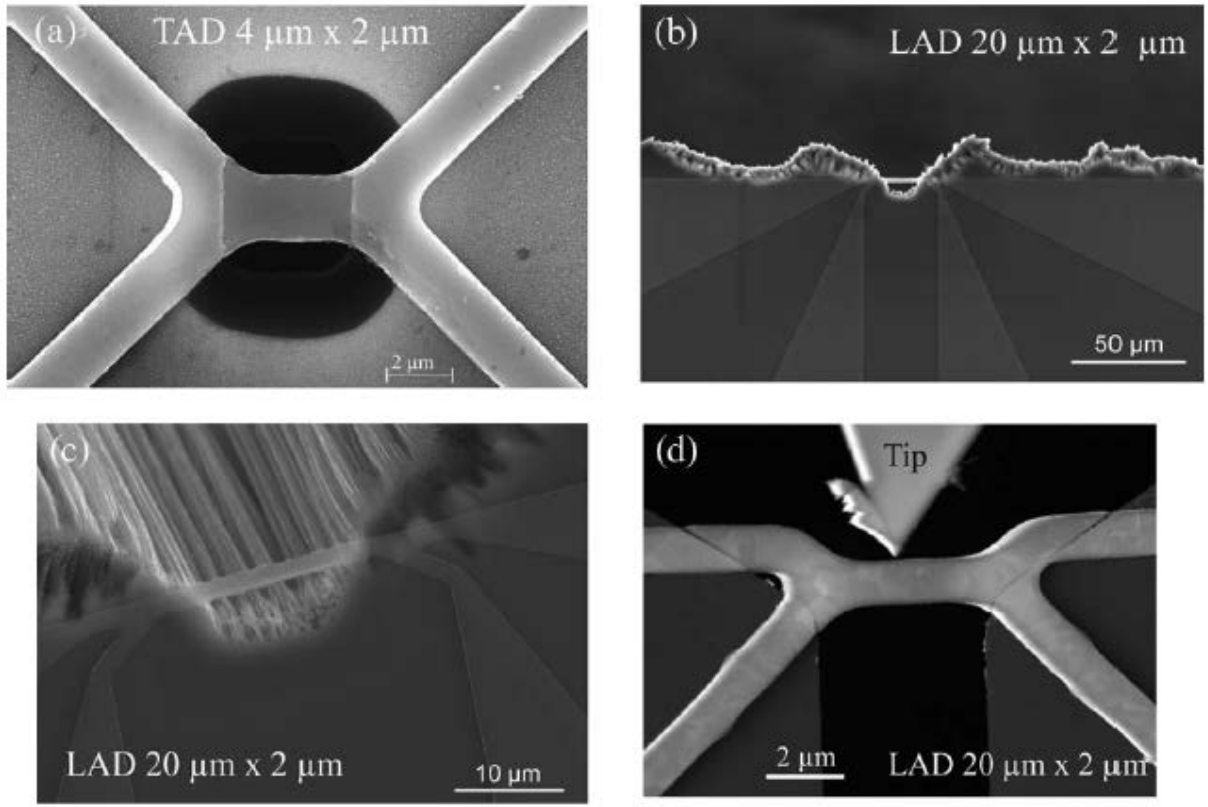

Fig. 4. SEM micrographs of the two testing devices. (a) TAD 4 μm $\times$ 2 μm. (b) LAD 20 μm $\times$ 2 μm. c) LAD 20 μm $\times$ 2 μm. (d) high angle annular dark field scanning TEM image of LAD (4 μm $\times$ 2 μm) in vicinity of the nanoindenter diamond tip.

Advanced Materials Processing and Microfabrication

Spannungsmesswafer und -chips

- Measurement of Si cantilever curvature
- Wafer level measurements
- Parallel stress measurements in materials libraries

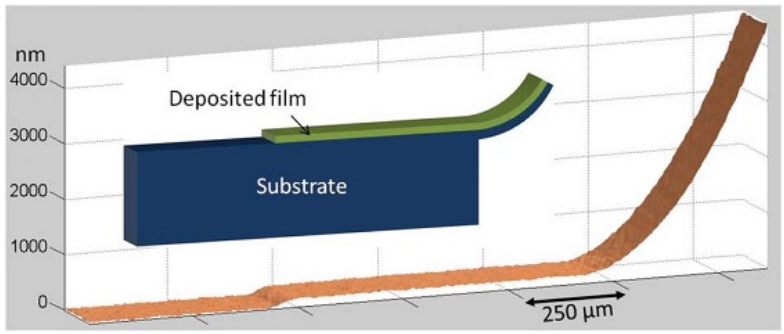

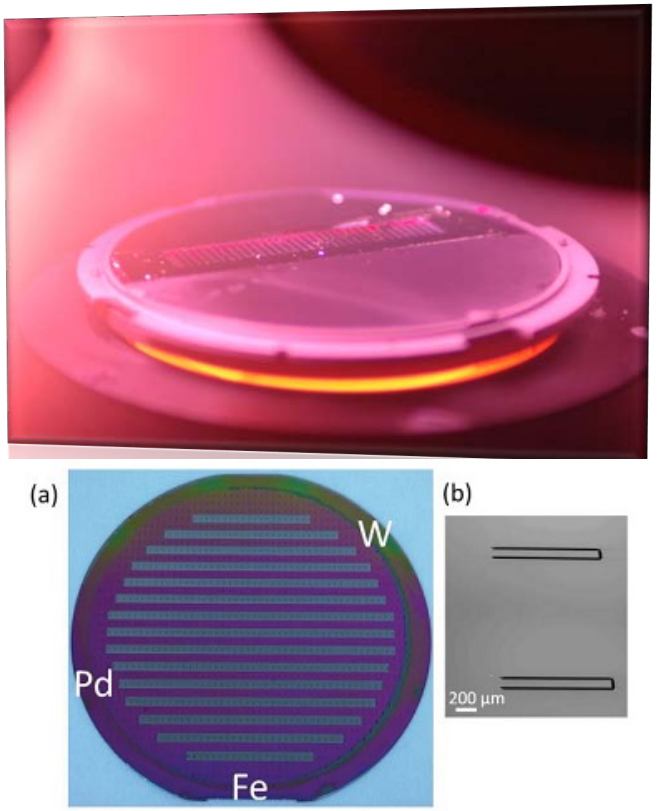

FIG. 2. (Color online) (a) Photo of a 4-inch cantilever array SOI wafer after deposition of a Fe-Pd-W thin film materials library through a micro-machined Si shadow mask. The deposited areas appear in gray. (b) A scanning electron microscopy image of un-coated cantilevers.

SFB-TR 87

Advanced Materials Processing and Microfabrication

Spannungsmesswafer

IOP Publishing — Journal of Physics D: Applied
J. Phys. D: Appl. Phys. **46** (2013) 084011 (10pp) doi:10.1088/0022-3727/46/8

Time- and space-resolved high-throughput characterization of stresses during sputtering and thermal processing of Al–Cr–N thin films

D Grochla[1], A Siegel[1], S Hamann[1], P J S Buenconsejo[1], M Kieschnick[1,2], H Brunken[1], D König[1] and A Ludwig[1,3]

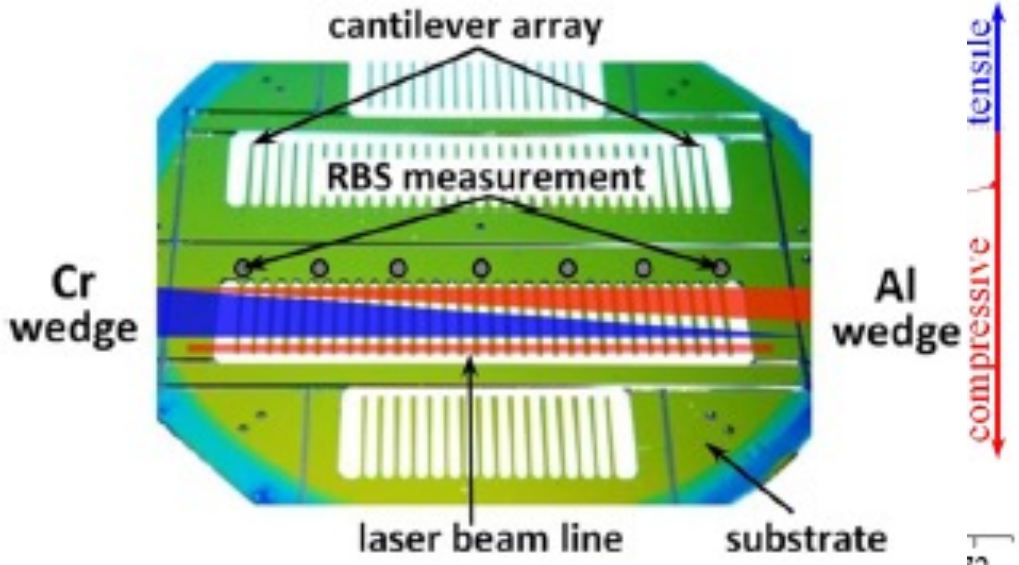

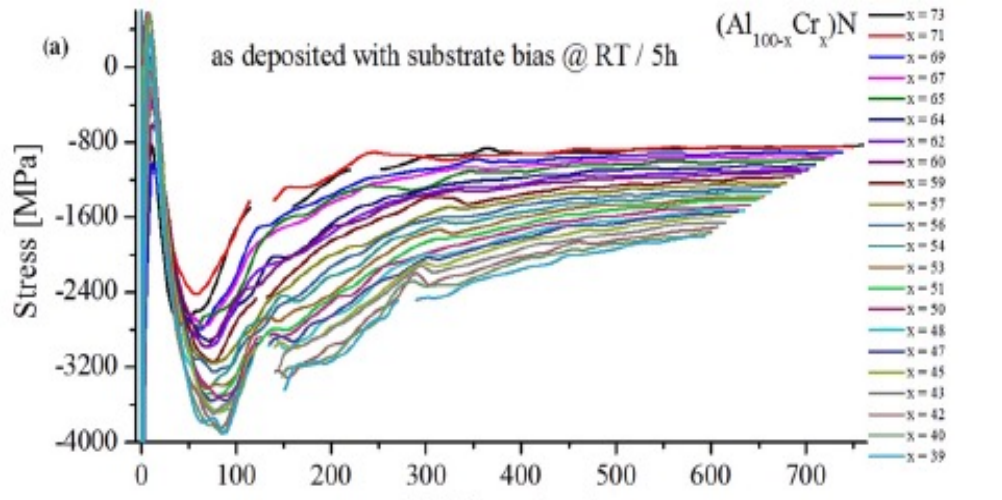

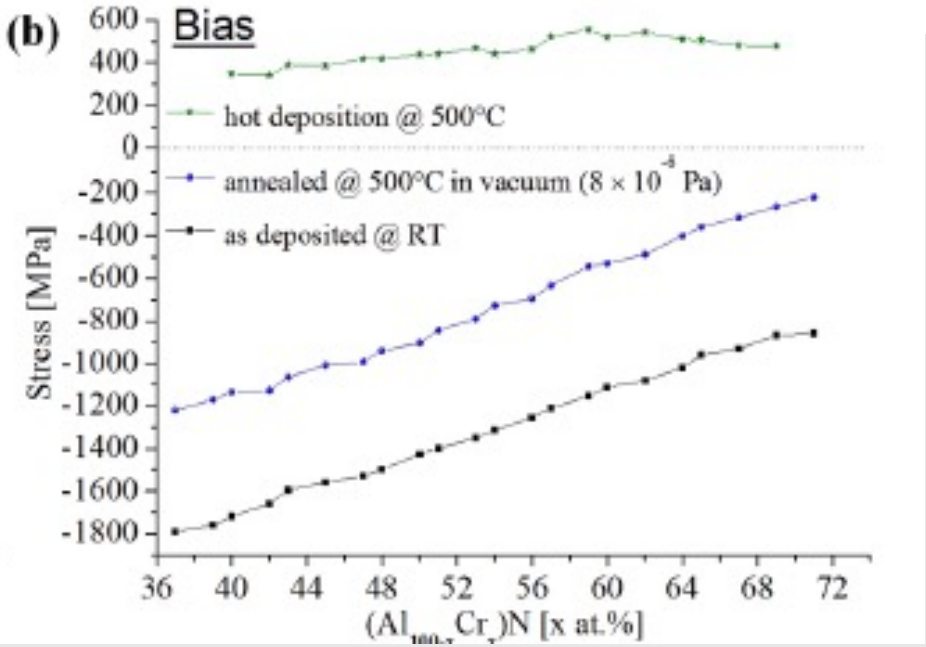

Advanced Materials Processing and Microfabrication

Spannungsmesswafer und -chips

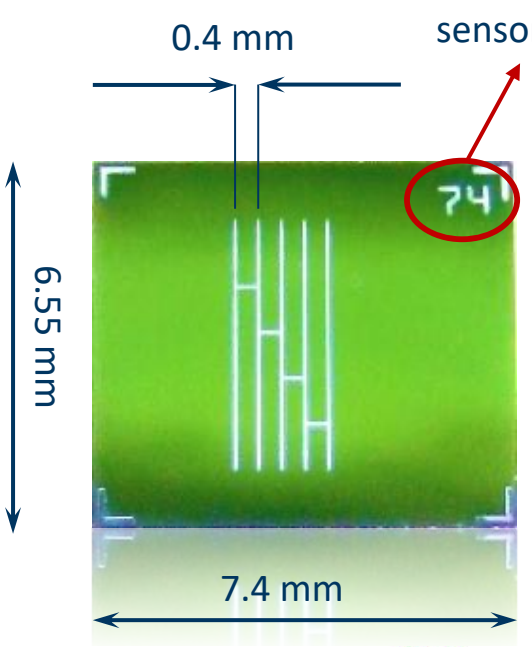

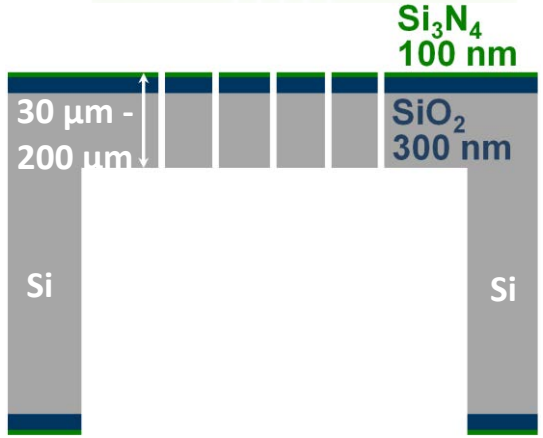

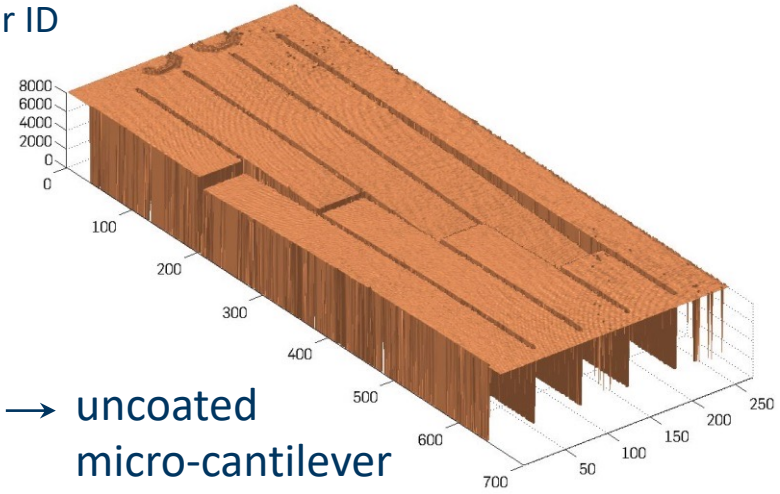

→ uncoated micro-cantilever

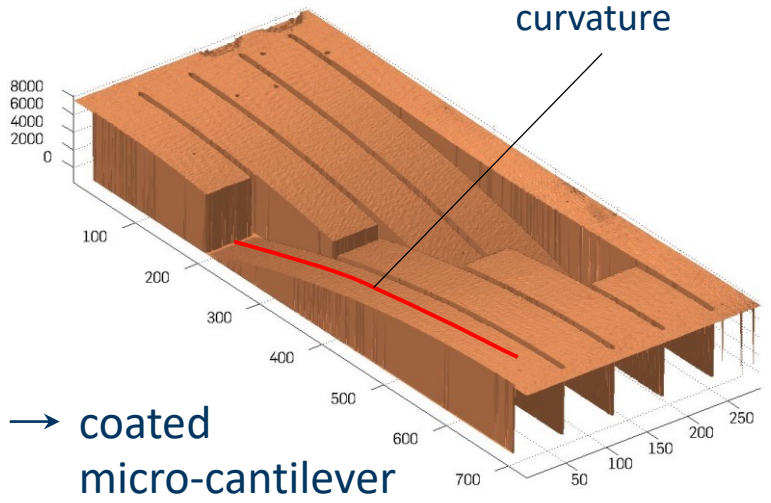

→ coated micro-cantilever

Stoney equation:

$$\sigma = \frac{Y_s t_s^2}{6(1-\nu)t_f R}$$

Y_s: Young's - Modulus of substrate

t_s: cantilever substrate thickness

t_f: film thickness

R: curvature radius

ν: Poisson's ratio of substrate

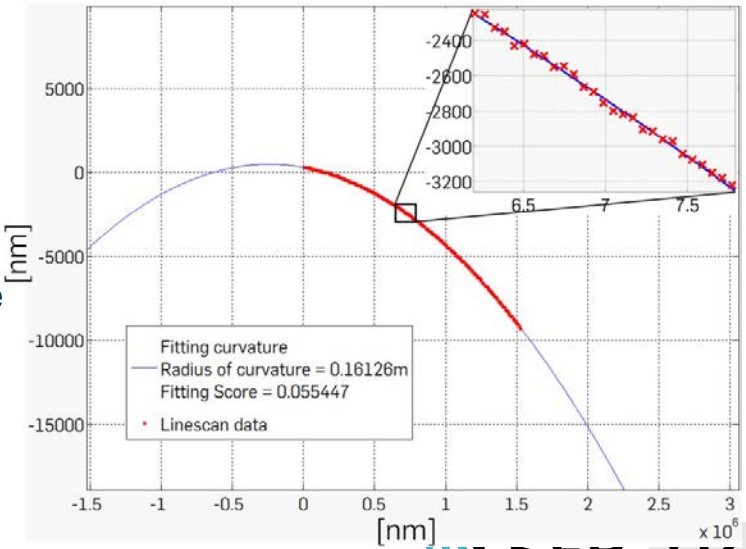

SFB-TR 87

Spannungsmesswafer und -chips

- chip handling system for industrial PVD-reactor

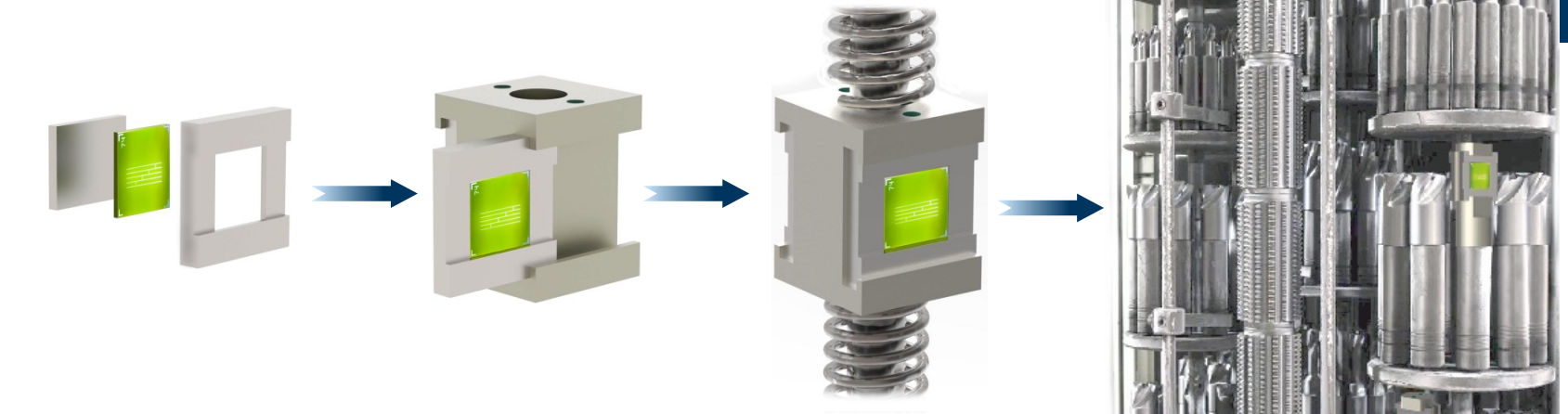

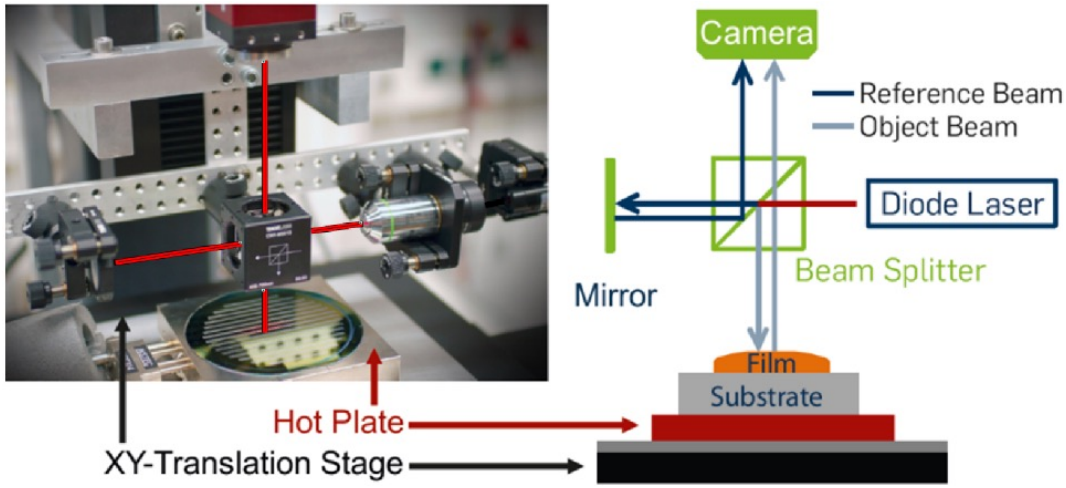

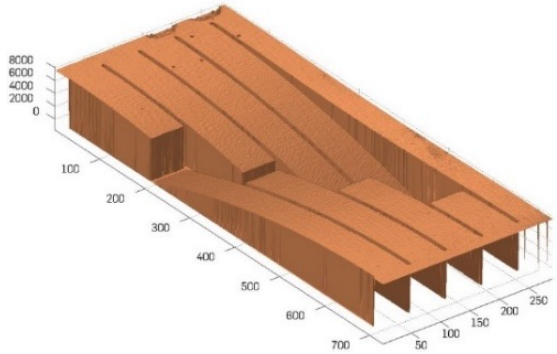

- application in static & dynamic coating processes
- space-resolved measurement
- determine stress state

SFB-TR 87

Atomic-scale mixture by co-deposition: Atom probe tomography (APT) analysis of co-sputtered Cr-Mn-Fe-Co-Ni forced solid solution

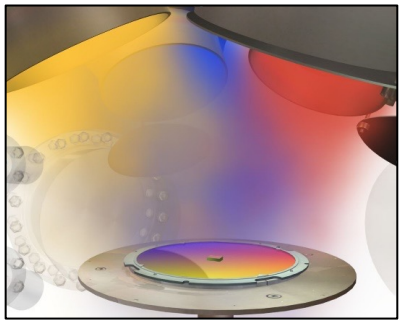

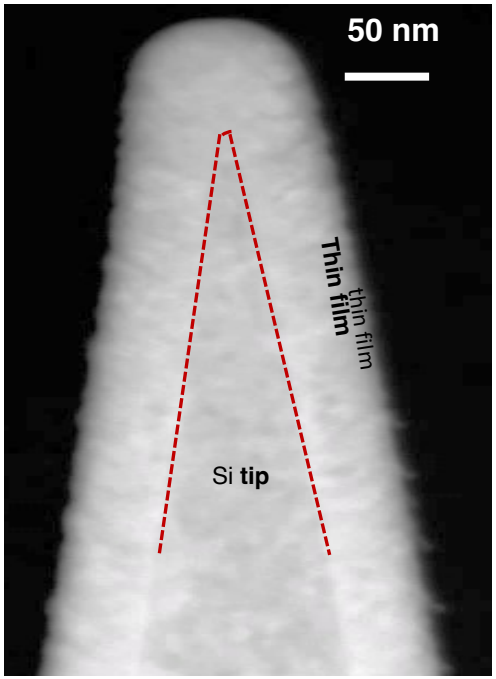

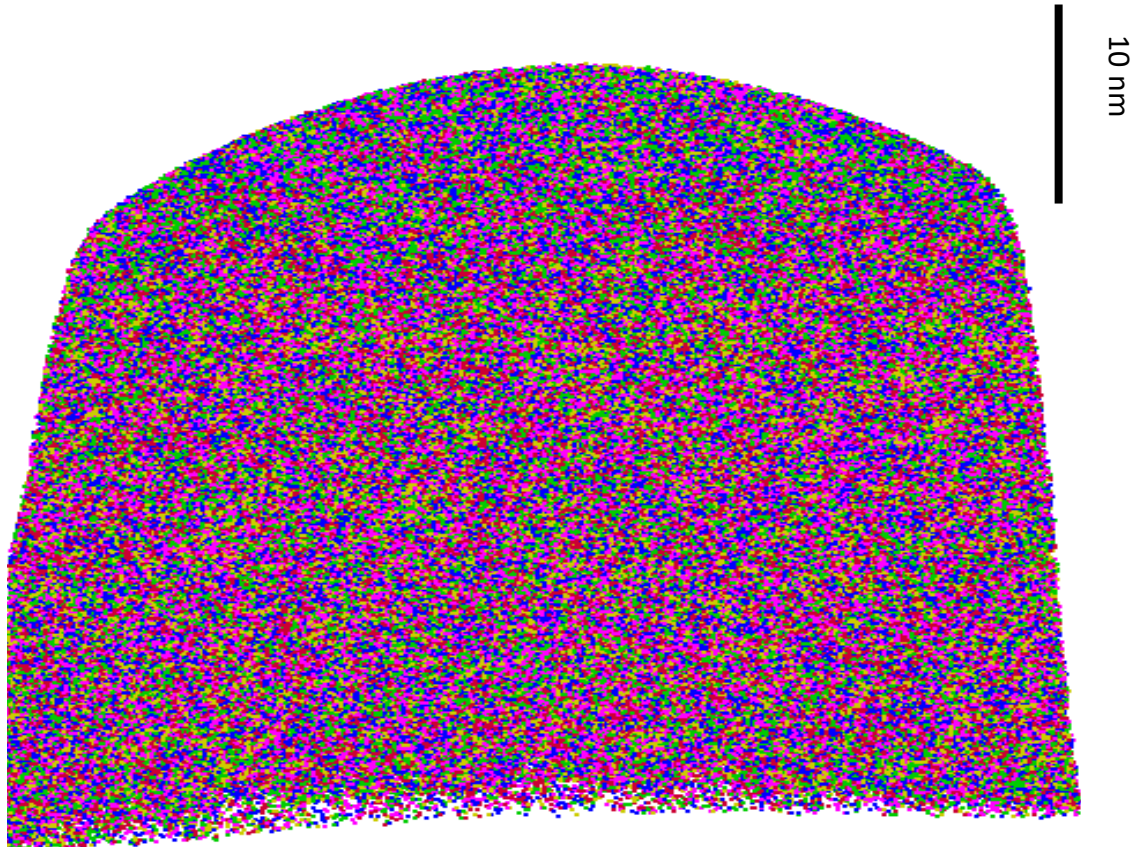

Y. J. Li, A. Savan, A. Kostka, H. S. Stein, A. Ludwig (2018) *Accelerated atomic-scale exploration of phase evolution in compositionally complex materials*, Materials Horizons 5, 86 - 92

Combinatorial processing platforms for accelerated phase evolution in CCAs

Fast synthesis of nc thin films (Combinatorial deposition)

5 targets, rotated substrate
MnCrFeCoNi, Cantor alloy

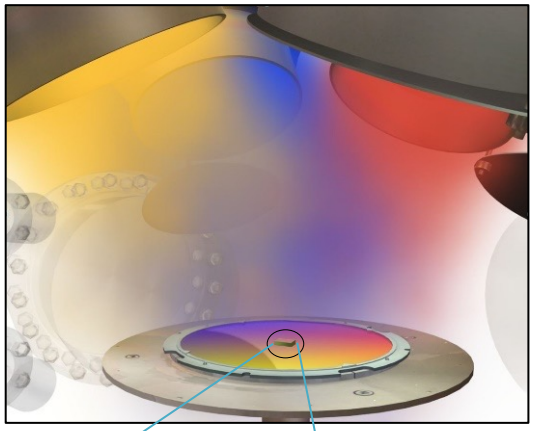

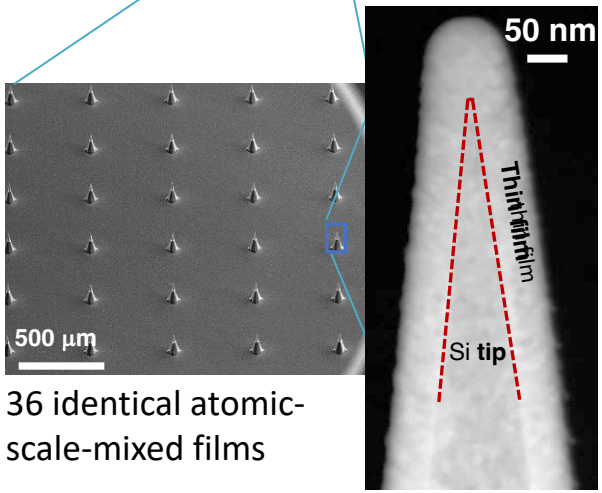

36 identical atomic-scale-mixed films

Fast annealing / oxidation (rapid phase evolution)

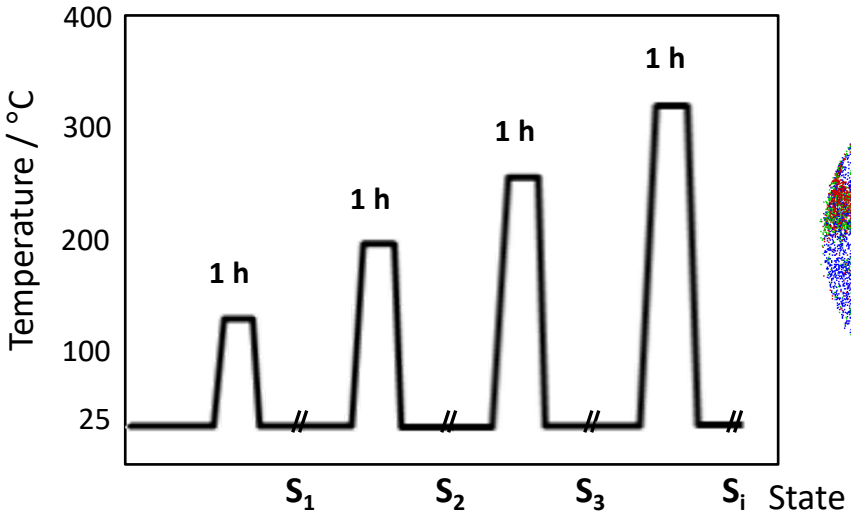

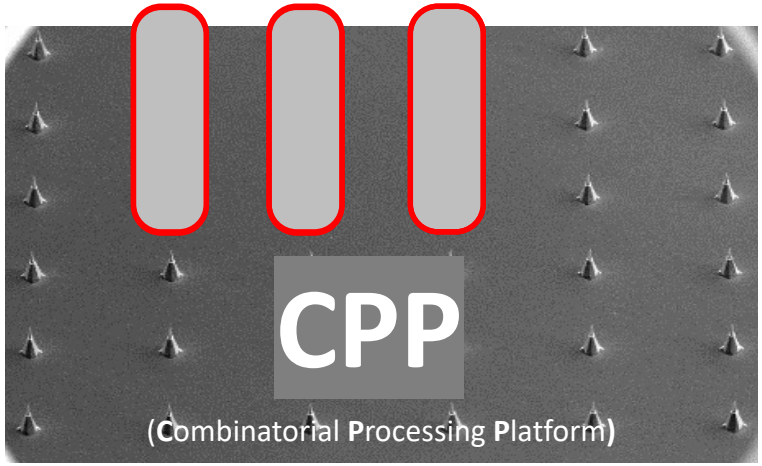

Direct atomic-scale analysis

APT
(chemical analysis)

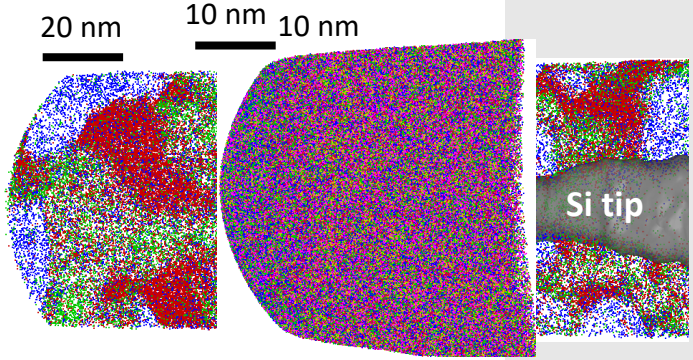

TEM
(crystal structure)

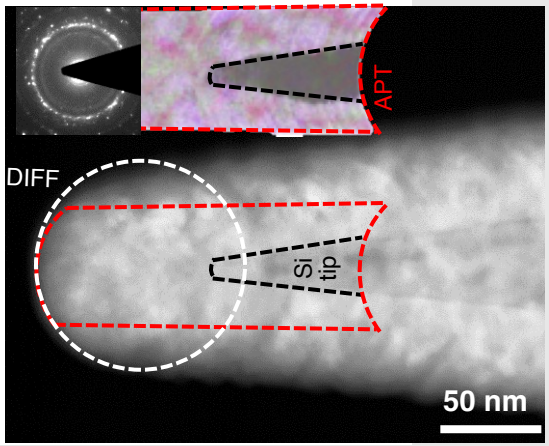

Y. J. Li, A. Savan, A. Kostka, H. S. Stein, A. Ludwig (2018) *Accelerated atomic-scale exploration of phase evolution in compositionally complex materials*, Materials Horizons 5, 86 - 92

Combinatorial processing platforms for accelerated phase evolution in CCAs

300°C, 1 h

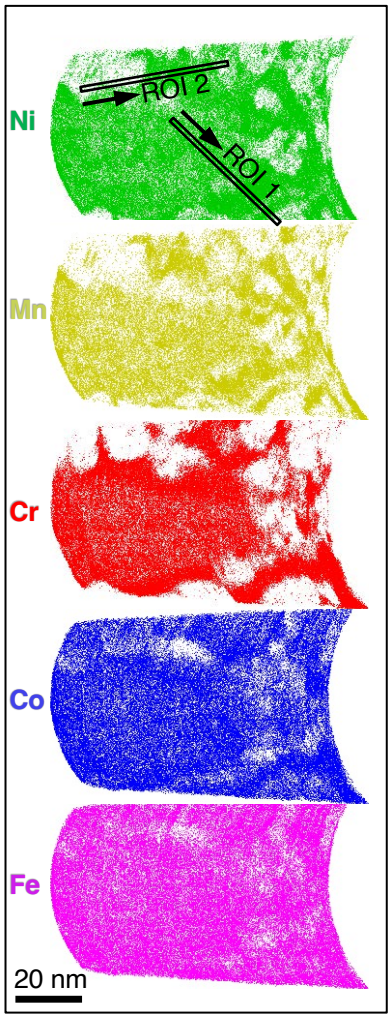

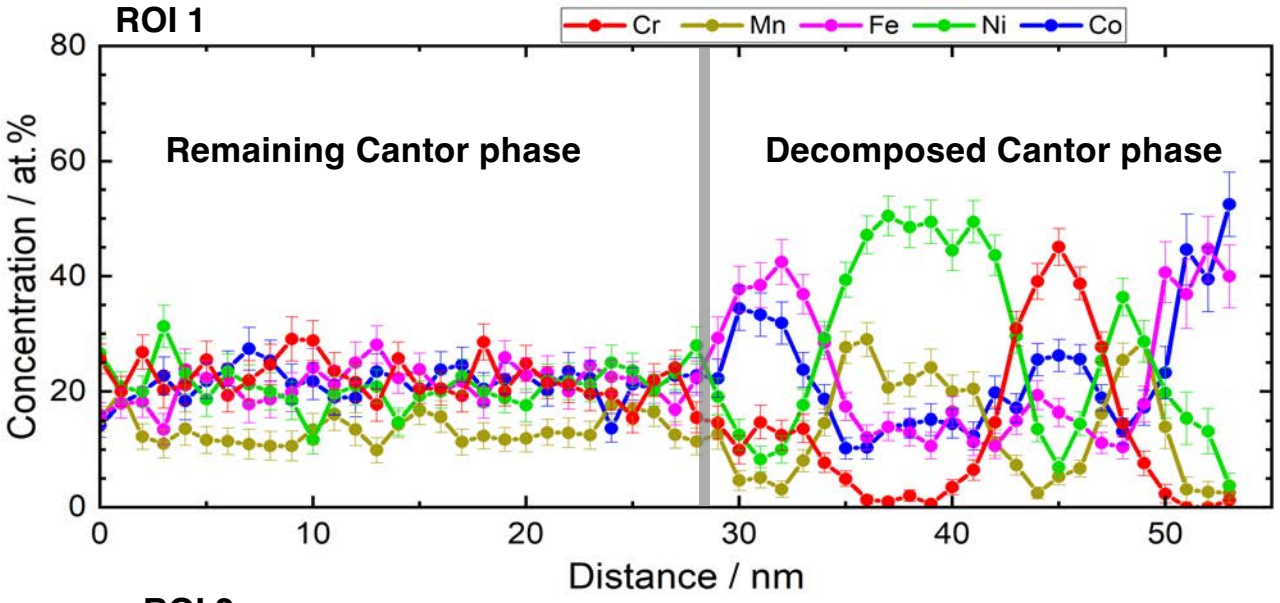

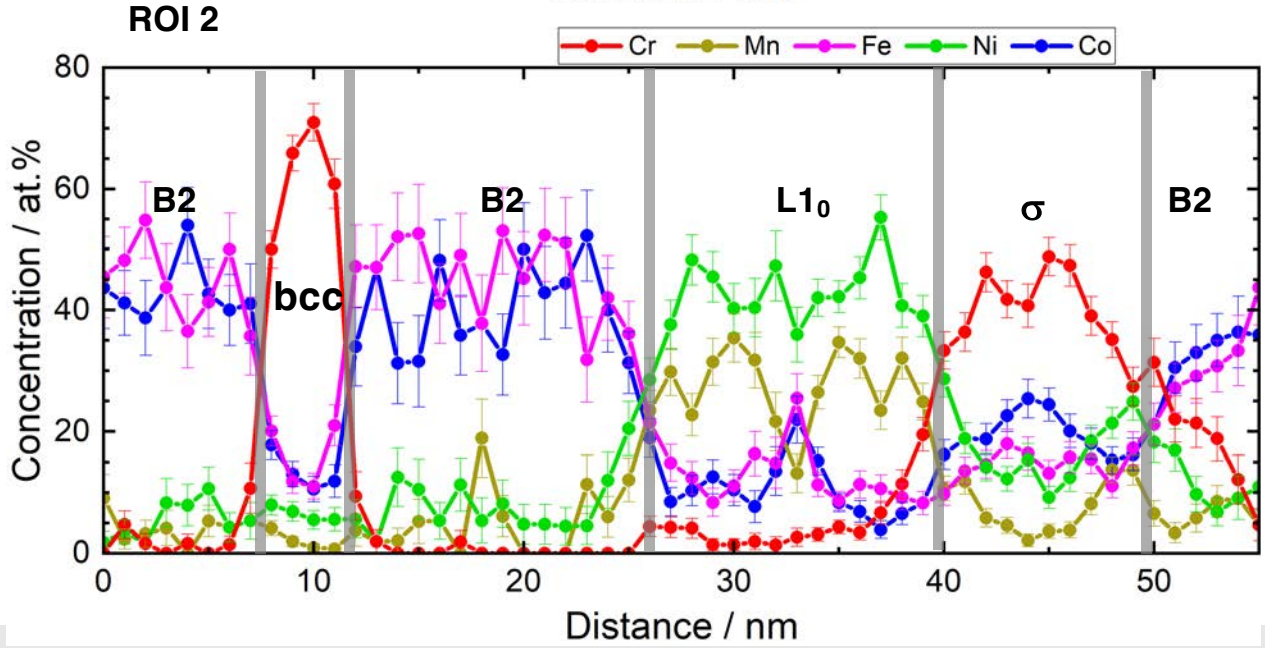

Bulk counterpart

500°C or higher
500 days

B2: 46 at.% Fe
46 at.% Co

bcc: 86 at.% Cr

$L1_0$: 51 at.% Ni,
42 at.% Mn

σ: 46 at.% Cr

Otto et al.,
Acta Materialia, 2016

Y. J. Li, A. Savan, A. Kostka, H. S. Stein, A. Ludwig (2018) *Accelerated atomic-scale exploration of phase evolution in compositionally complex materials*, Materials Horizons 5, 86 - 92

Combinatorial processing platforms for accelerated phase evolution in CCAs: Oxidation study

Bulk counterpart

↓ 600-900°C, 100 h

Mn_3O_4, Cr_2O_3

Laplanche et al., Oxid. Met., 2016

500°C, 5 min in air

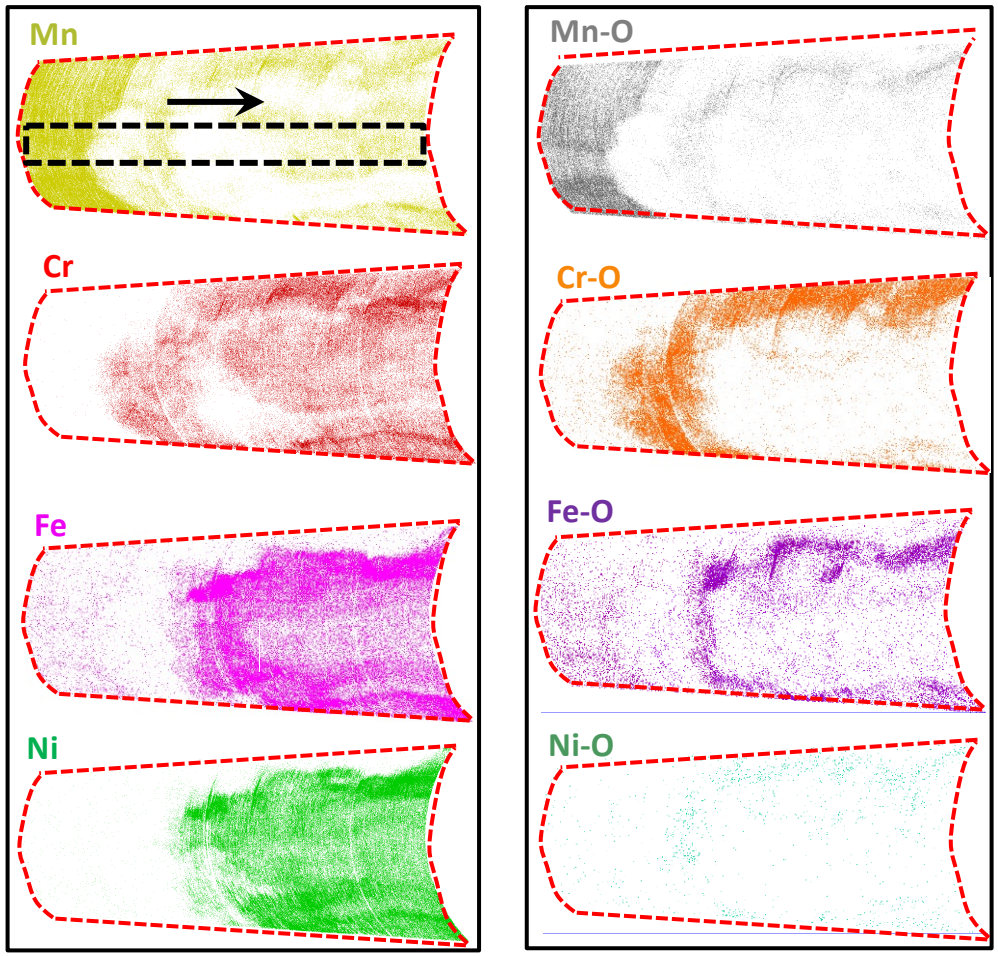

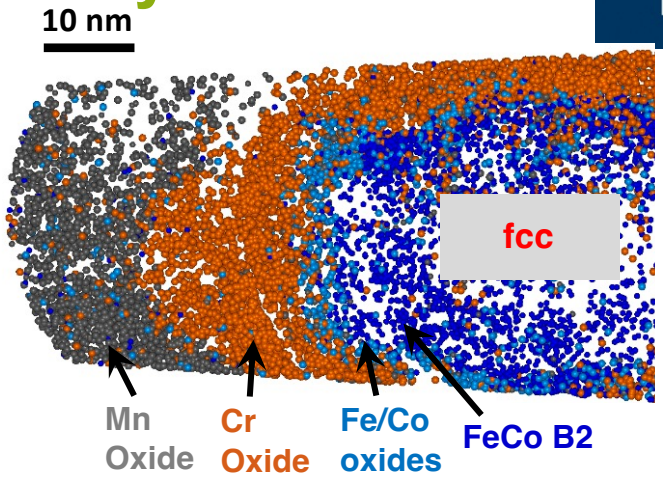

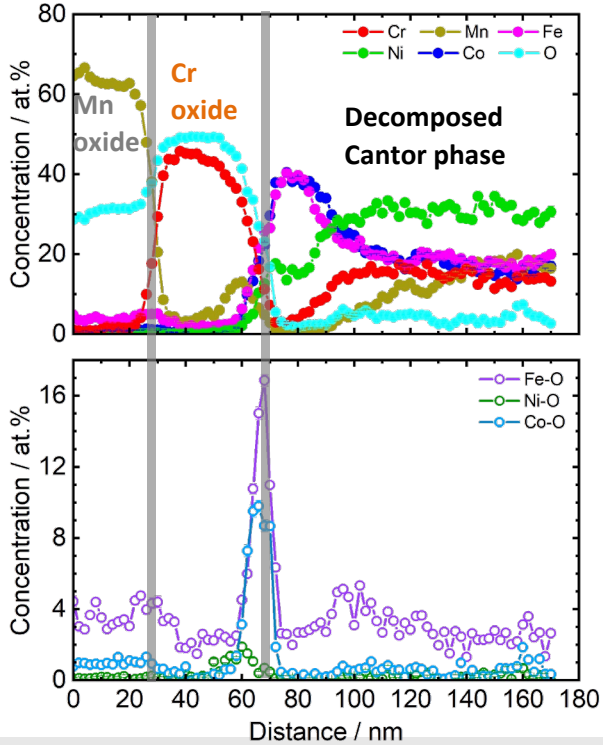

Y. Li, A. Kostka, A. Savan, A. Ludwig (2018) ***Atomic-scale investigation of fast oxidation kinetics of nanocrystalline CrMnFeNiCo thin films***, J. Alloys and Compounds 766, 1080 -1085

Combinatorial processing platforms for accelerated phase evolution in CCAs: Electrochemistry

OER: oxygen evolution reaction

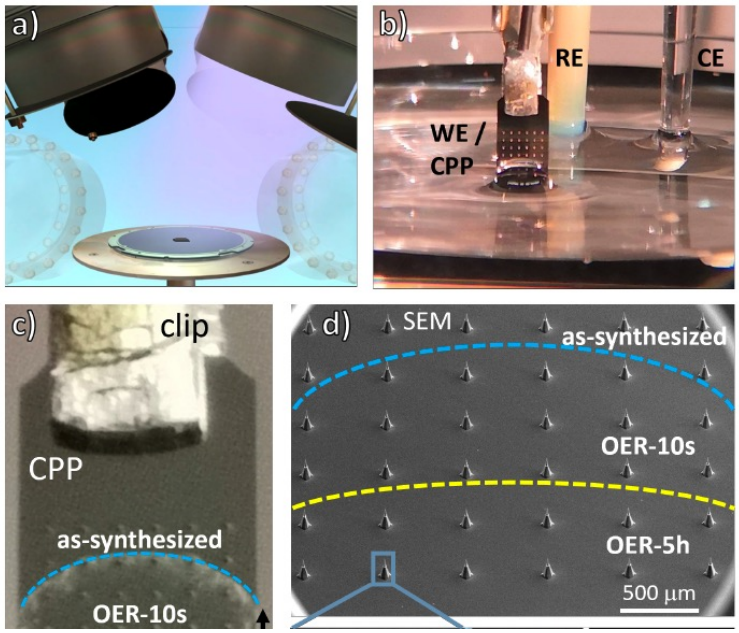

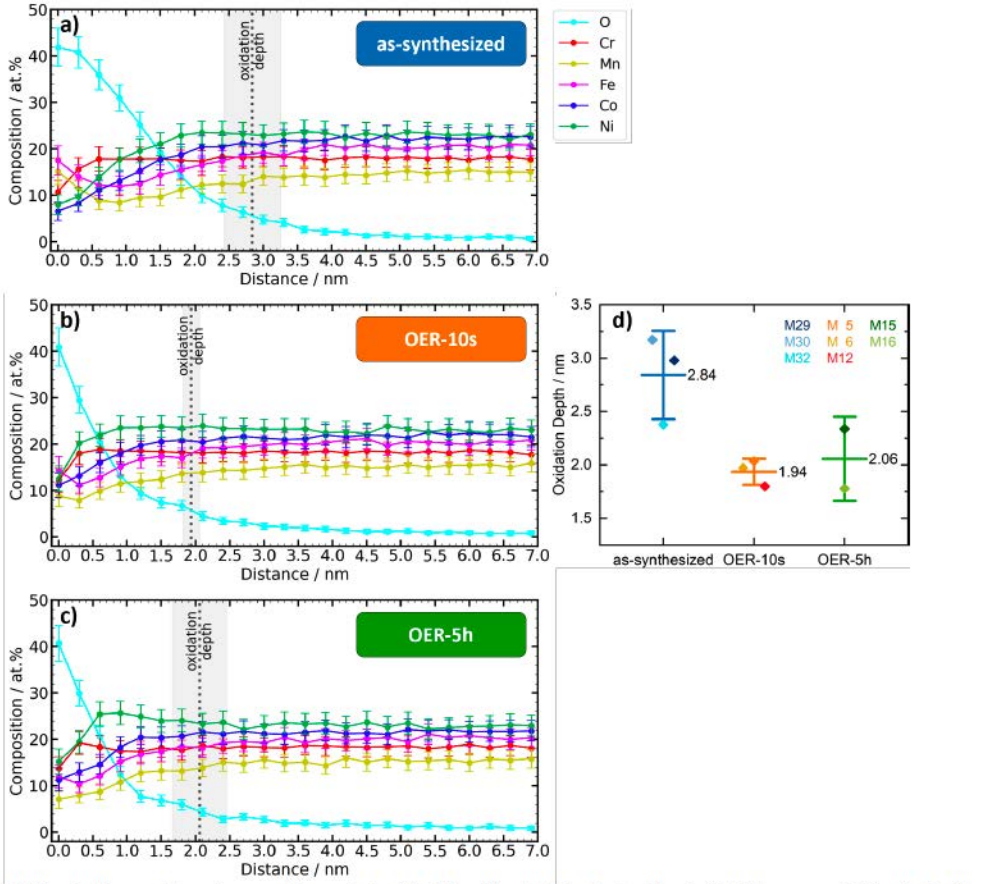

Fig. 3 | Oxidation depths. a-c, Element composition vs depth plots of the different states. Dashed lines indicate the mean oxidation depth with a standard deviation beyond which the oxygen content remains at low values. **d**, Plot of the oxidation depths of the different states with mean value and standard deviation. Each tip is represented by a different color.

V. Strotkötter, Y. Li, F. Lourens, A. Kostka, T. Löffler, W. Schuhmann, A. Ludwig (2024) *Self-Formation of Compositionally Complex Surface Oxides on High Entropy Alloys Observed by Accelerated Atom Probe Tomography: A Route to Sustainable Catalysts*, Materials Horizons, 11, 4932-4941, 10.1039/D4MH00245H

Advanced Materials Processing and Microfabrication

Übungsfragen

- Definieren Sie Grenzflächen und Oberflächen.
- Erläutern Sie die Bedeutung von pn Übergängen.
- Nennen Sie ein Beispiel für grenzflächendominierte Höchstleistungswerkstoffe.
- Erläutern Sie die Bedeutung der Oberfläche für elektrokatalytische Anwendungen.
- Nennen Sie Anwendungsbeispiele von Schichten im Maschinenbau.
- Nennen Sie zwei Verfahren zur Herstellung von bulk Einkristallen (Wafer).
- Wie können Einkristalle von Systemen hergestellt werden, die sich beim Schmelzen zersetzen würden?
- Wie werden einkristalline Schichten hergestellt?
- Was ist problematisch an Festkörperreaktionen?
- Wie können Materialien bei extremen Drücken hergestellt und untersucht werden?
- Erläutern Sie die Grundprinzipien der Photolithographie und Si-Mikrotechnik.
- Nennen Sie drei Beispiele für die Anwendung von Mikrosystemen in der Materialforschung.
- Welche Mikrosysteme eignen sich für TEM-Anwendungen?
- Was ist eine Mikroheizplatte und wie kann sie zur Materialprozessierung genutzt werden?
- Erläutern Sie den Aufbau und die Funktionsweise eines Spannungsmesschips auf mikrotechnischer Basis.

Advanced Materials Processing and Microfabrication

Literatur und Quellen

- A.R. West, Solid state chemistry and its applications, 2. Auflage, Wiley, 2014
- P. Rudolph, Handbook of crystal growth: basic techniques, 2. Auflage, Elsevier, 2015
- R. Haefer, Oberflächen und Dünnschicht-Technologie, Springer, 1987
- Paper sind auf den Folien gekennzeichnet

Basic research needs for synthesis science:

https://science.osti.gov/-/media/bes/pdf/reports/2017/BRN_SS_Rpt_web.pdf?la=en&hash=24BA7C6B4BCE086EC5F3877F24DCE1CBCCFD5303